MARMARA UNIVERSITY

INSTITUTE FOR GRADUATE STUDIES IN PURE AND APPLIED SCIENCES

AN INTEGRATED MODELING APPROACH TO INVESTIGATE PERFORMANCE OF SELECTIVE REDUCTION CATALYST

İSMAİL HAKKI SAVCI

Ph.D. THESIS

Department of Mechanical Engineering

Thesis Supervisor

Prof. Dr. M. Zafer GUL

ISTANBUL, 2015

MARMARA UNIVERSITY

INSTITUTE FOR GRADUATE STUDIES IN PURE AND APPLIED SCIENCES

AN INTEGRATED MODELING APPROACH TO INVESTIGATE PERFORMANCE OF SELECTIVE REDUCTION CATALYST

İSMAİL HAKKI SAVCI

(724609003)

Ph.D. THESIS

Department of Mechanical Engineering

Thesis Supervisor

Prof. Dr. M. Zafer GUL

ISTANBUL, 2015

MARMARA UNIVERSITY
INSTITUTE FOR GRADUATE STUDIES IN PURE AND APPLIED SCIENCES

İsmail Hakki SAVCI, a Doctor of Philosophy student of Marmara University Institute for Graduate Studies in Pure and Applied Sciences, defended his thesis entitled "**An Integrated Modelling Approach to Investigate Performance of Selective Catalyst Reduction**", on July 23, 2015 and has been found to be satisfactory by the jury members.

Jury Members

Prof.Dr. Zafer Gul (Advisor)
Marmara University .....

Prof. Dr. Cem Sorusbay (Jury Member)
Istanbul Technical University.....

Assoc.Prof. Hakan Serhad Soyhan (Jury Member)
Sakarya University .....

Assoc.Prof. Metin Gumus (Jury Member)
Marmara Üniversitesi .....

Assist.Prof. Mustafa Yılmaz (Jury Member)
Marmara Üniversitesi .....

APPROVAL

Marmara University Institute for Graduate Studies in Pure and Applied Sciences Executive Committee approves that İsmail Hakki SAVCI be granted the dégree of Doctor of Philosophy in Department of Mechanical Engineering, Mechanical Engineering Program o... 17.08.2015 (2015/18-02)

Director of the Institute
Prof. Dr. Uğur YAHŞİ

To my father;

Prof Dr Hikmet SAVCI

ACKNOWLEDGMENT

I would like to express to my sincere gratitude to my advisor Prof Dr. M. Zafer Gul for his strong support and continuous encouragement throughout my dissertation. In fact, it is a great honor to have worked with him.

This project would not have been possible without the help of countless others in my university and company.

Special thanks to Mr. Tolga Senoguz of Ford Otosan for making this opportunity a possibility.

Last but not the least, I want to thank my family members for their encouragement and support during all these years of research. Special thank to my father, Prof. Dr Hikmet SAVCI who has great support for my academic perspective and whole life. I would like to thank my wife, daughter for their faith, understanding, encouragement, and support.

June 2015 **İsmail Hakkı SAVCI**

TABLE OF CONTENTS

ACKNOWLEDGMENT vi

TABLE OF CONTENTS vii

ÖZET ix

ABSTRACT xi

CLAIM FOR ORIGINALITY xiii

SYMBOLS xiv

ABBREVIATIONS xv

LIST OF FIGURES xvi

LIST OF TABLES xxi

1. INTRODUCTION 1

1.1. Background 4

1.2. Diesel Exhaust Aftertreatment Systems 8

1.3. Selective Catalytic Reduction 10

1.4. Motivation and Research Contributions 15

1.5. Dissertation Outline 16

2. LITERATURE REVIEW 17

2.1. Diesel Engine NOx Emission and Regulations 17

2.2. SCR Aftertreatment System Control 19

2.3. Selective Reduction Catalyst Numerical Modelling 21

2.4. SCR Deposit Modelling 23

2.5. SCR Experimental Studies 26

3. METHODOLOGY 29

3.1. Simple Validation Cases 33

3.1.1. Validation of the Chemical Reaction Rate 33

3.1.2. Deposit Modelling 38
3.2. Experimental Setup 44
3.2.1. Spray droplet measurement 44
3.2.2. Flow rig development 51
3.2.3. Imaging techniques and testing methodology 55
3.3. Numerical Modeling of Inline Exhaust Aftertreatment System 57
3.3.1. CFD model description 59
3.3.2. Experimental set-up and optical diagnostics 66
3.3.3. CFD spray model setup 73
3.3.4. Mathematical modeling 74
3.3.5. CFD urea-water evaporation and decomposition 79
3.3.6. Conjugate heat transfer (CHT) 79
3.3.7. Spray wall interaction 80
3.4. CFD Deposit Prediction with test result 82
3.5. Emission Prediction using 1D with 3D effect 84
3.5.1. Geometrical sector based approach 84
3.5.2. Emission prediction model 85
4. RESULTS AND DISCUSSION 87
4.1. The Results of 3D SCR Simulation 88
4.1.1. The Flow field results 88
4.1.2. Spray particles distribution 90
4.1.3. Temperature distribution 101
4.2. Deposit Formation 105
4.3. NH_3 distribution at the inlet of the SCR 111
4.4. Urea Deposit Mapping 117
4.5. Emission Prediction Modelling 123
5. CONCLUSIONS 129
6. REFERENCES 131

ÖZET

Dizel emisyon gazları partikül, karbon monoxide, NOx içeren çok sağlığa zararlı gazlardır. lBu çalışmanın amacı seçici indigeyici katalist sistemler icin birbiriyle entegre ve çok boyutlu bir modelleme geliştirebilmektir. Bu modelleme tekniği ile katalistlerde yüksek NO_x çevrim verimi için gerekli emisyon tahminlerini yapabilecektir. Emisyon tahminin doğruluğunu arttırmak için egzoz sistemindeki 3 boyutlu bütün fiziksel etkiler detaylı bir çalışma ile modellenmiştir. Araştırmacılar farklı üre seçici indirgeyici katalist modellemeleri geliştirmektedir ancak modeller deposit oluşmasının emisyon üzerindeki etkilerini modelleyememektedir.

Tezde emisyon taminleri 3 boyutlu sayısal çalışmaları sonucunda secici indirgeyici katalistlerindeki NH_3 dağılımlarının bulunması ve üre-kristallerinin birikmesinin sıcaklık ve debiye bağlı haritalaştırılması sayesinde doğru olarak yapılamabilmektedir. Bu sayede daha gelişmiş üre kontrol stratejileri denenebilmekte, seçici indirgeyici katalist boyutlandırmaları ve kimyasal yükleme optimizasyon çalışmaları yapılırken egzoz sistem tasarımları iyileştirilebilmektedir.

Seçiçi İndirgeyici Katalist modellemeleri çok sayıda fiziksel modelleme gerektiren karmaşık bir modeleme tekniğidir. Bu modelleme püskürtme, kimyasal modelleme, katı-sıvı arasındaki ısı transferi ve deposit modellemesi içermektedir. Bu fazla sayıda modelleme yaklaşımlarının farklı çalışmalar ile doğrulanması yapılmıştır. Literaturde bulunan temel çalışmalar ile kullandığımız modelleme teknikleri karşılaştırmaları yapılmıştır. Bu sayede geliştirilen modeller gerçek egzoz sisteminin modellenmesinde kullanılmış ve PIV sistemi ile akış ve parçacık doğrulanmaları yapılmıştır.Kurulmuş olan akışkanlar mekaniği laboratuvarımızdan egzoz sisteminin değişik yerlerini termo eleman, basınç ve NOx sensorleri monte edilerek alınan datalar ile sayısal modeli iyileştirilmiştir. Akışkanlar mekaniği laboratuvarı motordan çıkan sıcaklık, hava, NOx debisi simule edilen ECU ile birlikte çalışan, kontrollu test yapmamızı sağlayan bir laboratuvardır.

Üre kristallerin modellemesi karmaşık olduğundan sadece sayısal modelleme teknikleri ile ürenin sistemde birikmesi ve yapısının ne olduğunu tahmin etmek mümkün değildir. Sayısal modellemesi ile sadece ürenin nerede birikebileceği tahmini yapılabilmektedir. Gerçek egzoz sistemine üre injektörünün bulunduğu yerden endoscope ile alınan

görüntülerden görüntü işleme teknikleri ile ürenin ne kadar biriktiğinin tahmini yapılabilmektedir. Bu datadan daha sonra üre kristallerinin birikme haritası çıkarılabilmektedir.

Üre kristalleri akışkanlar mekaniği laboratuvarında endoscope, quartz camlar ve sayısal ile detaylı incelendikten sonra oluşturulan harita ile 1 boyutlu emisyon modeline verilecek olan datalar düzeltilerek verilmektedir. 1 boyutlu emisyon modeli sayısal gelen düzgün olmayan NH3 dağılımları ve ile emisyon sonuçlarını bulabilmektedir. Bu sonuçlar motordan gelen emisyon sonuçları ile karşılaştırılmıştır.

Haziran 2015 **İsmail Hakkı SAVCI**

ABSTRACT

The emissions of the diesel engines consist of various harmful exhaust gases such as carbon monoxide (CO), particulate matter (PM), hydrocarbon (HC), and nitrogen oxides (NOx). Several technologies have been developed to reduce diesel emissions especially NOx reduction systems in last decades. The most promising NOx emission reduction technologies are exhaust gas recirculation (EGR) system to reduce peak cylinder temperature that reduces NOx form caused by combustion and active selective catalyst reduction (SCR) system using reducing agent such as urea-water-solution for exhaust aftertreatment system.

Recent years many different emission reduction application strategies were developed. One of the challenging approach to remove the EGR from engine and design the high NOx conversion efficiency SCR with reducing agent system. Thus the comprehensive SCR modeling approach is required to design compact aftertreatment systems that meet NOx emission legistration level.

In the first stage, To develop computational fluid dynamic (CFD) methodology with conjugate heat transfer, spray, deposit and chemical reaction modeling techniques is fundamental work for methodology development. Result of this methology include required parameters to optimize SCR system design.

In the second stage 1D emission prediction tool is developed whether the design meet the emission legistlation target. This emission prediction tool should be fast and accurate method with 3D simulation and deposit effect on the SCR system. Before freezing the design of SCR system, emission level of design should be predictable whether further design optimizations or advanced SCR technologies are required. 1D emission tool can predict to different SCR catalyst sizing, and different aftertreatment system layout.

Since deposit has a complex phenomogical physics for prediction, in this dissertation deposit modeling is developed in 3D CFD. To predict more accurate deposit prediction, image processing tool was developed in Matlab which uses endoscop camera deposit images. The calculated mass of deposit from matlab was correlated with deposit studies in Flow Test Bench. These results were developed to deposit map which is function of

temperature and mass flow rate over all operating conditions by using image processing tool.

The main objective of this work is to develop selective catalyst reduction CFD modeling with correction of the deposit map technique to focus on ammonia distribution at the SCR inlet and to observe its influence over NOx reduction process.

June 2015 **İsmail Hakkı SAVCI**

CLAIM FOR ORIGINALITY

The Selective Catalytic Reduction (SCR) is designed to reduce the NO_x emissions from the combustion system such as power plants and engines. Selective Catalyst Reduction system with urea water solution as reducing agent, is state of the art reduction technology among the NO_x reduction technologies for diesel engines.

Different emission strategies are used to meet emission legislation of European standard for heavy duty diesel engines as NOx and PM reduction. Active SCR, EGR and Diesel particulate filter (DPF) are used to meet Euro VI legistration. Recent challenging strategy is attempting to minimize fuel consumption with stand-alone SCR. To optimizing urea injection strategy as calibration work and optimized exhausts system layout as CFD work are key parameters to achieve high NOx conversion in this strategy.

In this dissertation, 3D CFD SCR modeling integrated with deposit map have been developed to investigate SCR performance accurately. Emission prediction including all the 3D effect of flow, species distribution and deposit map are used to predict legistration level of the exhaust aftertreatment system.

- 3D CFD for SCR are advanced modeling techniques which consist various physics such as spray, conjugate heat transfer, multi component chemisty.
- Deposit modeling are developed in CFD with good correlation to predict deposit location but CFD is poor tool to predict mass of deposit. Mass of deposit prediction method was developed in Matlab by using image processing tool.
- Deposit mass calculation in Matlab and deposit location prediction in CFD were correlated and combined in Flow Lab.
- 1D emission prediction model was developed to asses the emission performance of the system for each WHSC points. The models are performed by using NH3 distribution at the inlet of the SCR with deposit map correction from CFD. Thus the 1D emission models include 3D effect of the systems.

June 2015 **İsmail Hakkı SAVCI**

SYMBOLS

h_s : Stagnation enthalpy

k : Turbulent kinetic energy

ℓ : Dissipation length scale

$\dot{m}$: Mass flow rate

$r_p(t)$: Particle Position

$v_p(t)$: Particle velocity

m_p : Particle mass

$\dot{m}_p$: The rate of particle mass

F_d : Drag Force

F_p : The pressure gradient force

F_{vm} : The virtual mass force

F_g : The gravity force

U : Instantaneous velocity

Q_t : Convective heat transfer to the particle from the continuous phase

Q_{rad} : The rate of radiative heat transfer.

σ : Stefan-Boltzmann constant.

X_{is} : Raoult's law

We : Weber Sayısı

ABBREVIATIONS

CFD **:**Computational Fluid Dynamics

EGR **:**Exhaust Gas Recirculation

EC **:**European Commission

PM **:**Particulate Matter

SCR **:**Selective Catalytic Reduction

CO **:**Carbon Monoxide

UWS **:**Urea Water Solution

DPF **:**Diesel Particulate Filter

CAN **:**Controller area network

2D **:**Two-Dimensional

3D **:**Three-Dimensional

CHT **:**Conjugate Heat Transfer

PIV **:**Particul Image Velocity

RSM **:**Reynold Stress Modelling

NOx **:**Nitrogen Oxides

RANS **:**Reynolds average Navier-Strokes

SMD **:**Sauter Mean Diameter

WHTC **:**Word Harmonic Transient Cycle

WHSC **:**Word Harmonic Steady Cycle

LIST OF FIGURES

Figure 1.1. European Legistration trend for Heavy duty Emission Standards [6] 2

Figure 1.2. Emission legislation of " CO, HC, NO_x and PM" [2] 2

Figure 1.3. Improvement of emission reduction by using different strategies 4

Figure 1.4. Schematic of a typical automotive catalytic converter 5

Figure 1.5. The Reaction Energy Paths [12] 6

Figure 1.6. Catalytic converter's honeycomb structure 7

Figure 1.7. The structure of the catalyst 7

Figure 1.8. Diesel Engine Aftertreatment System Schematic 8

Figure 1.9. CO and HC conversion in DOC [17] 9

Figure 1.10. Diesel Particulate Filter 10

Figure 1.11. Selective Catalytic Reduction System 11

Figure 1.12. NOx Conversion and Ammonia Slip 14

Figure 2.1. The speed pattern of the world wide reference as WHTC cycle [36] 18

Figure 2.2. System Layout of Heavy Duty Application [13] 20

Figure 2.3. Structure of the control strategy for the SCR aftertreatment system [40] ... 21

Figure 2.4. Schematic overview of different droplet impact regimes 24

Figure 2.5. Side reaction of deposit 25

Figure 3.1. Multicomponent Evaporation model 29

Figure 3.2. CFD Model of the SCR modelling 30

Figure 3.3. Flow Chart of Work 31

Figure 3.4. Sketch of the experimental setup [66] 34

Figure 3.5. Numerical results of species and temperature in exhaust system 35

Figure 3.6. Calculated conversion to NH3 for different gas velocities [66] 36

Figure 3.7. Predicted conversion to NH3 at different gas temperatures. [66] 37

Figure 3.8. Chemical approach effect on NH3 distribution 38

Figure 3.9. Regime map for spray/wall-interaction [76]..... 39

Figure 3.10. Droplet Behaviour in gas phase and on wall 40

Figure 3.11. Sketch of the experimental setup for spray/wall interaction. 40

Figure 3.12. Spray pattern at 4 ms, 10ms and 20ms..... 41

Figure 3.13. Spray pattern of numerical models at 4 ms, 10ms and 20ms 41

Figure 3.14. Predicted wall film thickness with spray distribution 42

Figure 3.15. Calculated mass fraction of urea in the wall..... 43

Figure 3.16. Calculated mass fraction urea at plane lateral 43

Figure 3.17. Components of the PIV setup 45

Figure 3.18. Describes a simple schematic of PIVfor spray diameter distribution 46

Figure 3.19. Spray Angle Measurement 47

Figure 3.20. Droplet diameter distribution..... 47

Figure 3.21. Spray behaviour through the nozzle..... 48

Figure 3.22. Shows the computational grid..... 49

Figure 3.23. Comparision of high speed camera and CFD results for spray angle 50

Figure 3.24. Computational Fluid Dynamis Result for droplet diameter 51

Figure 3.25. Flow Test Bench 52

Figure 3.26. Schematic of Exhaust System Layout with Emission..... 54

Figure 3.27. Operating condition of burner..... 54

Figure 3.28. Configuration of the test section used for optical test..... 56

Figure 3.29. The PIV testing through 3 window pipe..... 57

Figure 3.30. SCR Aftertreatment Inline model 58

Figure 3.31. Shows the computational mesh for the mixer region..... 59

Figure 3.32. Shows the computational mesh for the whole model..... 59

Figure 3.33. Selective Catalyst Modeling in Converge 60

Figure 3.34. Selective Catalyst Modeling in Fluent 60

Figure 3.35. Parcel Number sensitivity testing 63

Figure 3.36. Boundary conditions of the inline exhaust aftertreatment system 66

Figure 3.37. The PIV and shadowgraph setup for the optical test bench 67

Figure 3.38. PIV measurement at the pipe window..... 68

Figure 3.39. PIV measurement comparison flow field 69

Figure 3.40. Velocity vector from PIV measurement..... 69

Figure 3.41. Velocity vector at the cone k-epsilon..... 70

Figure 3.42. Velocity vector at the cone RMS 70

Figure 3.43. Velocity vector distribution at the cone for k-epsilon model 70

Figure 3.44. Velocity vecot distribution at the cone for RSM model..... 71

Figure 3.45. Thermocouple layout in SCR catalyst..... 72

Figure 3.46. Temperature distribution correlation with flow distribution 72

Figure 3.47. Temperature Distribution at the inlet of the SCR 73

Figure 3.48. Liquid droplets impacting on wall [94] 78

Figure 3.49. Fluid Solid Coupling Methodology 80

Figure 3.50. Different deposit regime in inline exhaust aftreatment 82

Figure 3.51. Endoscopes capture the critical region image..... 83

Figure 3.52. Endoscope camera..... 83

Figure 3.53. Division of substrate face into equal area geometrical sectors..... 85

Figure 3.54. 1D modelling of the selective reduction catalyst 86

Figure 3.55. Perfomance Modelling Methodology..... 86

Figure 4.1. Operating conditions of deposit work 88

Figure 4.2. Velocity distribution for RMS model..... 89

Figure 4.3. The velocity vector along the sections of the system 89

Figure 4.4. Droplet Distribution into the system 90

Figure 4.5. Droplet Distribution across the system at 0.125 s..... 92

Figure 4.6. Droplet Distribution across the system at 0.1325 s..... 93

Figure 4.7. Droplet Distribution across the system at 0.1485 s..... 93

Figure 4.8. Droplet Distribution across the system at 0.204 s..... 94

Figure 4.9. Droplet distribution through the mixer at 0.124 s..... 95

Figure 4.10. Droplet distribution through the mixer at 0.204 s..... 96

Figure 4.11. Droplet distribution along the system for time 0.01s..... 97

Figure 4.12. SMD Value for Upstream and Downstream of the Mixer..... 98

Figure 4.13. Droplet count upstream and downstream of the mixer 100

Figure 4.14. Temperature variation along the system due to process..... 102

Figure 4.15. Temperature decrease due to evaporation process..... 102

Figure 4.16. Temperature cooled down due to evaporation..... 103

Figure 4.17. Temperature cooling down due to evaporation 103

Figure 4.18. Heat Transfer on the mixer wall 104

Figure 4.19. Deposit formation where the spray hits..... 106

Figure 4.20. Temperature reduced on the mixer due to deposit 107

Figure 4.21. Isocyanic acid form more complex deposit 108

Figure 4.22. Deposit accumulation on the mixer..... 109

Figure 4.23. Mass Thickness on different region of the system..... 110

Figure 4.24. NH3 distribution at the inlet of the catalyst..... 111

Figure 4.25. NH3 distribution at the inlet of the catalyst..... 112

Figure 4.26. NH3 distribution at the inlet of the catalyst..... 112

Figure 4.27. NH3 distribution at the inlet of the catalyst..... 113

Figure 4.28. Mass of the NH3 at the inlet 114

Figure 4.29. Gamma value of the NH3 116

Figure 4.30. Isocyanic product can be seen along catalyst 117

Figure 4.31. Optical window pipe 118

Figure 4.32. Deposit Characteristics for different impingement condition..... 119

Figure 4.33. Deposit accumulation at 400 kgh/h and 200 degree C..... 121

Figure 4.34. Deposit accumulation at 350 kgh/h and 300 degree C..... 122

Figure 4.35. Deposit Mapping from Image Processing Tool..... 123

Figure 4.36. Emission Prediction Modeling with 3D CFD results..... 124

Figure 4.37. Corrected NH3 value with deposit maping result..... 125

Figure 4.38. Temperature Distribution 125

Figure 4.39. Fluid Temperature across the catalyst..... 126

Figure 4.40. Velocity distribution across the catalyst..... 126

Figure 4.41. NOx reduction across the catalyst..... 126

Figure 4.42 WHSC point for different NH3 distribution from CFD..... 128

Figure 4.43. Emission Prediction on the inline exhaust aftertreatment system 128

LIST OF TABLES

Table 1.1. Emission Reduction Technologies [8]..... 3

Table 2.1. European standards for heavy duty Diesel engines NOx emission [6] 17

Table 3.1. List of flow test bench components..... 52

Table 3.2. Components of the optical test bench..... 67

Table 3.3. Mesh type and number sensitivity..... **Error! Bookmark not defined.**

Table 3.4. Boundary Conditions..... 64

Table 4.1. Predicted Deposit values for different operating conditions 122

1. INTRODUCTION

Diesel engines have been the dominant power source for medium and heavy duty commercial vehicle applications such as trucks, buses, off road vehicles in the past decades. Diesel engines are also used for light duty applications such as passenger cars in recent years. The main advantages of diesel engines are increased fuel economy, higher durability, increased torque and low taxes imposed by government in comparison similar engine displacement of gasoline engine.

The main disadvantages of diesel engine are harmful exhaust gases due to diesel combustion process. These exhaust emissions threat public health in three main pollutants. [1]

1. The particulate matters (PM) are complex mixture that is generated from diesel combustion. PM is made up hundreds of chemicals adsorbed which are mostly carcinogens. The small size of particulate matters which is around 1-2µm is directy effect the public health particulary for the lung. [2]

2. Carbon monoxide (CO) is toxic chemicals. It is produced from partial combustion.[3]

3. Nitrogen Oxides are produced from combustion in the presence of nitrogen at high temperatures. Nitrogen oxides can form nitric acid vapour. Nitric acid vapour can penetrate the lung and damage it.[4]

These three emissions should be removed from the environmental due to their hazardous effect on the public health.

Stringent legislative emission standards to protect public health for diesel heavy duty and light duty engines were introduced by European Commission (EC), United States and China government commissions. In Figure 1.1 present the significant reduction of PM and NOx for heavy duty vehicles. These reductions show the reduction progression from 1992 to 2015. [5] The standards are defined by energy output (g/kwh) of the vehicles. The emission standards based on test cycle which represent driver real driving style. Each emission standards refered to as Euro 1, Euro 2, Euro 3, Euro 4, Euro 5 and Euro 6. Euro 6 entered in force in January 2014.

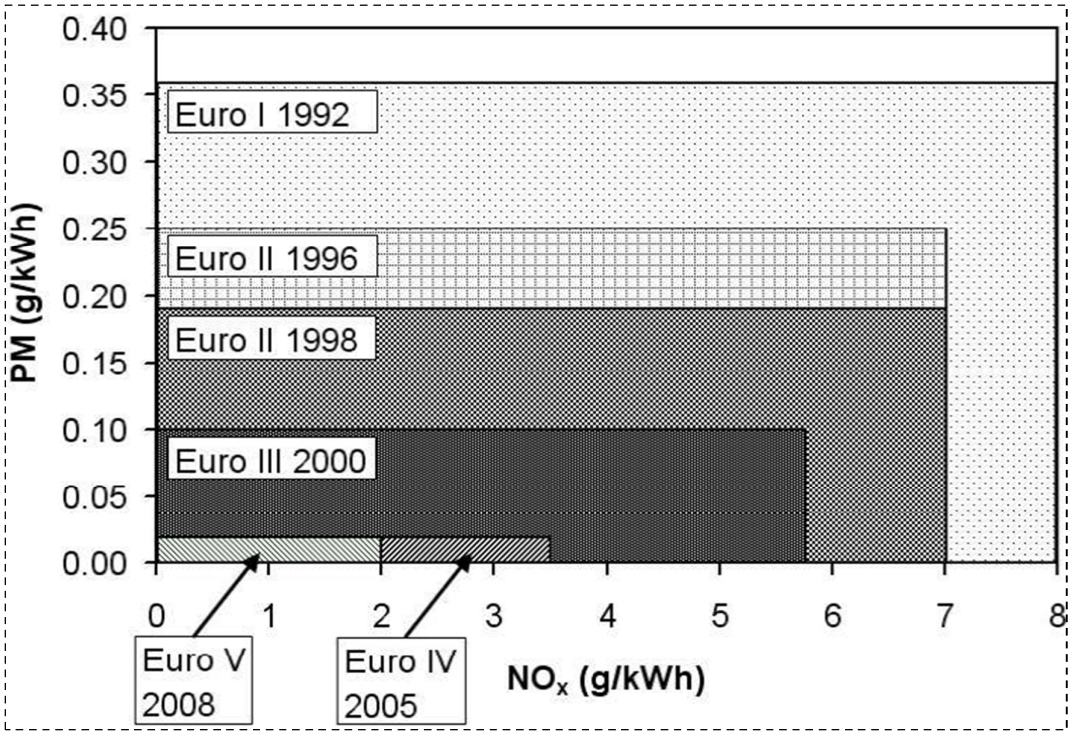

Figure 1.1. European Legistration trend for Heavy duty Emission Standards [6]

European emission legislation standards for commercial and passenger car is presented in Figure 1.2. The standards of heavy duty vehicle for Euro6 legistration include particulate matter (PM) emissions of 0.02 g/kWh, CO emission of 1.5 g/kWh and NO_x of 2 g/kWh. [7]

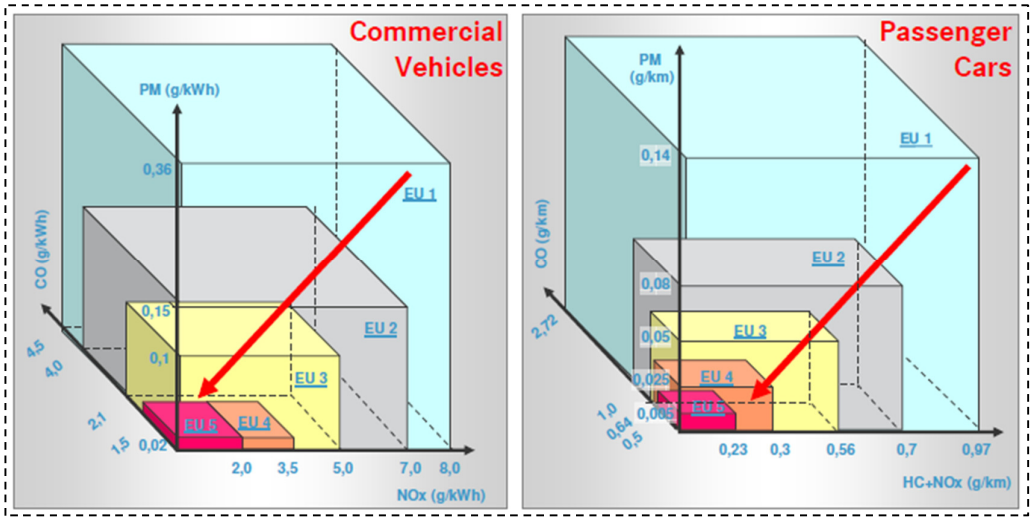

Figure 1.2. Emission legislation of " CO, HC, NO_x and PM" [2]

Many emission reduction technologies have been developed to meet emission standards for diesel engines. Particulate matter reduction is occured by regeneration using diesel oxidation and diesel filter catalyst. NOx reduction techniques are based either hardware design as exhaust gas recirculation (EGR) or standalone catalyst technologies as SCR or LNT NOx reduction systems. Active SCR system is state-of-the art technologies for NOx reduction technology. [8]

Table 1.1. Emission Reduction Technologies [8]

Emission Equipment	Description	NOx Efficiency	PM Efficiency	Status
Exhaust Gas Recirculation (EGR)	Recycles the exhaust gas back to the engine intake system	50% - 60%	n/a	Package issue, calibration effort
LNT	Adsorbes NO and oxygen during lean operation, uses CO and HC from periodic rich operation to convert to nitrogen	>80%	n/a	Light duty
SCR	Converts NOx to nitrogen and oxygen in the presence of urea	80% - 98%	30%	Urea-water-solution for ammonia
Diesel Oxidation Catalyst	Oxidizes HC and CO in catalyst	n/a	30%	DPF regen application
Diesel Particulate Filter	Collects particles in diesel exhaust	n/a	80% - 90%	Efficient catalyst for PM

Different calibration and hardware strategies are used for NOx and PM reduction. Recent advancement in exhaust after-treatment systems has identified two key promising technologies for reducing NOx emission which are the Lean NOx Trap

(LNT) and Selective Catalyst Reduction (SCR). [9] As illustrated in **Error! Reference source not found.**

Figure 1.3 the only combustion calibration can meet the Euro V emission legistration.

Using Selective Catalyst Reduction (SCR) NOx strategy, EGR and Diesel particulate filter (DPF) may be required to meet Euro VI emission standart. **Error! Reference source not found.**

Figure 1.3. Improvement of emission reduction by using different strategies

The most attractive emission strategy when using SCR involves a calibration of the engine for low PM (injection timing, high injection pressures), and using the SCR catalyst to reduce the increased NOx.

The recent strategies attempting to minimize fuel consumption, standalone SCR and DPF might be sufficient to meet Euro VI standard. The advanced strategy is required to optimize urea injection strategy and fuel consumption without EGR hardware which leads to a high emission reduction of NOx. SCR may be more advantages, especially in the heavy-duty truck application, than the competing EGR technology, which brings a fuel economy penalty. One needs to remember, however, that fuel savings in SCR engines are at least in part-offset by the cost of urea, which is consumed at about 3-5% of the fuel volume.This method results in a better fuel economy without additional hardware. The challenging part of this strategy is high NO_x reduction in exhaust aftrertreament. Thus optimized SCR system design and urea injection calibration are critical work to achieve this strategy.

1.1. Background

Automotive manufacturers widely used catalytic converter for exhaust aftertreatment applications in recent years. [10] Catalists are state of the art converter due to efficient and economical advantages to meet strict emissions legistration for European and USA. Shematic view of typical automotive catalytic converter is shown in Figure 1.4. The main challenge part is emission regulation becomes more stricker rules in near future so catalytic converter's efficiency should be improved.

A catalytic converter system is a "mechanical" device that contains an active catalyst

(coated substrate) that provides a "chemical" aftertreatment of pollutant exhaust gas. It's primary purpose is to aid in the conversion of exhaust HC, CO, and NO_x to less environmentally harmful products. [11]

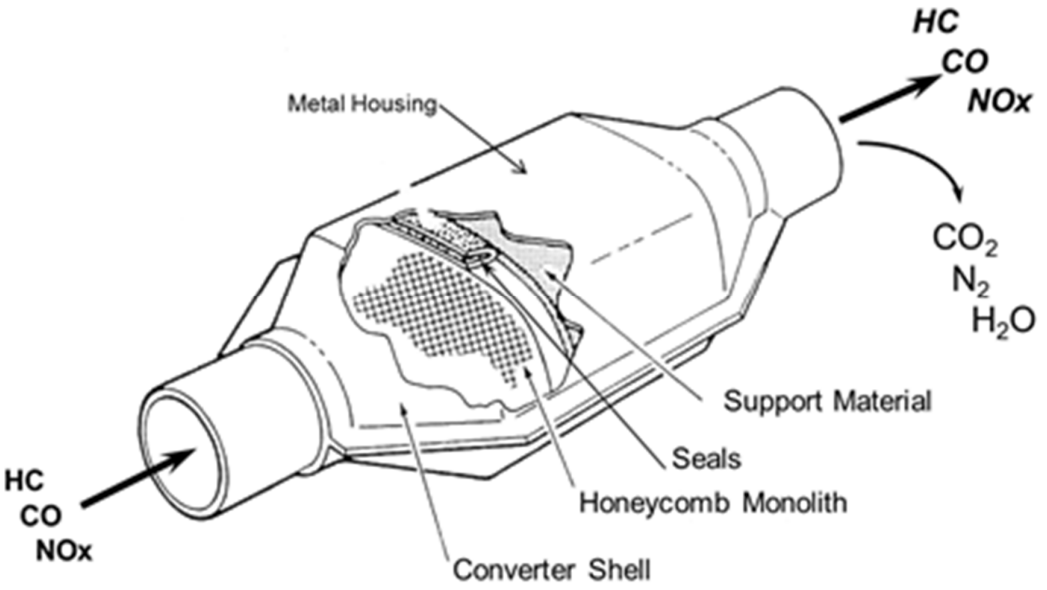

Figure 1.4. Schematic of a typical automotive catalytic converter

The catalyst is a substance which can increase the rate of a chemical reaction as seen in Figure 1.5**Error! Reference source not found.** But reactant and products are not altered or consumed during the reactions. [12]

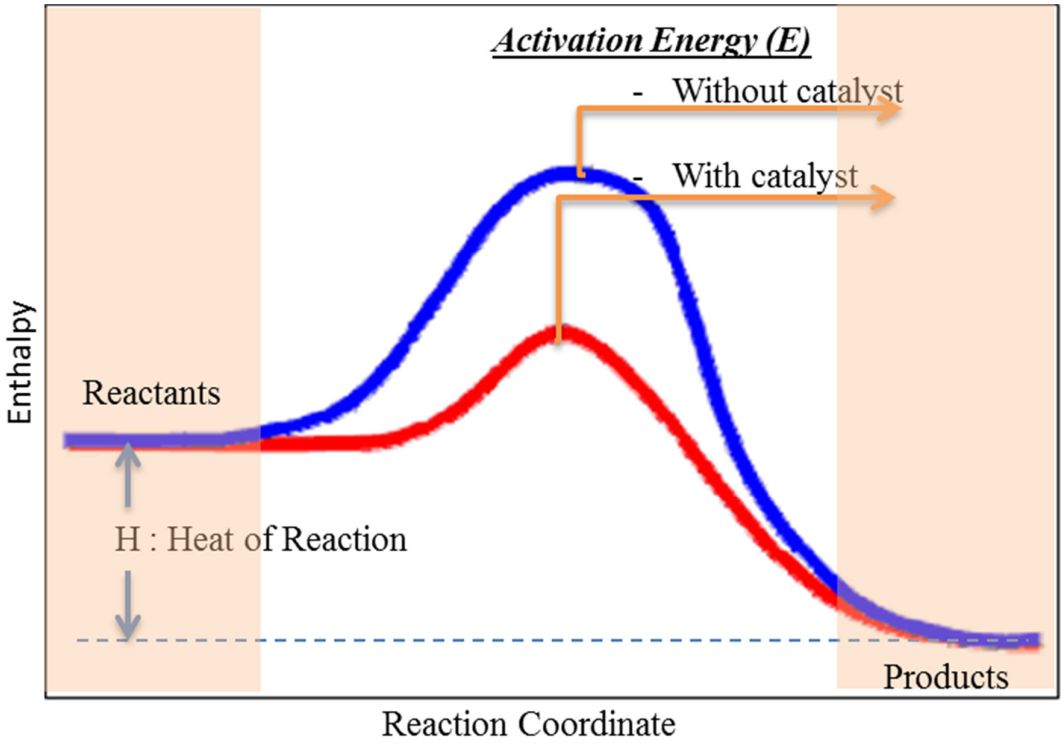

Figure 1.5. The Reaction Energy Paths [12]

The structure of the catalytic converter can be honeycomb or multilayer. The main shapes of the honeycomb catalysts are monoliths and plates. Monolithic type catalysts are characterized by the complex interactions of various physical and chemical processes. A simple cylindrical catalyt is shown in Figure 1.6 . It is comprised of a honeycomb monolithic ceramic structure that is made up of numerous parallel channels. Inner surface of these channels is coated with precious metals (such as platinum, palladium or rhodium). [13]

In automotive applications monolith structured substrates are widely used for the diesel oxidation catalyst, selective catalytic reduction (SCR). The main advantages of honeycomb catalysts are reduced pressure drop and increased surface chemical reaction due to the geometric surface area. [14]

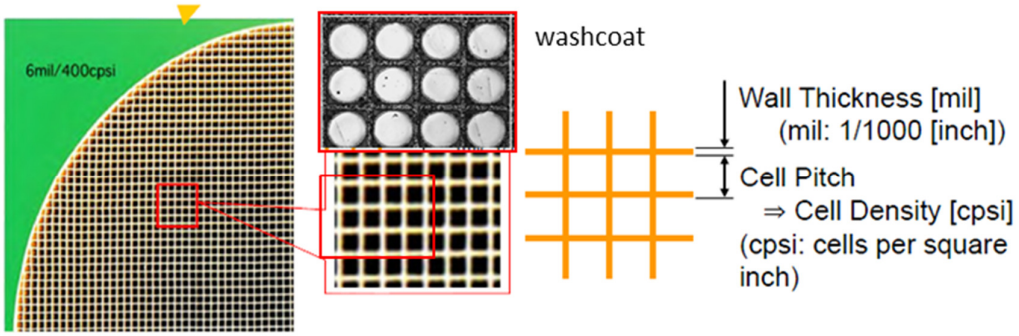

Figure 1.6. Catalytic converter's honeycomb structure

The porous support layer is made of washcoats that have high surface area layer for effective surface reaction in Figure 1.7. Ceramic monolith are manufactured from cordierite or silicone carbide that has thermal shock resistance due to a low thermal expansion coefficient; porosity and pore size distribution that is require of washcoat application.

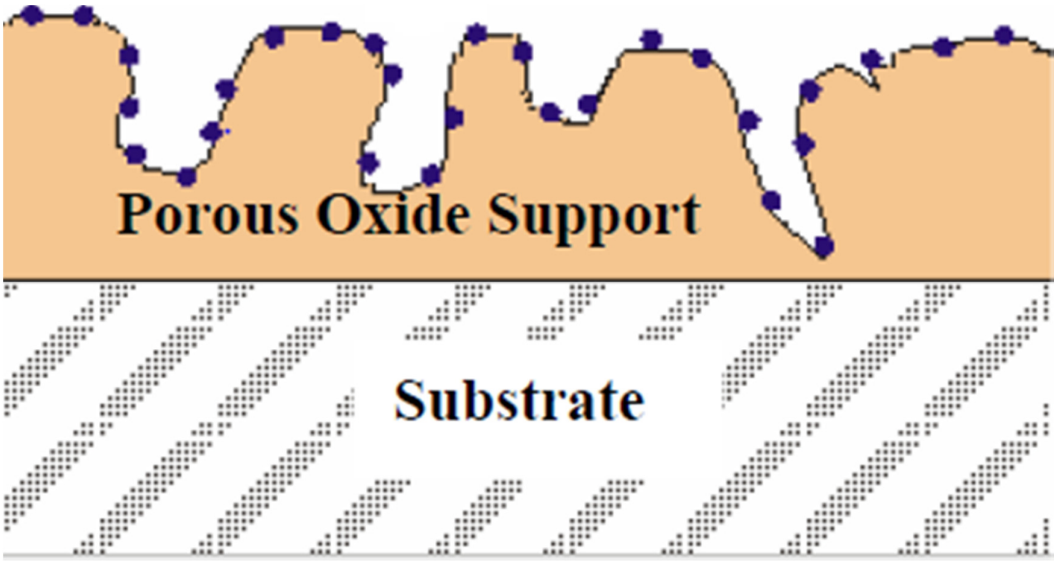

Figure 1.7. The structure of the catalyst

Catalysts are typically manufactured by applying washcoat onto catalyst supports. The washcoat, which serves as the carrier for a precious metal catalyst, is a porous refractory oxide layer which is applied to the substrates from an acidified aqueous slurry, dried and calcined. Aluminum oxide is the most common washcoat material. Other materials, used either as catalyst carriers or as promoters and stabilizers, include silicon oxide, cerium dioxide, titanium dioxide, zirconium oxide, and zeolites. [15]

1.2. Diesel Exhaust Aftertreatment Systems

Figure 1.8 is a schematic of a diesel exhaust gas aftertreatment system. The diesel oxidation catalyst (DOC) and diesel particulate filter (DPF) have been widely used to remove hydrocarbon and particulate matter in diesel engine.

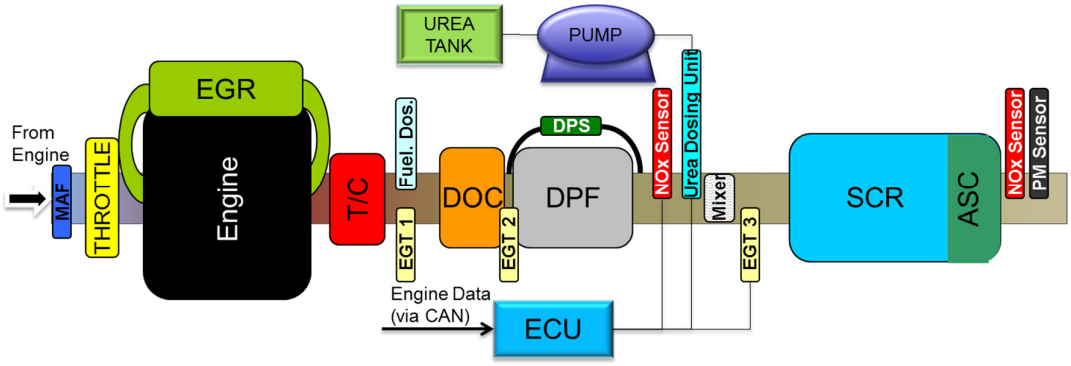

Figure 1.8. Diesel Engine Aftertreatment System Schematic

The diesel oxidation catalyst (DOC) is one of the oldest technologies originated from the early two way catalyst for controlling CO, HC and PM. DOC is ability to promote oxidation of unburned fuel in the exhaust to product such as CO2 and H2O. DOCs come in metallic or ceramic through honeycomb substrates coated with an oxidizing catalyst such as platinum, palladium or both due to low temperature activity for HC conversions [16]. The diesel oxidation catalyst is very effective catalyst for carbon monoxide and hydrocarbon emissions from diesel engines. **Figure 1.9** illustrates the catalyst performance as a function of temperature. The catalyst shows no activity at lower temperature. At high temperature rate of chemical reaction rate increases. [17]

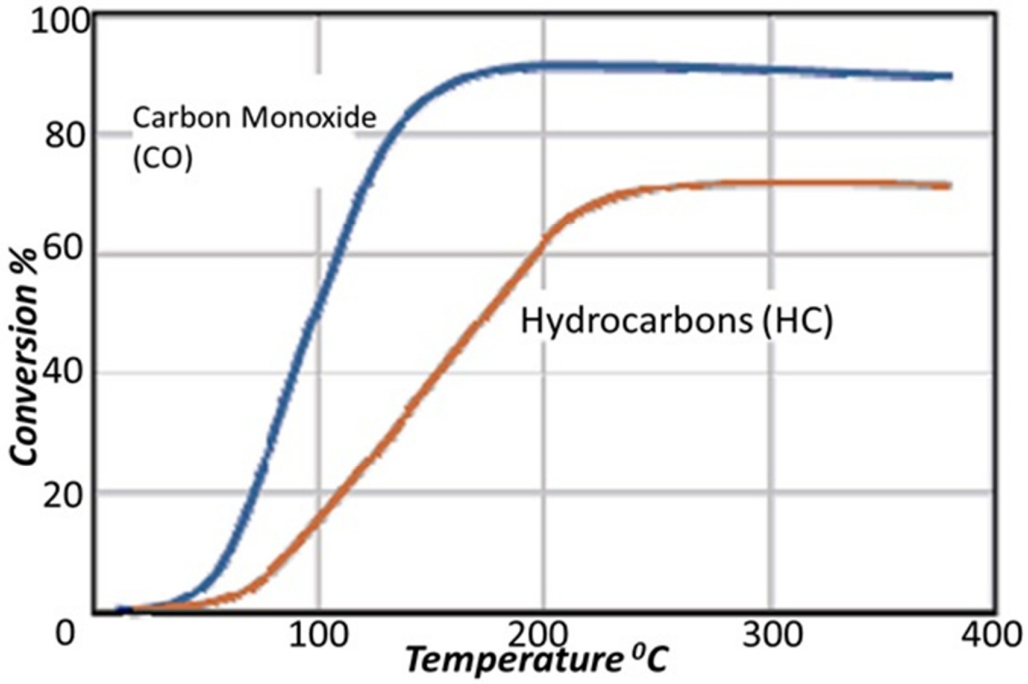

Figure 1.9. CO and HC conversion in DOC [17]

Diesel Particulate Filters (DPF) are mechanical device that physically filters the Particulate Matter (PM) in exhaust gas through a ceramic (cordierite or silicone carbide) honeycomb monolyth. 95% of pariculate matter (PM) is filtered by DPF . The filters consist open and closed channel as illustrated in Figure 1.10. Soot particle can be trapped by closed channel until pressure increased become high through DPF. The pressure sensor measure pressure increase to start cleaning process. [16]

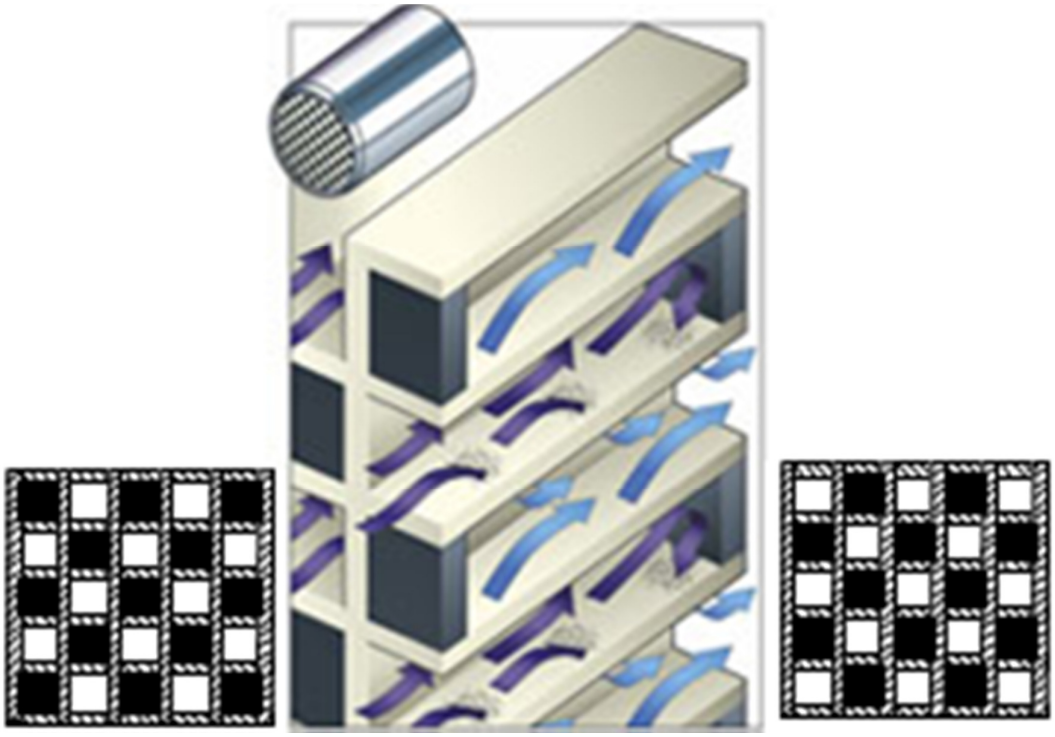

Figure 1.10. Diesel Particulate Filter

The trapped soot has been removed from the filter through oxidation to gaseous products, in a process called regeneration. The active regeneration is occured by fuel injection trough the DOC and temperature increase burnt the soot. The passive regeneration is occured by high temperature from combustion. [18]

1.3. Selective Catalytic Reduction

The Selective Catalytic Reduction (SCR) was designed to reduce the NO_x emissions from the combustion system such as power plants and engines. SCR which is using urea solution is called active SCR system. Active SCR system is state of the art NOx reduction technology for diesel engines. [19] The SCR technology was first applied in power plants in Japan in the late 1970 and followed by Europe from the mid 1980 and widely used in the world. In the USA, SCR systems were introduced for gas turbines in the 1990, with increasing potential for NOx control from coal-fired powerplants. [20] Nissan developed first SCR exhaust aftertreatment system for heavy duty vehicles in 2004. [21]

In the automotive applications, the Selective Catalytic Reduction (SCR) with NH_3 injection are widely used emission reduction technique to convert the NO_x emissions to N_2 (nitrogen) and H_2O (water). [7] However, pure ammonia (NH_3) is toxic reducing agent for mobile application. [22] Urea Water Solution (UWS) has transport and storage advantages over ammonia. [23] Urea should decompose to ammonia and carbon dioxide over SCR with NH_3 process with lower conversion ratio. [24]

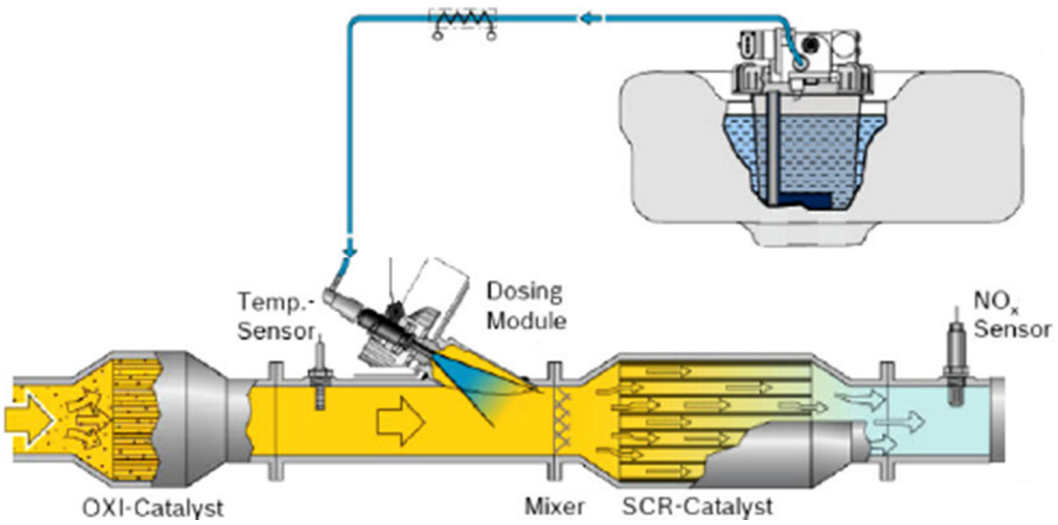

Figure 1.11. Selective Catalytic Reduction System

The major components of active SCR system are an dosing module which control the mass flow rate of the urea-water-solution (UWS), the honeycomb SCR catalyst which accelerates a chemical reaction, NO_x and gas temperature sensors which are located downstream and upstream of the catalyst.

The control system should be installed to the system for signal conditioning for injector and sensor. Controller area network (CAN) is required to communicate the signals between injector actuator, controller and engine data such as NO_x and temperature value. The parameters of the urea injector control are only opening time of the injector. It adjust the mass flow rate of the urea-water solution. More advanced injector can be adjusted with frequency, pressure and mass flow rate of the system.

SCR tank is essential for the urea solution storage. Urea solution storage system consist of urea tank, urea pump and urea level sensors.

Main equipment of dosing module is urea water solution (Adblue or DEF) which is mixture of 32.5% urea and 67.5% water, which is actually injected through the exhaust system, then it converts to the ammonia with 3 reaction step.

The first step is when urea-water solution (N_2H_4CO) is injected through the exhaust system, the water is evaporated then urea converts to liquid phase.

$$N_2H_4CO(UWS) \rightarrow N_2H_4CO(liquid) + 6H_2O(gas) \quad (1.1)$$

Liquid urea (N_2H_4CO) decomposed into ammonia (NH_3) and isocyanic acid ($HNCO$) in the exhaust system.

$$N_2H_4CO(liquid) \rightarrow NH_3(gas) + HNCO(gas) \quad (1.2)$$

Hydrolysis reaction is to convert from isocyanic acid with water vapor to ammonia as shown in equation 1.3. The thermolysis reaction of urea is endothermic reaction and the required heat is provided by the exhaust system. [25] [26]

$$HNCO(gas) + H_2O(gas) \rightarrow NH_3(gas) + CO_2(gas) \quad (1.3)$$

The system layout and dosing control of the urea injection rate should be optimized due to three major mechanism which are undesired slip of ammonia and iso-cyanic acid and deposit accumulation. Lower injection rate will result low conversion efficiency of the NO_x reduction, higher amount of injection rate will result deposit accumulation and slip of ammonia. [27]

While urea starts to decompose already at around 160°C, the decomposition cannot reach completion in the gas phase at temperatures typical for diesel exhaust and at the residence time in SCR systems. It is believed that only up to about 20% of the urea decomposes to HNCO and NH3 in the gas phase at 330°C, and only about 50% decomposes at 400°C. The remaining urea decomposes only after reaching the surface of the catalyst. It was also shown that HNCO is very stable in the gas phase, requiring an oxide surface to catalyze its decomposition to NH3. [28] In effect, most of the urea decomposition—especially at low temperature conditions—will occur on the catalyst

surface, rather than in the gas phase. In laboratory bench tests, the effects of urea decomposition were visible in the inlet section of the SCR catalyst. [29]

Urea decomposition processes and their impact on SCR catalyst performance are still not fully understood and require further research. Especially in low temperature SCR can not predict well. In addition to reactions in the gas phase and on the catalyst surface, storage and release of materials in the catalyst washcoat may play a role in the SCR catalysis. Ammonia is stored in the catalyst, as evidenced by the delayed appearance of the NH3 slip at the catalyst outlet, several minutes after the beginning of the SCR process. [30]

If urea is fed into the SCR system at low temperatures, a number of undesired byproducts may be formed, including cyanuric acid (C3N3(OH)3, from trimerization of HNCO), biuret, or melamine. Catalyst manufacturers have been aware of the possibility of SCR catalyst fouling by products of incomplete decomposition of urea, which may be a serious consideration for low temperature applications. Some proposed SCR system configurations include a dedicated urea hydrolysis catalyst placed between the urea injection point and the SCR catalyst. [31]

A typical SCR converter is honeycomb monolith structure with washcoated which are zeolite or vanadium based. The chemical reaction is very complex in SCR catalyst. Ammonia reacts with NO,NO_2 and oxygen in number of different reactions.

There are three main reactions that take place in NO_x reduction using NH3. First reaction is “standart” reaction which the nitrogen oxides of Diesel exhaust gas are primarily composed of NO, which converts into Nitrogen and water vapor by happens of Oxygen, as follows.

$$4NH_3 + 4NO + O_2 \rightarrow 4N_2 + 6H_2O \quad (1.4)$$

The second reaction is “Fast” SCR reaction. It is faster than the “standard” SCR reaction and occurs at the low temperature condition and presence of NO2. [32]

$$2NH_3 + NO + NO_2 \rightarrow 2N_2 + 3H_2O \quad (1.5)$$

The third reaction is slow reaction that happens only with NO2.

$$8NH_3 + 6NO_2 \rightarrow 7N_2 + 12H_2O \quad (1.6)$$

In addition to these reactions, the overall NOx reduction process is affected by many factors such as the catalyst types, gas temperatures, amount of dosing, NH3 distribution, deposit accumalation.

The SCR process requires precise control of the ammonia injection rate. An insufficient injection may result in unacceptably low NOx conversions. An injection rate which is too high results in release of undesirable ammonia to the atmosphere. These ammonia emissions from SCR systems are known as ammonia slip. The ammonia slip increases at higher NH3/NOx ratios. According to the dominant SCR reaction, the stoichiometric NH3/NOx ratio in the SCR system is about 1. Ratios higher than 1 significantly increase the ammonia slip. In practice, ratios between 0.9 and 1 are used, which minimize the ammonia slip while still providing satisfactory NOx conversions. **Error! Reference source not found.** presents an example relationship between the NH3/NOx ratio, NOx conversion, temperature, and ammonia slip.

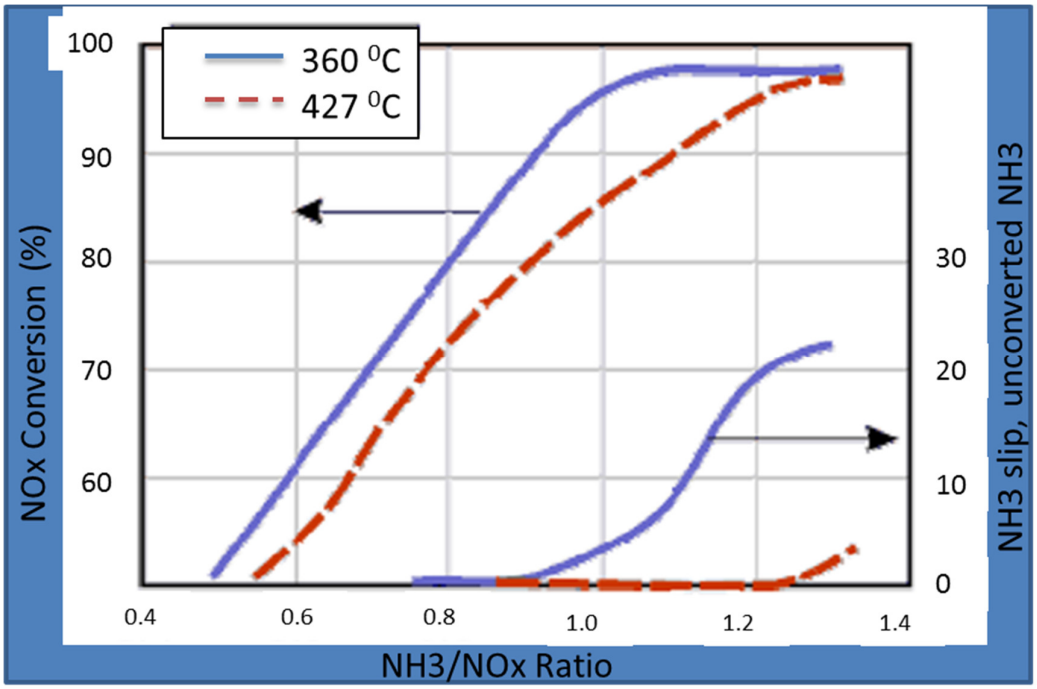

Figure 1.12. NOx Conversion and Ammonia Slip

The ammonia slip decreases with increasing temperature, while the NOx conversion in an SCR catalyst may either increase or decrease with temperature, depending on the particular temperature range and catalyst system. [10]

1.4. Motivation and Research Contributions

The aim of this work is to develop comprehensive approach to predict exhaust emission for selective catalyst reduction. The emission prediction is assesed by 1D modeling tools in GT-Power. The complex physics are modeling by 3D simulations of exhaust gas aftertreatment systems.

The CFD software calculates the conjugate heat transfer, flow field, spray modeling, species distribution and deposit modeling in the SCR systems. These results are calibrated by using the experimental data coming from the PIV, shadowgraph measurement in flow test bench and dyno test bench. The measurements are performed under a wide range of transient and steady state operating conditions. For this work flow test bench is built with compressor, burner and automation system.

Since deposit has a complex phenomogical physics for prediction, in this dissertation for deposit prediction image processing tool was developed in Matlab which uses endoscop camera images. The calculated mass of deposit from matlab was correlated with deposit studies in Flow Test Bench. In addition deposit map which is function of temperature and mass flow rate over all operating conditions was generated by using image processing tool. The map based classical method is the most widely adopted because of its simplicity and stable performance.

1D emission prediction tool is required whether the design meet the emission legistlation target. This emission prediction tool should be fast and accurate method with 3D simulation and deposit effect on the SCR system. Before freezing the design of SCR system, emission level of design should be predictable whether further design optimizations or advanced SCR technologies are required. 1D emission tool can predict to different SCR catalyst sizing, chemical kinetic effect and different aftertreatment system layout on emission level.

The objective of this work is to develop selective catalyst reduction CFD modeling with correction of the deposit map technique to focus on ammonia distribution at the SCR

inlet and to observe its influence over NOx reduction process. In the automotive exhaust gas aftertreatment applications, the reaction kinetics are strongly non-linear and often involve highly transient evolution adsorbed species, which is quite difficult to implement directly into a conventional CFD software. All processes inside the Fe-Zeolite catalyst are then simulated by the 1D the chemical surface kinetics with deposit map from 3D CFD model that play a determinant role in emission prediction of the system under steady state condition.

1.5. Dissertation Outline

In the first work of this thesis is dedicated to the development a three-dimensional CFD model was introduced to describe the multi component lagrangian spray model, heat transfer, multi component liquid film and conjugate heat transfer model inside aftertreatment system. The model for spray and velocity distribution was calibrated using the PIV system. The spray distribution inside the exhaust aftertreatment was visualized by shadowgraph technique.

Flow Lab is built with advanced test equipment for this thesis. The inline exhaust aftreatment system was calibrated in terms of temperature, flow and species in flow test bench.

The second work deposit accumulation map is generated by using 3D CFD model. 3D CFD model can predict deposit location well which is correlated in flow lab. Endoscopic deposit visualization technique can calculate the deposit mass with image processing.

The third work of the thesis proposes deposit accumulation correction map is used to correction ammonia distribution data from 3D CFD model. Detailed numerical model was then conducted to transfer the ammonia distribution and velocity distribution at front face of the catalyst for 1D modeling performance technique.

In the last work comprehensive integrated modeling models were used for each WHSC point to understand the emission prediction level. This techniques provide the emission level with this system layout and calibration.

2. LITERATURE REVIEW

This chapter includes a review of literature relevant to the selective catalyst reduction research. The review is starting from emission regulations and SCR basics. The later is also included on 3D CFD modelling technique of the selective catalyst reduction, and deposit modelling as well. Discussion is also1-D models for characterize catalyst parameters and trends. Experimental studies in particular optically accessible instruments are finialized in literature studies.

2.1. Diesel Engine NOx Emission and Regulations

Diesel exhaust gases consist of several harmful gases such as carbon oxide, nitrogen, hydrocarbons and particulate matter. Aftertreatment emission control technology are used to reduce exhaust gases specially by particulate matter and NOx. [5]

European legislations have been introduced and standards are being tightened to control NO_x. Table 2.1 reported the standards for NOx emission of heavy duty Diesel engines in European Union. [6], [33]

Table 2.1. European standards for heavy duty Diesel engines NOx emission [6]

Legistration	Date	NOx (g/kWh)
Euro I	1992	8.00
Euro II	1998	7.00
Euro III	2000	5.00
Euro IV	2005	4.00
Euro V	2008	2.00
Euro VI	2013	0.40

An emission test cycle is developed to asses the emission performance of the different engines. Emission test cycle represents the driving profile of customer in actul use for Europe, USA and China. [34] Various international governments have different test cycle for their driving profile. The basis of the test cycle was analysis of driving behaviour data about heavy-duty vehicle use for the different regions of the world.

These test cycle include a range of operating temperature, speed, and load. To asses the emission level of the engine, specific test conditions are required in the test cycle. Test cycle is more stable over the all engine range than road cycle due to various speed, load and temperature conditions. The OEM developed their emission hardware based on these test cycle. [35] In real world, the real emission level on the road is higher than the test cycle emission level.

WHTC test is based on transient engine dynamometer test cycle. The regulation of Euro 6 is based WHTC real heavy commercial vehicle use. WHTC test cycle both cold and hot requirements and hot start steady state test cycle (WHSC). WHTC test cycle were used by Euro 6 emission legistration for heavy-duty engines.

The WHTC is a transient test of 1800 s duration. Engine speed and torque values over the WHTC cycle are schematically shown in Figure 2.1.

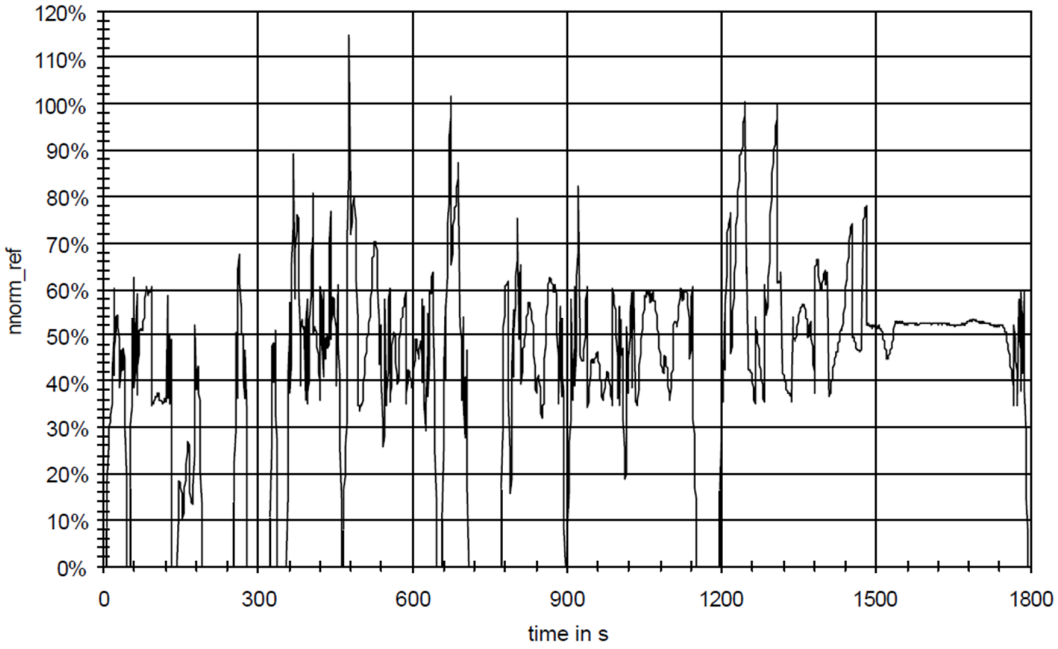

Figure 2.1. The speed pattern of the world wide reference as WHTC cycle [36]

WHSC test is a steady-state engine dynamometer schedule. The WHSC consist of 12 mode points with defined speed and torque criteria. [36] The parameters of the WHSC are listed in Table 2.2.

Table 2.2. World Harmonized Stationary Cycle (WHSC)

Mode	Speed	Load	Mode Length
-	%	%	s
1	0	0	210
2	55	100	50
3	55	25	250
4	55	70	75
5	35	100	50
6	25	25	200
7	45	70	75
8	45	25	150
9	55	50	125
10	75	100	50
11	35	50	200
12	35	25	250
13	0	0	210

Exhaust emissions regulations have traditionally been met by modifying and improving the engine technologies, specifically: combustion system, boosting system, fuel injection system, the EGR system and exhaust aftertreatment system.

2.2. SCR Aftertreatment System Control

The Selective Catalytic Reduction (SCR) was introduced state-of-the-art urea injection aftertreatment systems for reducing the NO_x emissions. Urea based SCR systems typically contains a pulse width urea injector to control the amount of urea water solution (UWS). The urea water solution is injected as a spray into the exhaust gases. The amount of UWS is controlled by urea injector based NO_x sensor and temperature sensor information into the exhaust system. These sensors are located at downstream and upstream of the catalyst. Based on the input from these sensors, the control unit adjust width of injection duration, frequency and amount of urea. The control system is most critical system to achieve efficient SCR system. [37] Urea injector with control unit called Denox was developed by Bosch and is shown in Figure 2.2. The urea injector in pumped urea from a tank.

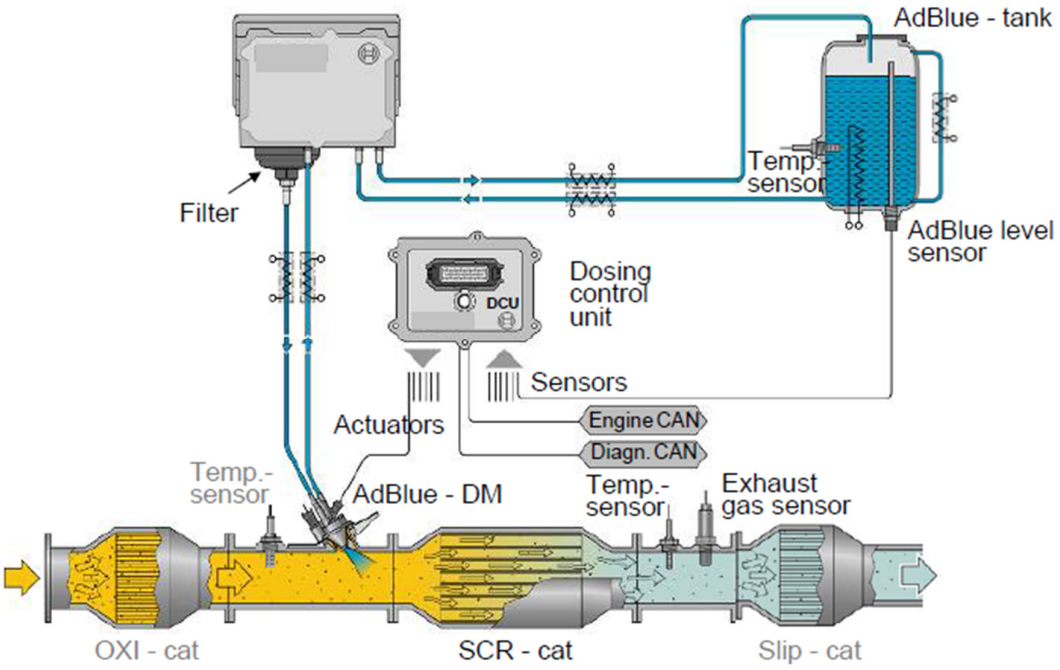

Figure 2.2. System Layout of Heavy Duty Application [13]

Dosing accurate amount of the urea injection is essential parameter for efficient SCR systems. High dosing urea result NH3 slip from the tail pipe and high conversion efficiency in SCR cataly. Low dosing urea result low NOx conversion in SCR with low NH3 slip. Ammonia slip is not easily predictable. Control of SCR is particularly difficult in an automotive application because of the highly transient conditions. To achieve the reductions required to meet emissions regulations, several SCR control system have been proposed by numerious researchers. [38] [39] [40] [41] [42]

There are many approaches for different control strategies. Most of control strategy is on feed-forward controller and they are designed as linearized SCR model for feedback controller. [39] [40] [43] [44] [45] Recent years model-based control systems have been developed for more efficient SCR catalyst with less urea consumption. [46] A 1-D SCR model was developed and validated, considering ammonia adsorption and desorption, SCR NOx reactions. The control logic used the SCR model to determine SCR surface coverage, based on engine speed, pedal position, mass air flow, inlet NOx (map or sensor) and SCR inlet pressure.

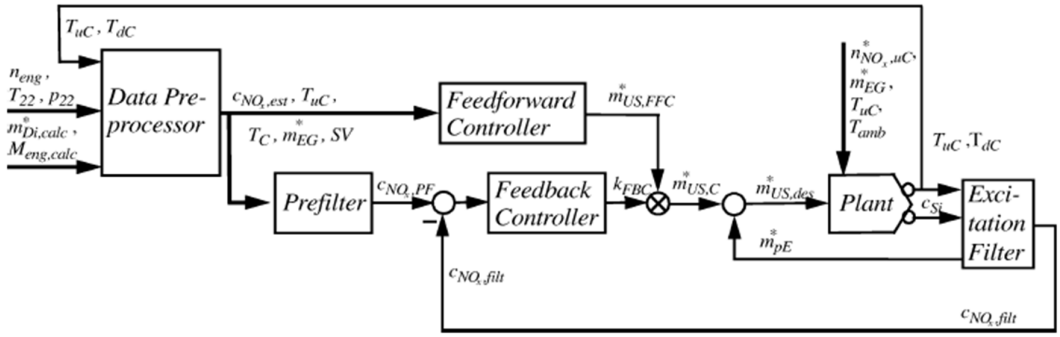

Figure 2.3. Structure of the control strategy for the SCR aftertreatment system [40]

2.3. Selective Reduction Catalyst Numerical Modelling

In order to meet emission standards, efficient exhaust aftertreatment design is required for vehicles. Urea Water Solution (UWS) is sprayed through the exhaust aftertreatment system for NOx system reduction mechanism. It is commonly believed that water evaporates first and then the NOx reducing agent ammonia is generated by a thermolysis reaction then hydrolysis reaction is occured. [47] The intensive use of numerical methods are used to develop SCR system.The precise modeling of SCR system is fundamental requirement to achieve accurate prediction. [47]

To reach efficient SCR system design fundamental requirements are uniform NH3 distribution upstream of the SCR catalyst. Flow field solution and spray distribution should be modeled accurately. Subsequently to accurate model of thermolysis and hydrolysis reactions provide mass flow of NH3 upstream. Species of reactions are transported by convective and diffusive process. So turbulence modeling provide required flow field, spray distribution and species distribution as well.

Numerious simulation was based on RANS turbulence modeling due to low computational effort. [48] [49] Reynolds stress model capture strong swirl flow effect than two-equational model. [50] The RSM can underpredict scalar transport of species. [51] LDA measurement data have good velocity field correlation againt numerical simulation of updated schmidt number for RSM modeling case. [47] For incylinder application RANS and RMS models are compared in term of mean velocity. The prediction for each models are in good agreement. For turbulence anistropic models RSM can predict accurately. Two equation RANS models have not capable to predict

strong swirl effect. [51] [52] RSM and RANS models are compared for SCR application. RSM has been found to predict turbulent kinetic energy and disspation for swirl that cause from bend pipe and mixer. RSM models predict flow field in two percent difference with twenty percent time penalty. [53]

Ammonia production from UWS contains physical and chemical processes. Water evaporates from UWS particles and solid/liquid urea decomposes into ammonia and other chemical species. There is no clear understanding about the physical state of urea during the evaporation and thermolysis processes. Surveying the literature, different physical states of urea during thermal decomposition could be found. [54] [55]But, the dominant hypothesis is that thermal decomposition of urea starts after the end of water evaporation. In this case, solid urea first melts and then decomposes into ammonia and isocyanic acid and eventually other components. [54] [56] [57] [58] [26] This is the one of the basic idea that can not model the UWS behaviour correctly. More simpliest modeling approach is to model only water as solution. [59] The other modeling approach was developed based on two component but not influnce each other. [60]

In this methodology was developed based on the partial pressure of water during the UWS decomposition. That approach was used by many researchers. [61] [57] [62] The partial pressure of water in UWS is very close to ideal assumption. Many researcher also work to model evaporation based on non linear assumption. [63] [64] [65]

Several numerical modeling approaches of thermoylsis and hydrolysis for SCR systems has recently been conducted. [66] [22] [56] [55] [67] [68] [58] [69] The evaporation and thermolysis of UWS droplets modeled urea depletion from UWS either as a vaporization process or a direct thermolysis process from molten urea to ammonia and isocyanic acid. [69] Single-step thermolysis models for urea in different physical states, suggested in the literature, are presented. Multi-step thermolysis model is proposed and validated against experimental data. Multidimensional modeling with urea injection are developed for active SCR systems. [57] 3D numerical modeling of injection are developed for urea water solution. This modeling consider spray gas interaction. [54] Thermolysis model for urea based on experimental Kimi Lundstrorm and Schaber work are developed to limit molten urea. [70]

It was shown how UWS droplets or liquid film undergo heating and water vaporization leading to high urea concentration near droplet or film surface. Dissolved urea at the droplet surface causes the vapor pressure of water to decrease which consequently decreases the evaporation rate of water in UWS compared to the pure water. [71] [72] In the same time, urea decomposes through thermolysis.

Rapid Mixing model (RM model) is developed to evaluate the influence of dissolved urea on the evaporation of water. [54] In the RM model, infinite high transport coefficients are assumed for the liquid phase, resulting in spatial uniform temperature, concentration and fluid properties in the droplet, with the temporal change in quantities. [71] [73] [74] Multi component evaporation model developed that takes into account a modified Stephan velocity and enthalpy diffusion of gaseous species to compute the evaporation rate. [63]

2.4. SCR Deposit Modelling

Deposit is major modelling issue to achieve comprehensive SCR modelling technique. Due to complex deposit physics very detailed understanding of deposit mechanism is required to improve CFD models. Deposit modelling involves heat and mass transfer models, accurate spray behaviour,flow field distribution and complex chemical reactions. Various models have been proposed for fuels. These models are adapted for the UWS deposit. [75], [76]

Deposit is built by droplet impingement. It is characterised by a different interaction regimes. A schematic overview can be found in Figure 2.4.

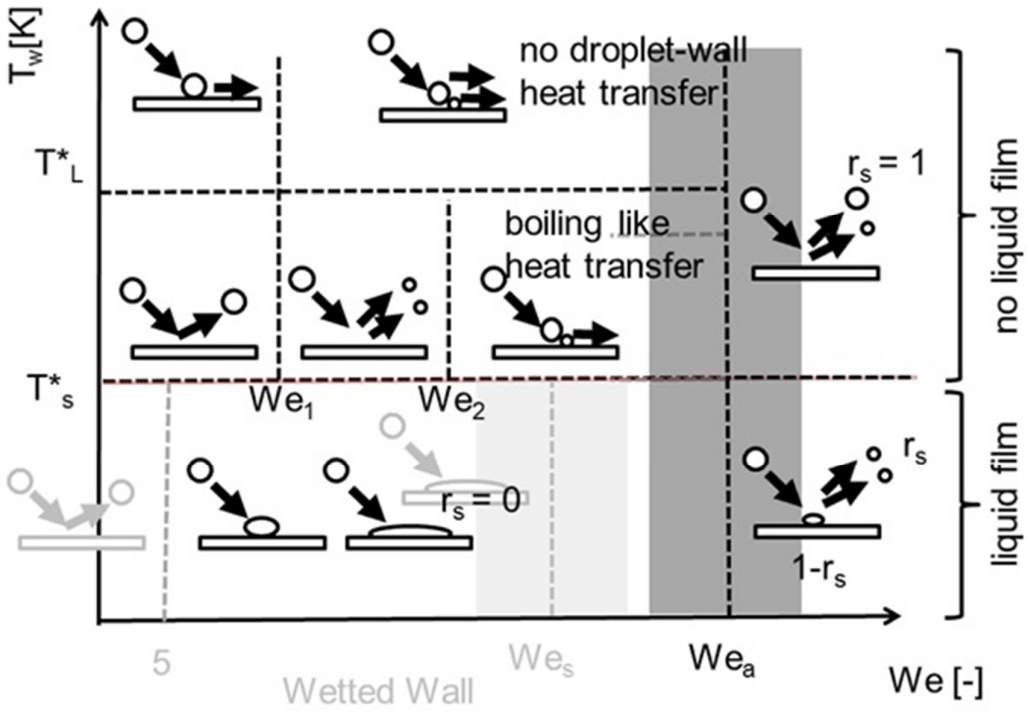

Figure 2.4. Schematic overview of different droplet impact regimes

The chemical complexity of the deposits that form in the active SCR system is due to the incomplete thermal decomposition of urea to NH3 at low exhaust temperature. NH3 generates by thermal decomposition of urea generates with below reactions. [77]

$$N_2H_4CO \rightarrow NH_3 \uparrow + HNCO \uparrow \quad (2.1)$$

$$HNCO + H_2O \rightarrow NH_3 \uparrow + CO_2 \uparrow \quad (2.2)$$

First reaction is decomposition step which urea converts to ammonia and isocyanic acid. [28] Then second reaction isocyanic acid reacts with water and converted to ammonia and carbon dioxide. The urea deposits are formed due to poor evaporation of urea. The isocyanic acid reacts with urea and forms biuret (N_2H_4CO), cyanuric (CYA), ammelide, ammeline and melamine in Figure 2.5.

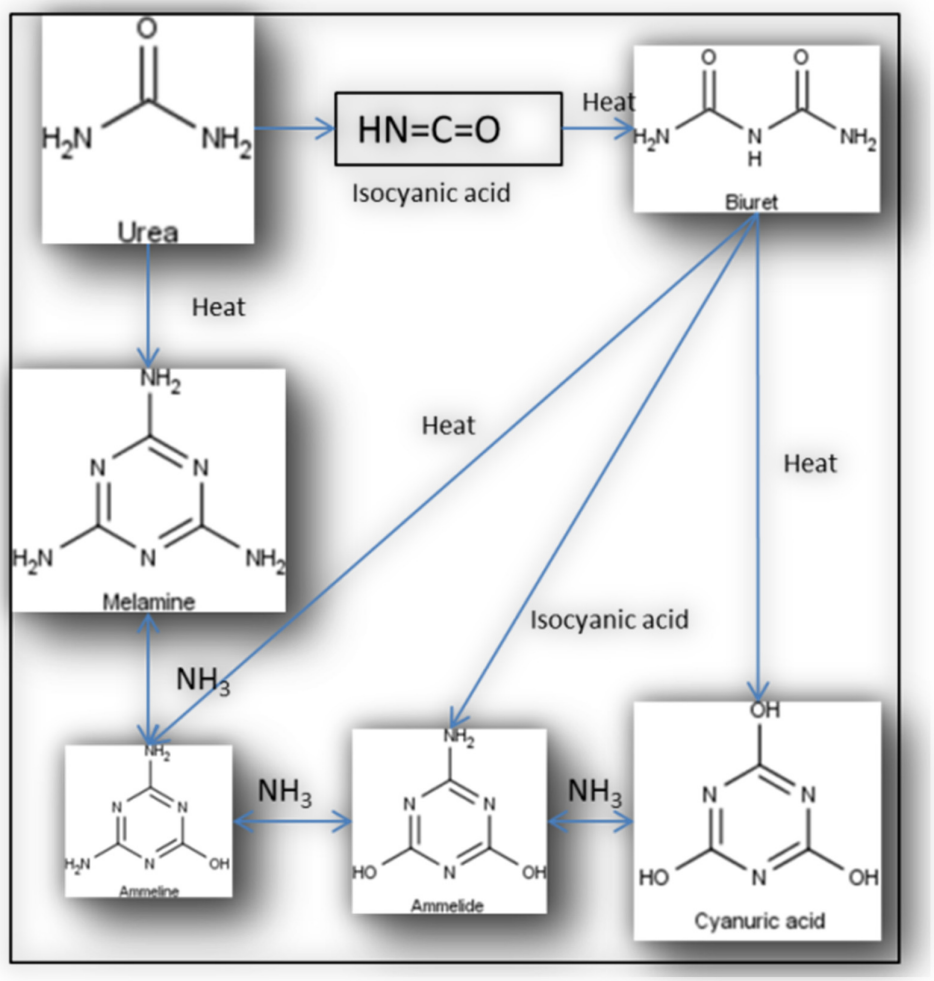

Figure 2.5. Side reaction of deposit

These chemical reactions contribute to deposit formation due to exhaust temperatures being lower than 300°C, which yield several undesirable products such as biuret ((H2NCO)2NH), cyanuric (CYA) acid ((HNCO)3), ammelide, ammeline, and melamine. [78] [28]. These reaction processes have been studied in the past and the main reactions are listed in the following. [43]

$$N_2H_4CO + HNCO \rightarrow (H_2NCO)_2NH \quad (2.3)$$

$$N_2H_4CONH + HNCO \rightarrow CYAacid + NH_3 \quad (2.4)$$

$$N_2H_4CONH + HNCO \rightarrow ammelide + H_2O \quad (2.5)$$

$$ammelide + NH_3 \rightarrow ammeline + H_2O \quad (2.6)$$

$$ammelide + NH_3 \rightarrow mela\min e + H_2O \quad (2.7)$$

The non-decomposed urea and deposit forms in crystal are left inside the exhaust system. If the urea dosing rate is given as a function of engine conditions, the insufficiency in ammonia generation and supply to the SCR catalyst may induce lower NOx reduction efficiency and an increase in operating cost from oversupply of urea. [79] [80] Higher NOx conversion can be achieved with high dosing rate but its result is ammonia slip and deposit accumulation. This tradeoff critical parameters should be considered.

Accumulation of the corrosive deposits on the walls of the exhaust pipes and catalysis surfaces create concerns for material deterioration and backpressure. In particular, the deposits were found to degrade the performance and the structural properties of both vanadia and zeolite based catalysis [29] [81] [82]. In some situations, the deposit can even block the pipe flow cross-section, causing engine to lose power.

The formation mechanism of urea deposits is complicated. In essence, urea deposit is an outcome of multiple influential factors including: (1) thermal and fluid transport; (2) system mixing structure design; (3) urea dosing strategy / NOx reduction targets; (5) engine features and measures in emission technical direction.

2.5. SCR Experimental Studies

There are a number of different type experimental works in literature for urea-water-solution decomposition and ammonia generation mechanism to better understand phenological physics of active urea-SCR system.

The first type of experimental work is laser-camera, high speed camera and shadowgraph testing to understand spray and flow field distribution, deposit accumulation charachteristics. [83] [84]

The second type experiments are urea-water-decomposition which is occured when spray is injected through hot exhaust system. The decomposition products such as isocyanic acid, ammonia, residence time has been studied. [85] [66] The decomposition processes of urea and deposits are experimentad and investigated with thermal gravimetric analysis (TGA) and fourier transform infrared spectroscopy (FTIR). [78]

The deposits of SCR systems by lab urea dripping test, and studied the impact of temperature on the urea-related deposits using TGA, FTIR and X-ray diffraction.

Detailed model of the evaporation and the thermal decomposition of UWS are developed to simulate the decomposition processes of urea. [63] The mechanisms of deposits formation on mixer blade surface are investigated by optical experiment and numerical study. [50] [86]

The third one is analyze the phenological mechanism of deposit, incompleted decomposition mechanism. This investigations were done in test bench or simple reactors. [43] [87] [88] [89] The thermolysis of urea under flow reactor conditions using a differential scanning calorimeter (DSC) and Fourier transformed infrared spectroscopy (FT-IR) have detailed studied. [87] Two different experiments were investigated. In the first one, they administered urea solution in a cordierite monolith and they recorded the concentration of ammonia and iso-cyanic acid. In the second experiment, a vertically suspended silica cup was loaded with small granular pellets of solid urea. In their work, they have shown that depending on the way the sample is administered, (cup or monolith), different behaviors in the gas were observed. The cup experiment showed higher gas phase concentration of reactants due to lower mass transfer rates as compared to the monolith. The production of by-products like biuret and Cyanuric acid (CYA) is also observed in their experiments. The thermal decomposition of urea and related compounds with thermogravimetric analysis (TGA) and differential scanning calorimetry (DSC) measurements have been studied, together with evolved gas analysis (EGA). [90] Thermal decomposition have been published using simultaneous TGA, DTA and mass spectroscopy (MS). [91] These studies focus on the decomposition of urea under purge gas conditions. In these reports, tracking of residue species and accounting for the production of solid by-products like ammeline and ammelide and accompanying synthetic details were not included. The thermal decomposition of urea are investigated under open reaction vessel conditions by thermogravimetric analysis (TGA), high performance liquid chromatography (HPLC), Fourier transform-infrared (FT-IR) and an ammonium ion-selective electrode (ISE). [43] Evolved gases and urea were analyzed and profiles of substances obtained from different reactions of urea thermolysis (i.e. biuret, cyanuric acid (CYA), ammelide, ammeline and melamine) versus temperature were given. In their work, major reaction

intermediates are identified and production of biuret, cyanuric acid, ammelide, ammeline and melamine as a function of temperature were investigated. They also showed that in the thermolysis process, to complete a reaction, the temperature should be high sufficient.

3. METHODOLOGY

The understanding of the physical and chemical phenomena of the urea-water-solution will provide detailed knowledge of the SCR process. Thus the development of more compact SCR systems of new generation aftertreatment systems will be assesed with new control strategies. The generation and distribution prediction of NH_3 from urea decomposition is a main step for the SCR simulation process. All steps of chemical reactions and spray of UWS are modeled to predict NH_3 upstream of SCR.

Three main chemical reaction steps are occured after the spray is injected through the exhaust aftertreatment system. The first step is the water evaporation step. In the inline exhaust aftertreatment configuration, water evaporation takes times so evaporation widely dependent to the length of the SCR process. Evaporation of UWS spray is thus a step that deserves a particular attention to numerical modelling. [92]

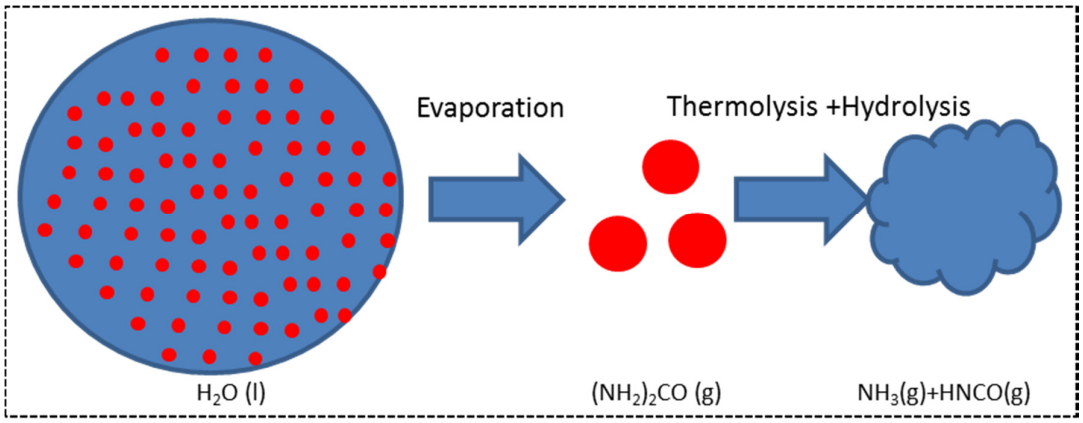

Figure 3.1. Multicomponent Evaporation model

Thermolysis and hydrolysis steps are modeled to convert urea to ammonia. The arrhenius coefficient of these reactions are taken from simple experimental validation cases from literature.

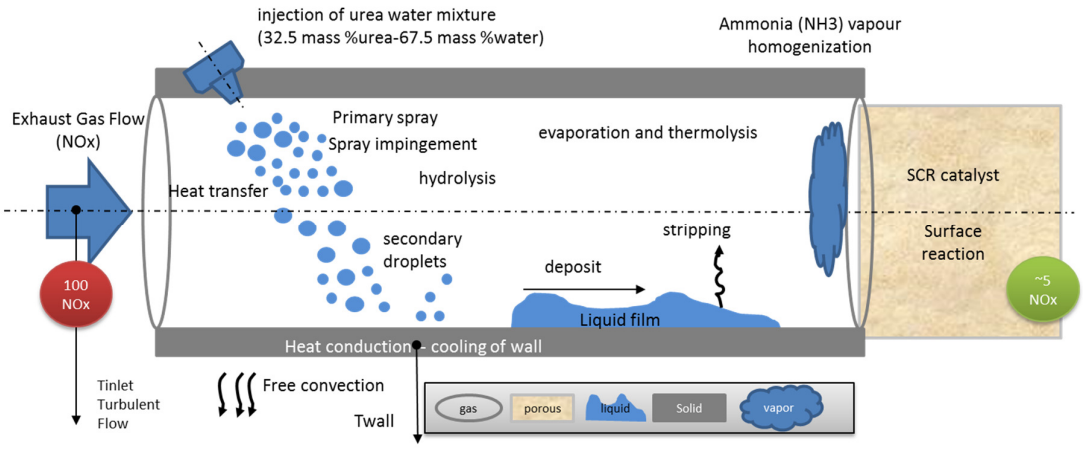

Figure 3.2. CFD Model of the SCR modelling

The numerical model of the SCR system consists of flow field, spray and spray/flow interaction modeling with turbulence effect. The flow field modeling one of the crucial step to accurate prediction of main flow behavior. Different turbulence modelings were experimented as k-e turblunce model and Reynolds Stress Modeling. Due to computational time penalty LES modeling was not considered.

The urea vapor modeling, thermolysis and hydrolysis modeling step have been validated by comparing CFD calculation and experimental result from literature. In SCR system spray wall interaction is expected in exhaust wall. The complex deposit modeling was included the CFD model with validated result from literature. For the accurate deposit modeling conjugate heat transfer modeling was conducted from spray to wall. This whole models yields conversion to ammonia. Figure 3.2 shows the all physics that are modeled in current numerical simulations.

There are mainly two approaches to the assess the performance of the Selective Catalyst Reduction such as experimental measurement and numerical simulation. They are both limited capabilities to perform efficienct SCR system design nowadays. Experimental measurement is high cost, time consuming method due to building a flow rig or setting up an engine test bench. Experimental method could not obtain all phenomenological and complex models behind the physics. Uncertanities and errors associated the measurement techniqes could not explore all the physics. Many configurations should be

build to investigate various controlled parameters that affect selective reduction catalyst performance. Therefore numerical modeling approach is highly desireable. Computational Fluid Dynamics modeling provides much more predictive information about complex physics but it is impossible generated confident results without experimental studies. Because numerical model should be validated especially for models of complex physics such as spray and deposit modeling.

To design efficient selective catalyst reduction system to meet emission legistrations, CFD simulations with experimental validation and advanced testings arerequired for complex physics. Due to the above considerations both experimental and numerical approaches were used in this study. Figure 3.3 represent the flow chart of the methodology. This flow chart represent the combination of experimental and numerical approaches to capture all physics that enhance the numerical modelling capability.

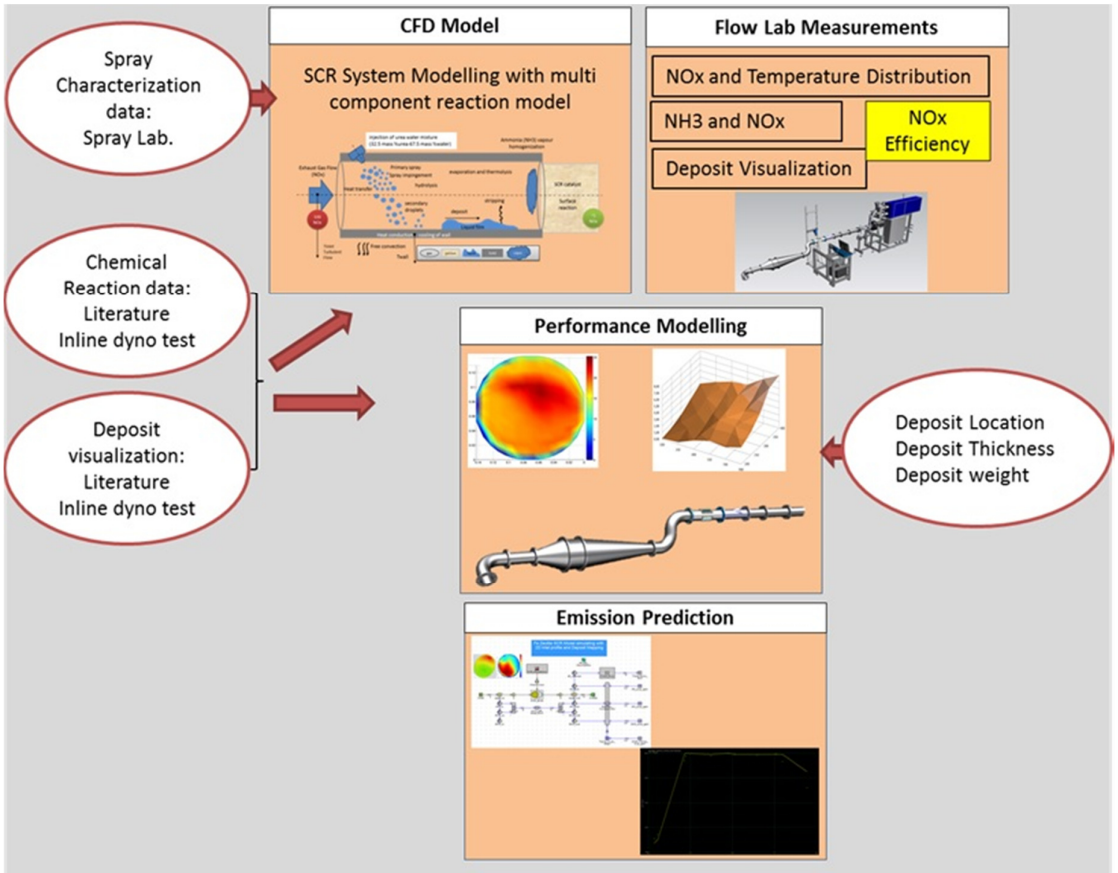

Figure 3.3. Flow Chart of Work

The first phase of the work is numerical spray validation. This is one of the initial steps in performing CFD simulation. The work starts with description of numerical spray validation process, challenges and the different steps involved in the process. A brief overview of the spray measurement techniques which is PIV measurement technique.

This is followed by a section on the tuning the chemical reaction rate of two step reaction which are hydrolysis and thermolysis. Experimental work from chemical reaction tuning setup is introduced to validate studies with representing applications. Experimental setup validation consists two chapter. First one is validate temperature of the wall and gas, velocity vector and spray validation, second is chemical reaction rate. Following work is deposit validation case from literature.

The third work is built numerical modelling of exhaust aftertreatment system at flow lab with tuned parameters from previous simulation. This numerical modelling built with models such as validated flow field, validated spray parameters, heat transfer, chemical reaction and deposit. The deposit modelling should enhanced due to complex phyiscs.

To predict accurate deposit modelling numerical modelling and experimental modelling should combined. Numerical modelling predicts the location of the deposit in good correlation. Deposit is built from droplet wall interaction. It is expected to occur in real exhaust gas systems, the derived approach includes application of a sophisticated droplet wall interaction model. Deposit modeling is not not capable model to account accurate deposit prediction. The thickness and mass of deposits should be calculated by experimental setup. The visualization of endoscope camera system with developed image processing tool are generated deposit map for the exhaust aftertreatment system. The maps from image processing tool enhance deposit modeling capabilies of the system.

The last one is 1 D modelling approach with 2D SCR upstream ammonia distribution with corrected deposit map in GTPower to asses the SCR catalyst performance accuately.

3.1. Simple Validation Cases

Saturation pressure, latent heat of vaporization and specific heat are required parameters to model evaporation process accurately. In this study values of these parameters depend on the temperature are taken from literature. These values are implemented into the Star-CCM and the UWS properties are internally calculated by scripts based these parameters. Saturation pressure is calculated from antonie equation. The Antoine equation for saturation pressure is based Psat/Patm.

$$\log_n\left(\frac{P_{sat}}{P_{atm}}\right) = A - \frac{B}{T + C} \quad (3.1)$$

where Patm is 1 bar, T is temperature (K), n is the base of the logarithm, and A, B and C are equation coefficients. [93] Latent heat of vaporization is calculated by the Clausius-Clapeyron. This method uses the Clapeyron equation with the assumption of ideal gas equation of state for the vapor. It is related the latent heat of vaporization to the saturation pressure.

$$L = \frac{RT^2}{P_{sat}} . \frac{dP_{sat}}{dT} \quad \textbf{(3.2)}$$

the need for dPsat/dT which limits the choice of compatible methods for Psat. The ideal gas constant implies that the Molecular Weight material property must be supplied. [94]

3.1.1. Validation of the Chemical Reaction Rate

UWS (Urea-water-solution) is injected through the exhaust aftertreatment system. [93] The generation of ammonia into the exhaust gases proceeds in three steps. [66]. First step is water form by the evaporation of the UWS droplets.

$$N_2H_4CO(UWSsolution) \rightarrow N_2H_4CO(liquid) + H_2O(g) \quad (3.3)$$

The second step is ammonia and iso-cyanic acid generation. They are produced after thermolysis reaction.

$$N_2H_4CO(UWSsolution) \rightarrow NH_3 + HNCO(g) \quad (3.4)$$

Ammonia are produced after hydrolysis of isocyanic acid,

$$HNCO(g) + H_2O \rightarrow NH_3 + CO_2 \quad (3.5)$$

The evaporation, thermolysis and hydrolysis reactions are crucial reaction models to predict accurate conversion of NOx. To evaluate the arrhenius parameters of thermolysis and hydrolysis reaction, simple CFD model is built in Star-CCM based on experimental results from UWS to ammonia. [66] 6 holes urea injector is used for simple pipe exhaust system. The gas temperatures are varied from 573 K to 623 K and velocity of exhaust system are varied from 6 m/s to 10.8 m/s. The results are samplied several point that are 3m, 4.5 m and 6 m far from downstream of injector. Rosin-Rammler distribution is defined for droplets.

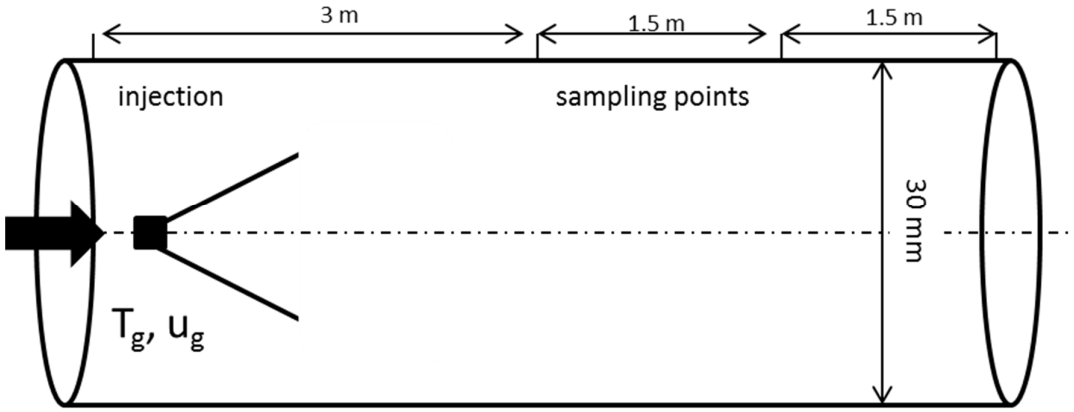

Figure 3.4. Sketch of the experimental setup [66]

Two step reactions are modeled based on arrhenius type reaction rate. The thermolysis and hyrolysis reaction are modeled. The coefficient of the arrhenius reaction are validated againt this simple model results. The CFD model predicts results of species are presented in Figure 3.5.

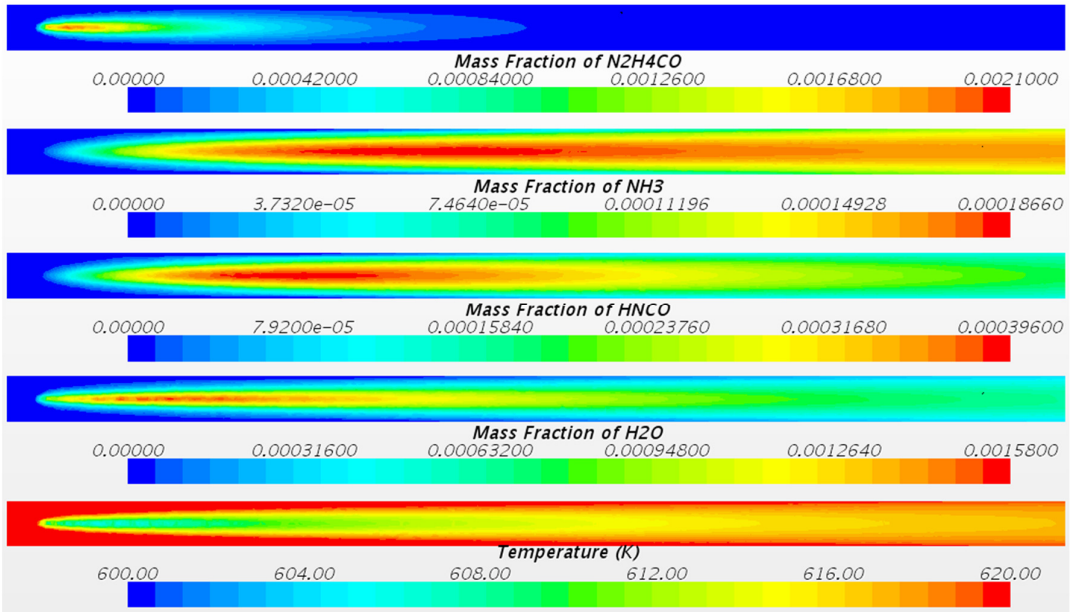

Figure 3.5. Numerical results of species and temperature in exhaust system

The CFD results are compared with experimental results.The conversion of NH3 and HNCO is a result from thermolysis and hydrolysis of urea-water solution. The thermal decomposition results same amount of both gaseous products at the 573 temperature as seen in **Figure 3.6**. In this literature work single step reaction modeled as thermohydrolysis reaction to correlate this simple exhaust aftertreatment system. This approach is not capable to predict iso-cyanic acid. Iso-cyanic acid is key parameters for deposit modelling. Without iso-cyanic acid deposit accumulation could not predict well. With tuning arrhenius reaction rate, one step chemical reaction modeling techniques are correlated with test results. The simulations are also validated well with experimental results at 623 K. With lower temperature prediction is occured underestimates but higher temperature it is correlated well. Beacuse higher temperature thermolysis becomes dominant effect for NH3 conversion.

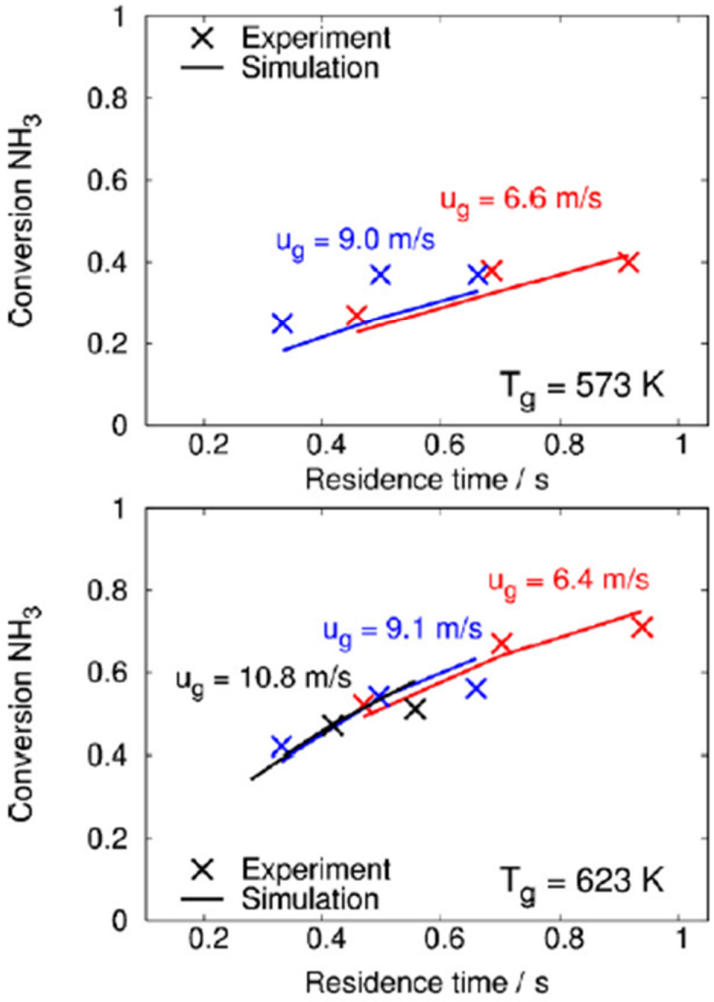

Figure 3.6. Calculated conversion to NH3 for different gas velocities [66]

Figure 3.7 shows the calculated conversion to NH3 and HNCO at different gas temperature with differnt time. The residence times provide HNCO conversion at high temperature.The conversion rate of HNCO and NH3 in time is decreased with residence time. Evaporation and thermolysis becomes slow due to large droplets.

High temperature results show more dominant effect of the conversion of the HNCO and NH3. The conversion rate is increased with temperature due to thermolysis effect. The kinetic parameters for the thermolsis and hydrolsis has been validated by comparing numerical CFD simulations with experimental data. The results are agree sufficiently. These values are implemented to Star-CCM for further calculations.

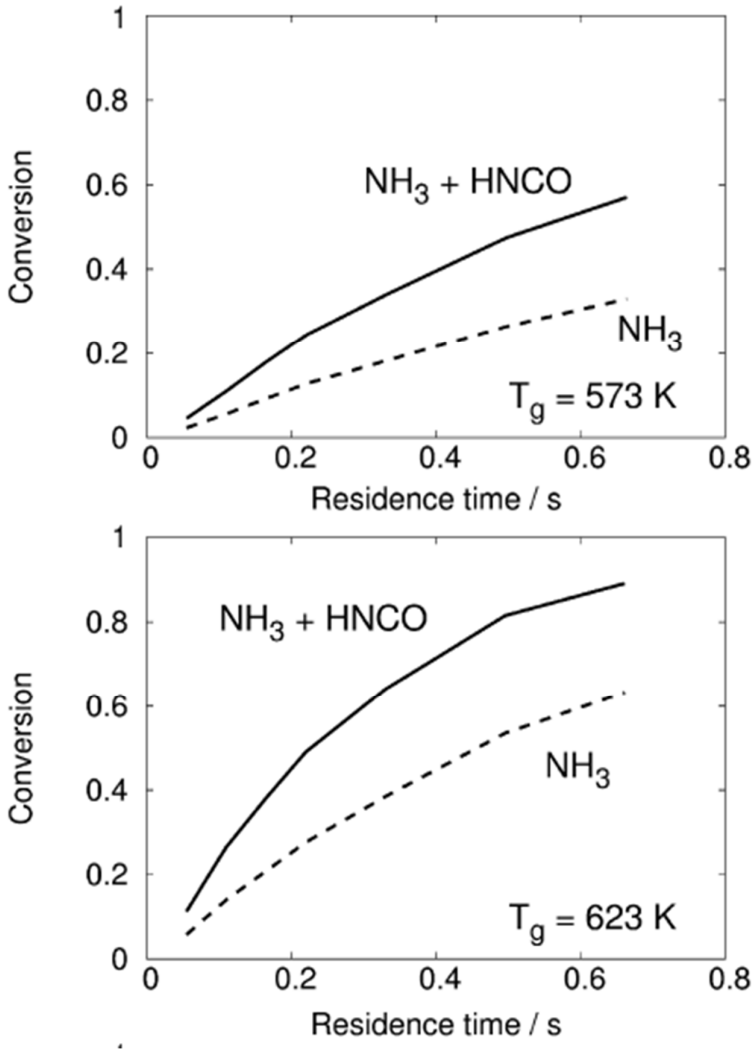

Figure 3.7. Predicted conversion to NH3 at different gas temperatures. [66]

During this work different chemical reaction approach was experimented such as one equation model againt two equation model. This approach consist of thermohydrolysis chemical reaction modeling with tune the arrhenius coefficient.

$$N_2H_4CO(UWSsolution) + H_2O \rightarrow NH_3 + CO_2 \quad (3.6)$$

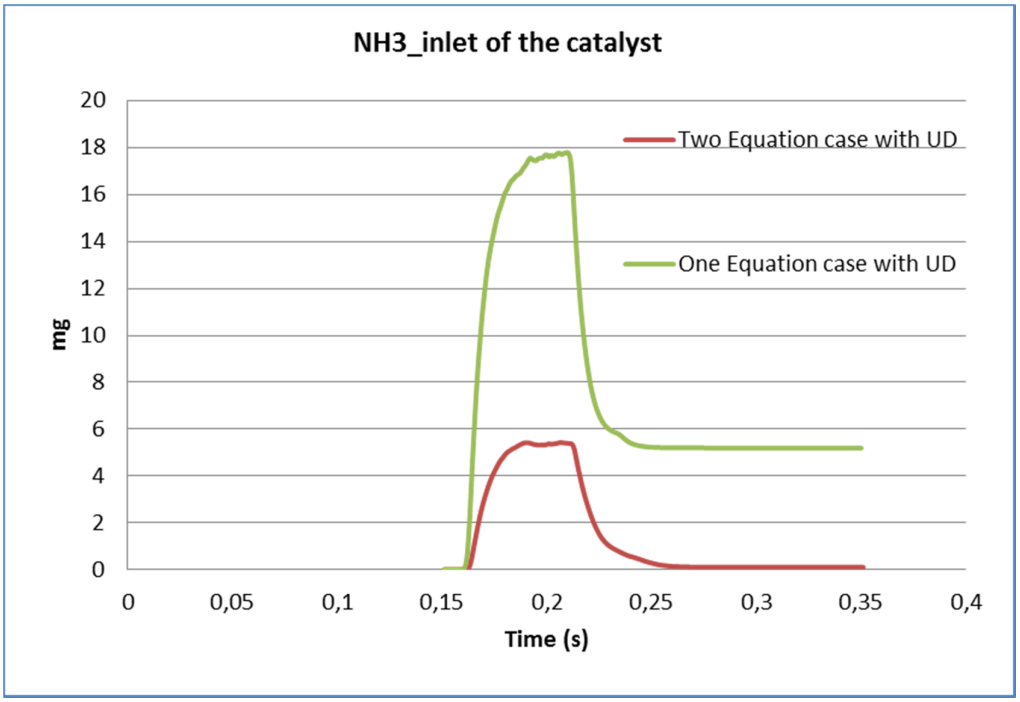

Figure 3.8. Chemical approach effect on NH3 distribution

One equation model was over predicted as %400 according to two equation model. The arrhenius reaction rate could not correlated to tune NH3 values. By modifying arrhernius reaction rate this values can be tuned with experimental data but it would not be physical values.

3.1.2. Deposit Modelling

To understand the complex physics of deposit which is occured during the spray/wall interaction and wall film formation, many numerical models are developed. The deposit is occured due to many parameters combined effects such as velocity of the droplet, droplet diameter, flow fluid charachteristics as swirl, wall temperature and wall film height. The Kuhke model consider deposit phenomena into four regimes as deposition, splash, rebound and thermal breakup which is based on two parameters. [94]

$$K = \frac{(\rho D) d^{3/4} u_d^{5/4}}{\sigma^{1/2} \mu^{1/4}} = C\alpha^{5/4} L\alpha^{3/4} \quad (3.7)$$

$$T^* = \frac{T_w}{T_{sat}} \quad (3.8)$$

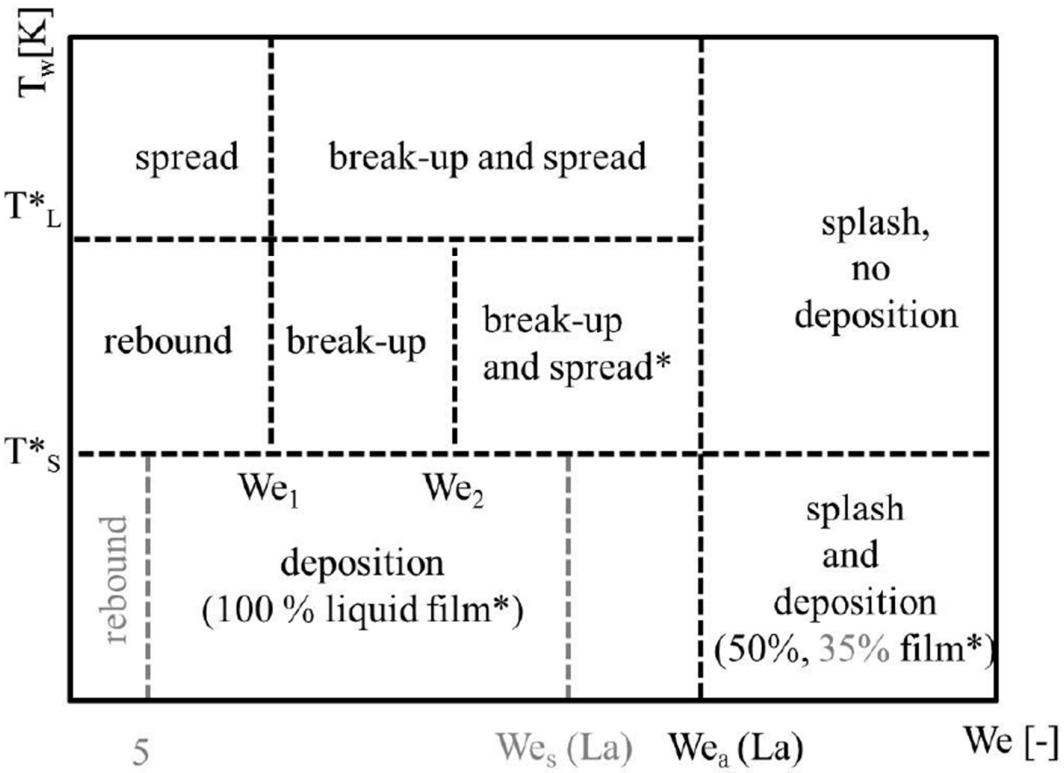

Figure 3.9. Regime map for spray/wall-interaction [76]

Figure 3.10 represent the spray distribution on the wall and spray characteristics such as splash, rebound and fluid film. Spray can breakup before it hits the wall due to flow interactions. The small droplets can evaporate fastly.

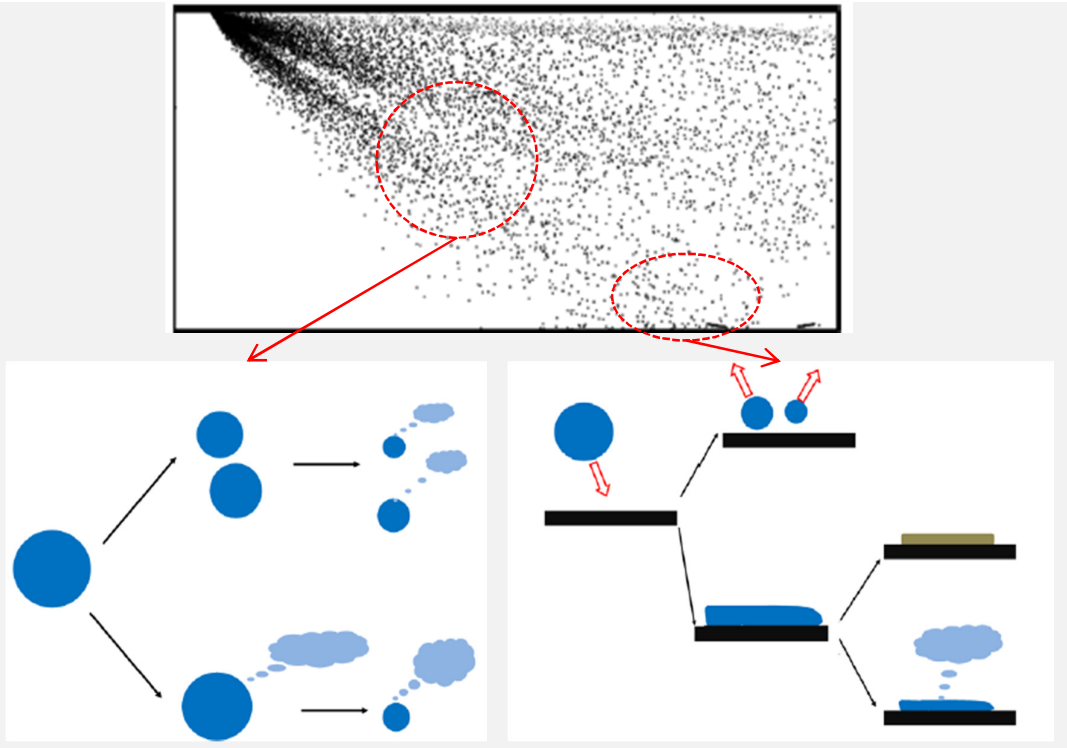

Figure 3.10. Droplet Behaviour in gas phase and on wall

The spray/wall interaction and deposit accumulation are investigated in glass window installed pipe. [54] A metal plate is installed in the center of the pipe for deposit visualization in Figure 3.11.

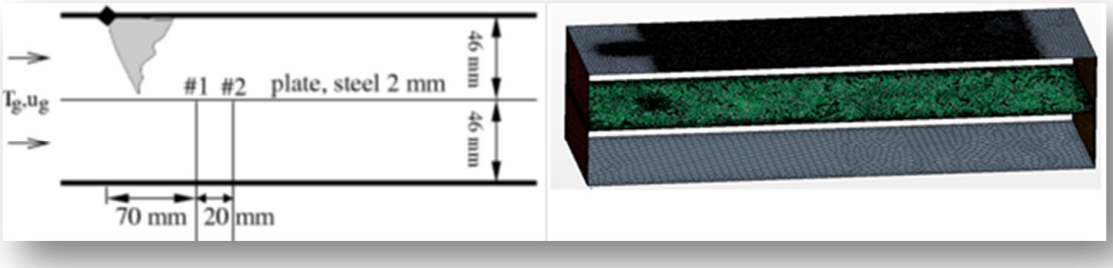

Figure 3.11. Sketch of the experimental setup for spray/wall interaction.

Figure 3.12 shows a side view of the predicted spray penetration at different times. The model predicts small droplets due to thermal breakup.

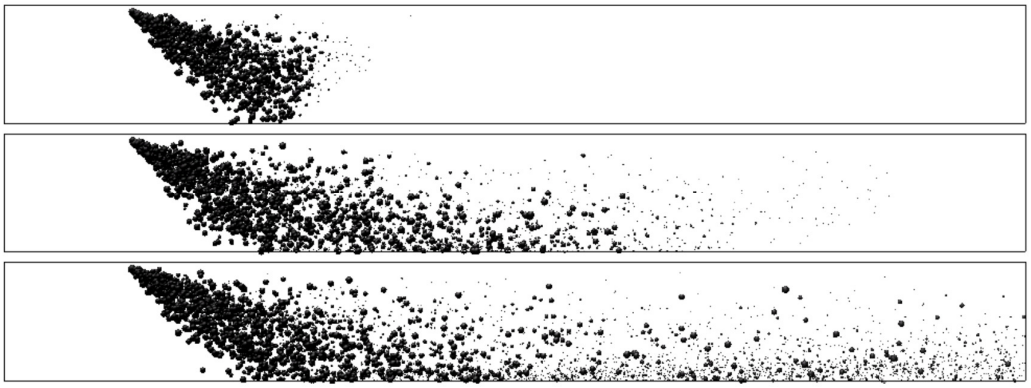

Figure 3.12. Spray pattern at 4 ms, 10ms and 20ms

Figure 3.13 shows numerical result of defined geometry in Star-CCM. The results are compareble with test result.

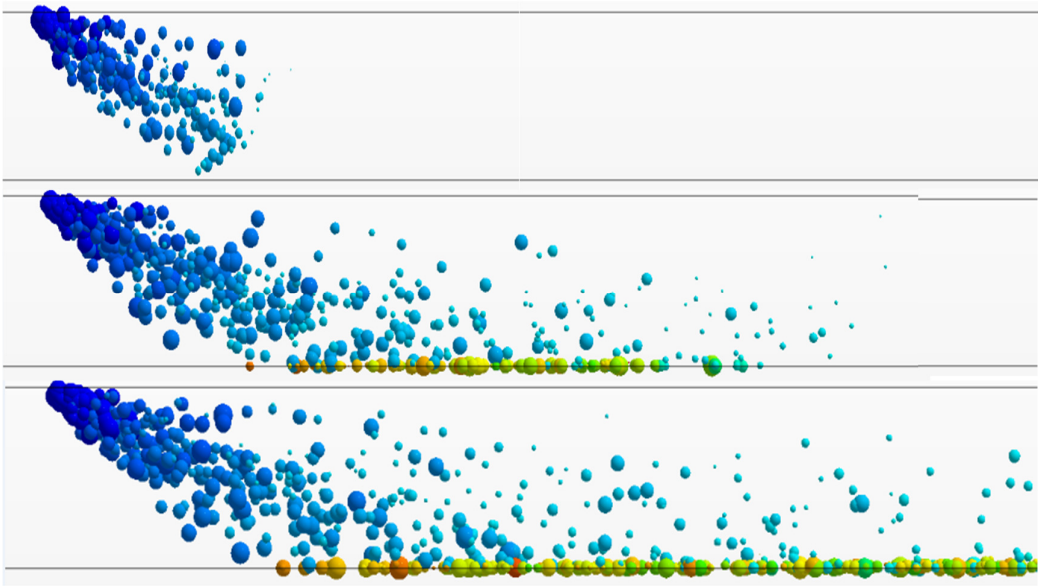

Figure 3.13. Spray pattern of numerical models at 4 ms, 10ms and 20ms

The predicted wall film thickness in Figure 3.14 reflects spray character with the film thickness in the spray impact region. This wall film characteristics are in good correlation with visual observations during the experiment.

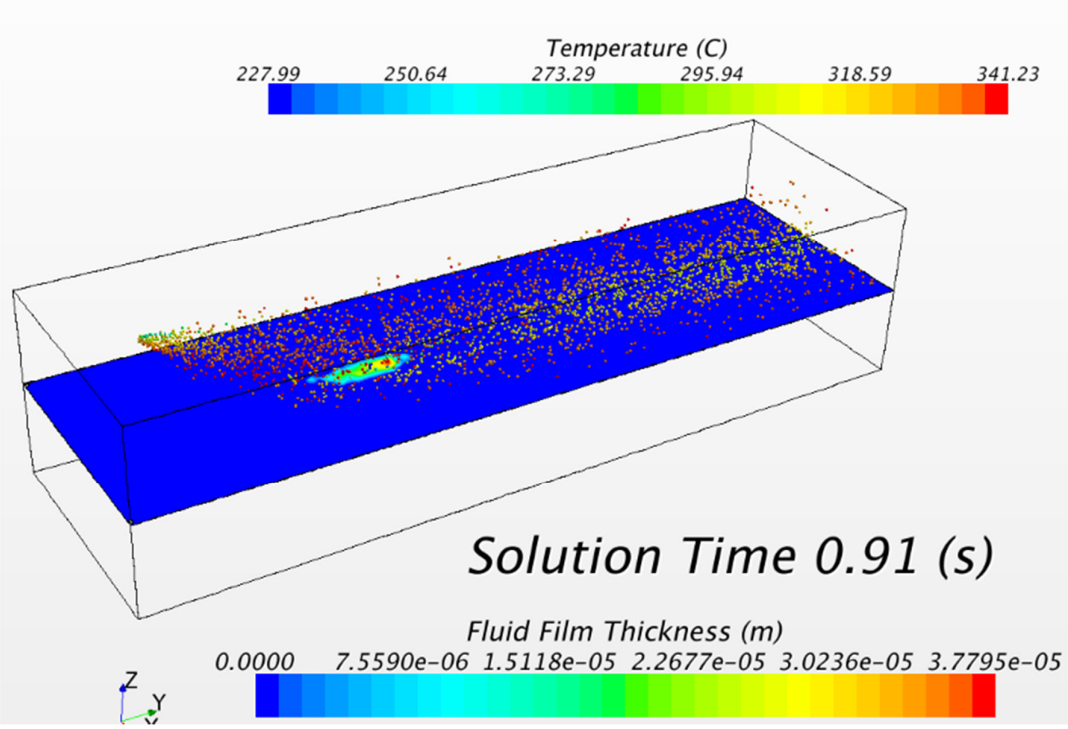

Figure 3.14. Predicted wall film thickness with spray distribution

Figure 3.15 shows the urea concentration in the wall film. In the spray impac region, the urea concentration is occured by the urea fraction of the droplets. Due to evaporation of water from the droplets concentration of urea increased significantly. As the wall film is moved to the downstream with small droplet impingement, higher urea concentrations are occured due to the evaporation of water. After evaporation of water is completed, thermolysis of urea begins in these regions. Thermoylsis reactions become dominat for NH3 conversion.

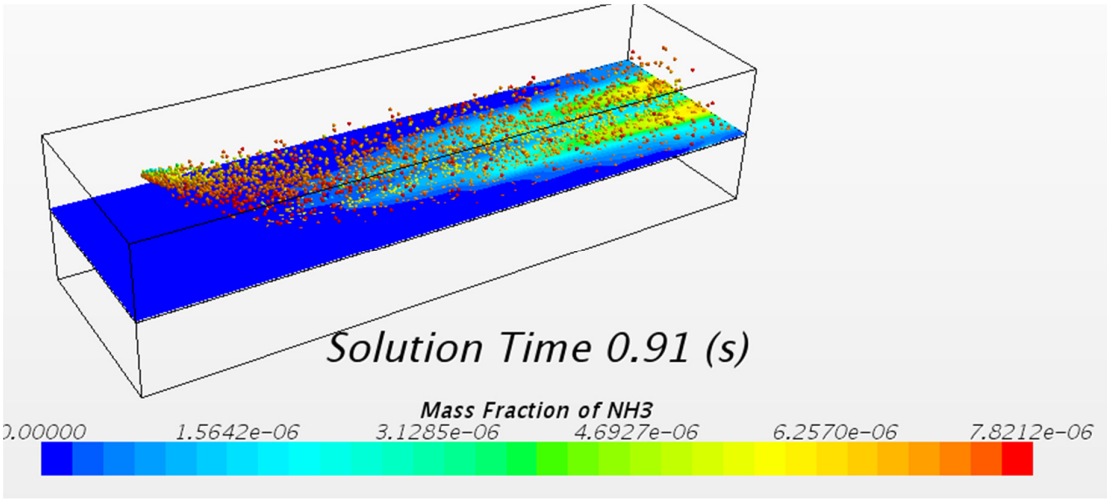

Figure 3.15. Calculated mass fraction of urea in the wall.

Figure 3.16 present views of the ammonia at the the center of the model. In the center of the model ammonia is produced significantly higher thant the the other parts of the model. The main reasion behind of this results is to thermolysis reaction of small droplets. Ammonia generation can be observed by urea decomposition from the boundaries of the models. Small droplets leads the evaporation and faster thermolysis so on the surface more NH3 conversion can be observed.

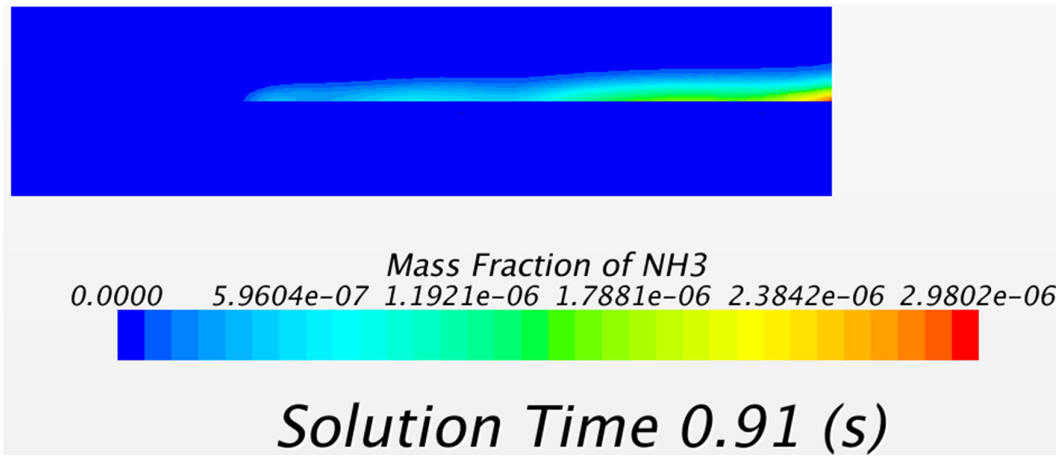

Figure 3.16. Calculated mass fraction urea at plane lateral

3.2. Experimental Setup

3.2.1. Spray droplet measurement

The most commonly used experimental techniques for spray characterization of urea injectors are Phase Doppler Particle Analyzer and Particulate Image Velocity (PIV). Phase Doppler Analyzer are not available for this work . PIV was used to examine spray characterization such as cone angle, spray range, spray distribution, drop size and velocity data of spray across the laser sheet area. Many works were conducted to measure sauter mean diameter (SMD) of the droplets by using shadowgraph technique with long distance miscroscope.

PIV is an application of the laser sheet technique. A laser sheet is double pulsed laser sheet in very short time interval.. The laser sheet is pulsed twice and illustrated region can be captured by a CCD camera. These technique based on the lagrangian approach. The positions of the particles are tracked for the calculations. The first laser sheet illustrate the initial positions of these droplets and these frozen images are captured by camera. Then droplets are advanced and the second image of the camera is exposed to the light scattered by the particles from the second laser pulse. Hence two images are collected, the first images shows the first position of the particles and the second picture shows advanced position. The velocity vector is calculated by measuring the particle displacement in the certain time.

PIV technique can also used with several exposed frames strategy, each particle is moved in several times to different locations on the same picture. Where PIV performs an average of the velocity field vector, autocorrelation or cross-correlation functions were post processed between two images. This technique has the advantage, is not biased by the gradient, since the individual particles are tracked individually to get velocity vector.

Phase-Doppler particle anemometry is a well established technique for spray droplet particles. This technique provide information of velocity and size of spherical particles. PDPA is based on the principle of light scattering. Two laser beams are pulsed into same area to measure frequency of the particles which is proportional to the velocity of the particle. The phase shift observed by two different detectors is

proportional to the size of the particle. By this technique velocity vector and particle size can be calculated. The correct emplacement of the system is guaranteed by a three-axis, computer-controlled positioning device whose z and y axes are respectively collinear with the flow direction and the PDPA emitter, whereas the x axis points towards the PDPA receiver. In this work PDPA was not used.

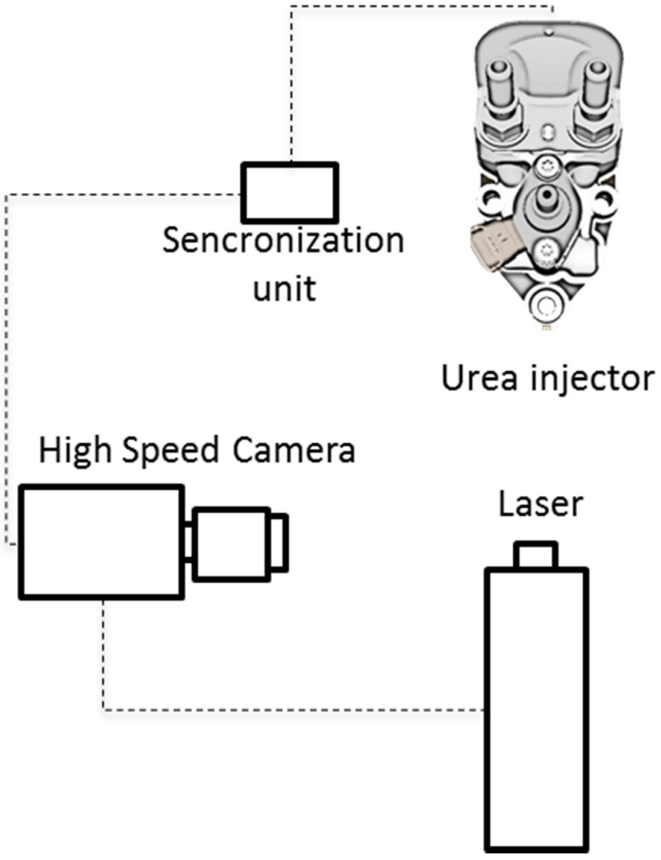

Figure 3.17. Components of the PIV setup

The sencronization unit are developed for laser, camera and injection module sencronization.

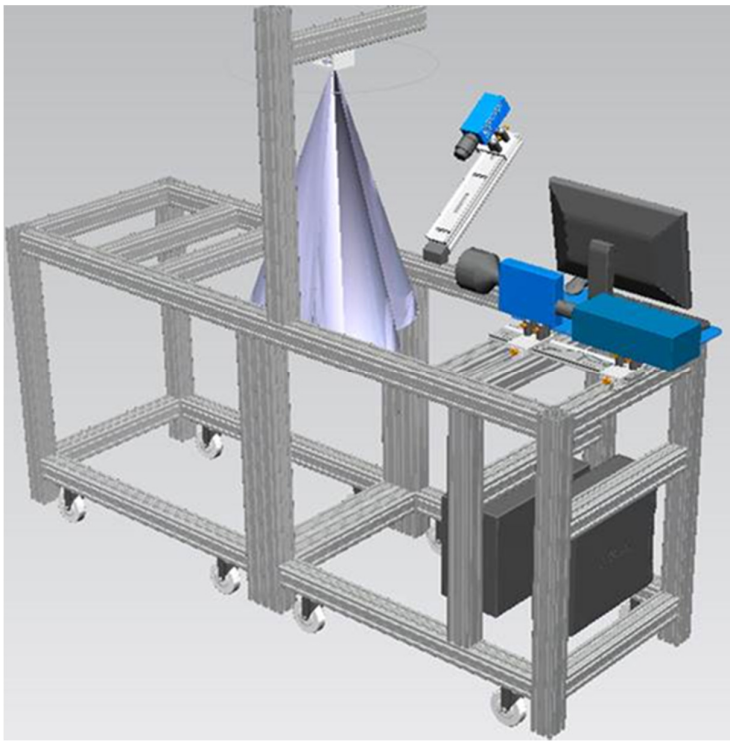

Figure 3.18. Describes a simple schematic of PIVfor spray diameter distribution

As shown in Figure 3.20, in experimental spray calibration process, droplet distribution is measured 50 mm below of the injector tip through spray. This data is then proceded to calculate the SMD, velocity data over the beam.

The spray angle are measured by the intersection of the two outside edges of the spray at the nozzle, was determined to be 33° for the three-hole injector in Figure 3.19.

There is injection to injection variation due to injector pumps. The spray cone angle is varied from 33° to 48°. To eliminate this noise factor, many measurement was done and average data was extracted for the post processing. Then the spray angle was determined 33°.

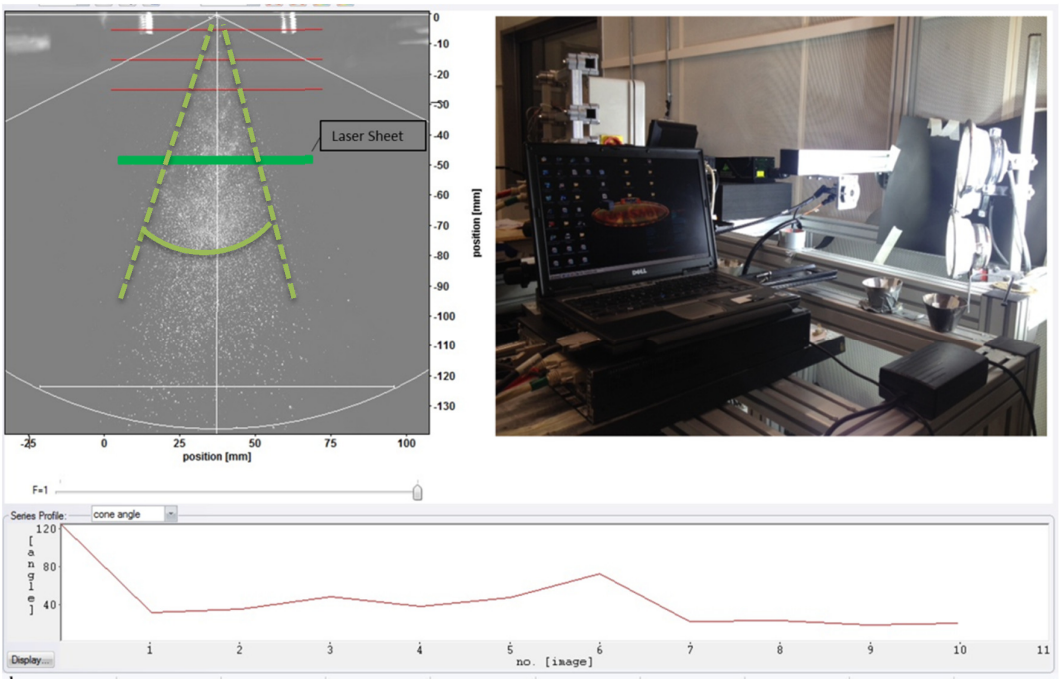

Figure 3.19. Spray Angle Measurement

After sampling many instantaneous images, an average spray particle diameter distribution is determined in Figure 3.20.

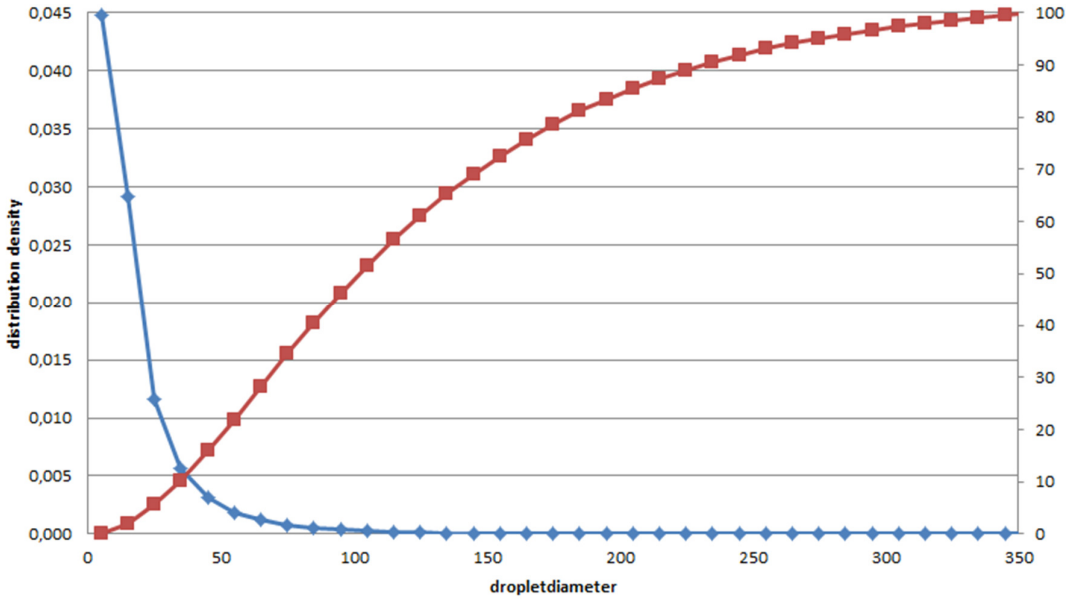

Figure 3.20. Droplet diameter distribution

The spray distribution through the spray nozzle was captured with high speed camera. The each nozzle was not discharge same amount of urea. The injector

problem was detected. New injector based on correct specification was ordered and

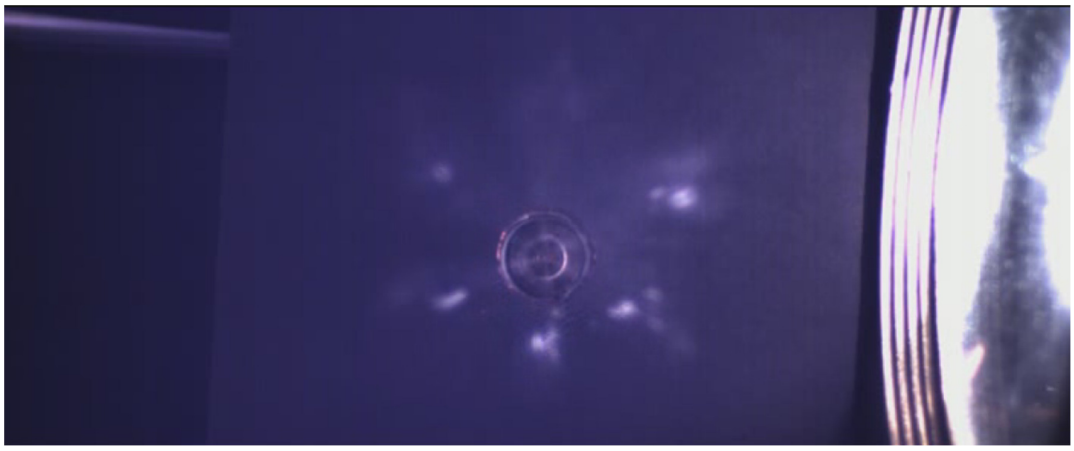

used in this work.

Figure 3.21. Spray behaviour through the nozzle

To tune spray parameters in Star-CCM model with experimental test result, the computational domain is built as cylindrical region with dimensions 90mm diameter, 115 mm height with three-hole injector at the top center, directed in axial direction in Figure 3.22.

A cylindrical chamber mesh is used to representing the calibration chamber (also known as Glass Bomb). Local refinement is applied to the tips of the nozzle to improve resolution. Boundaries are set to pressure boundary. Because the size of the domain is sufficient large, there is no evidence to show that droplets have passed through the pressure boundary. Since the test is usually carried out with the injector pointing toward to the ground, the gravity should be set to the same direction.

Air in the cylindrical domain was modeled as ideal gas. Standard k- ε model was employed. Energy equation was not solved. All the walls of the cylindrical domain were modeled with free slip condition. The flow was assumed to be stagnant to begin. This section describes the modelling approach based on StarCCM+.

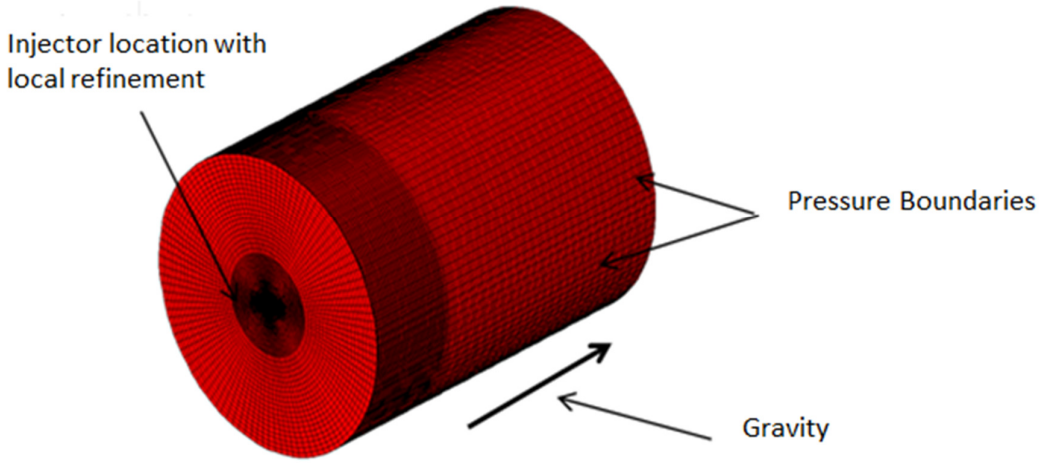

Figure 3.22. Shows the computational grid

High-speed shadowgraphy images of the one spray injection in ambient conditions highlight the its structures. The three-hole injector produced three distinct jets of fluid with long breakup lengths. Three-hole injector could not produce uniform distribution of spray across its cross-section. The atomisation of spray from the injector was seen to be consistent across the duration of each dosing event. Only injection starting internal time the spray oscillation was observed. 200mg/s, 500 mg/s and 1000 mg/s were experimented and dosing rate effect can not be observed.

Experimental data on lateral plane is compared with numerical data on corresponding plane to arrive to better empirical model constants in Figure 3.23.

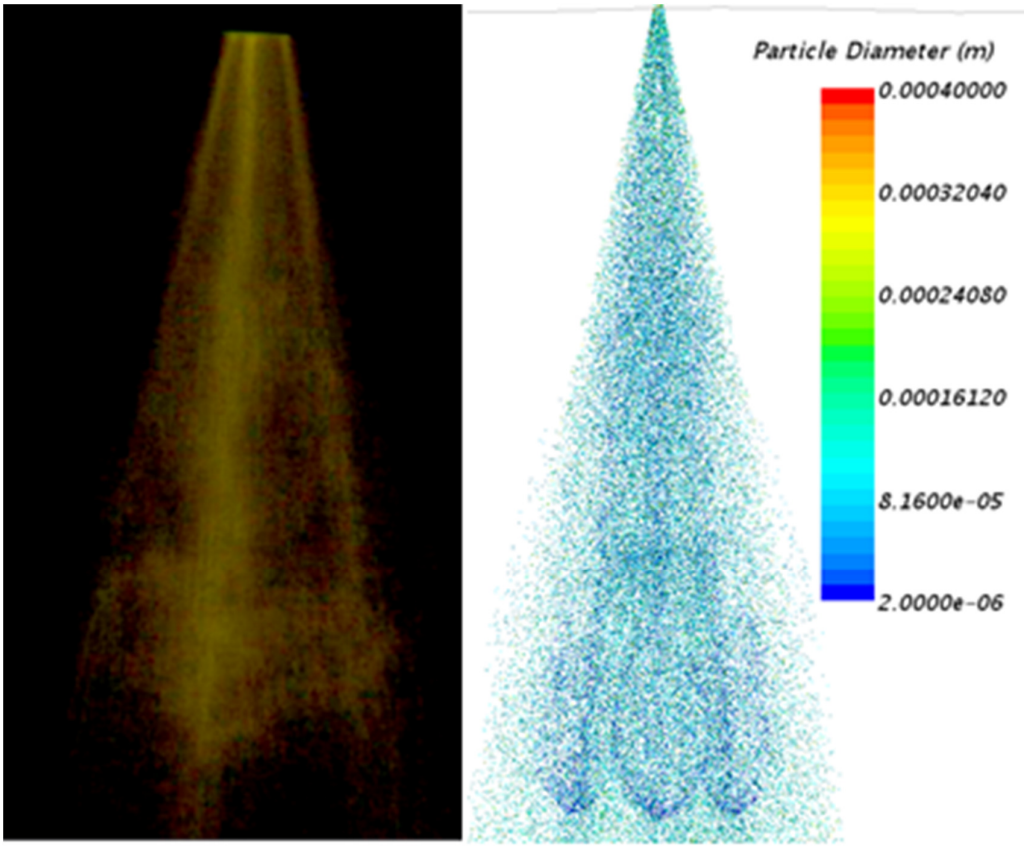

Figure 3.23. Comparision of high speed camera and CFD results for spray angle

Figure 3.24. shows some representative results from computational fluid dynamic model. Droplet diameter was be extracted using the CFD and compared with that results of the PIV test. The correlation seems well with experimental result. The droplet diameter tabulated data was extracted to use in further Star-CCM calculation.

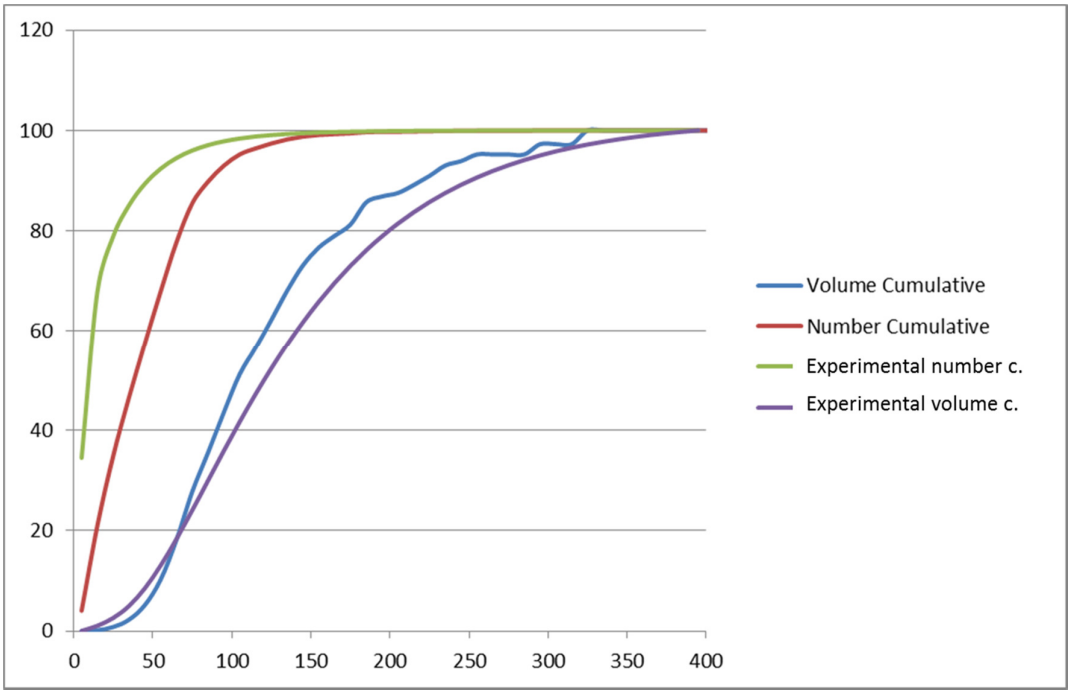

Figure 3.24. Computational Fluid Dynamis Result for droplet diameter

3.2.2. Flow rig development

The hot gas test rig is natural gas burner-based system which is developed for aftertreatment performance assesment. This system provides exhaust flow, temperature, NO_x concentration within the heavy duty vehicle operating condition.

The system can operate air mass flow rate and temperature up to 2500 kg/h and 1200 ^{0}C respectively. The external air is drawn into the system by the compressor, passes through the flow meter and burn with natural gas. At the end of the burner the flow enters the test section, which simulates the real exhaust conditions and serves to analyse the behaviour of the urea-water spray.

The flow rig test components are in Table 3.1. Each components are selected and designed for aftertreatment application. In Figure 3.25 present the flow test bench without exhaust aftertreatment system installation.

Table 3.1. List of flow test bench components

1	Compressed Air Line
2	Natural Gas Line
3	Heat Exchanger
4	Data Logger
5	Test Speciment Inlet
6	Electronic Control
7	Burner Unit

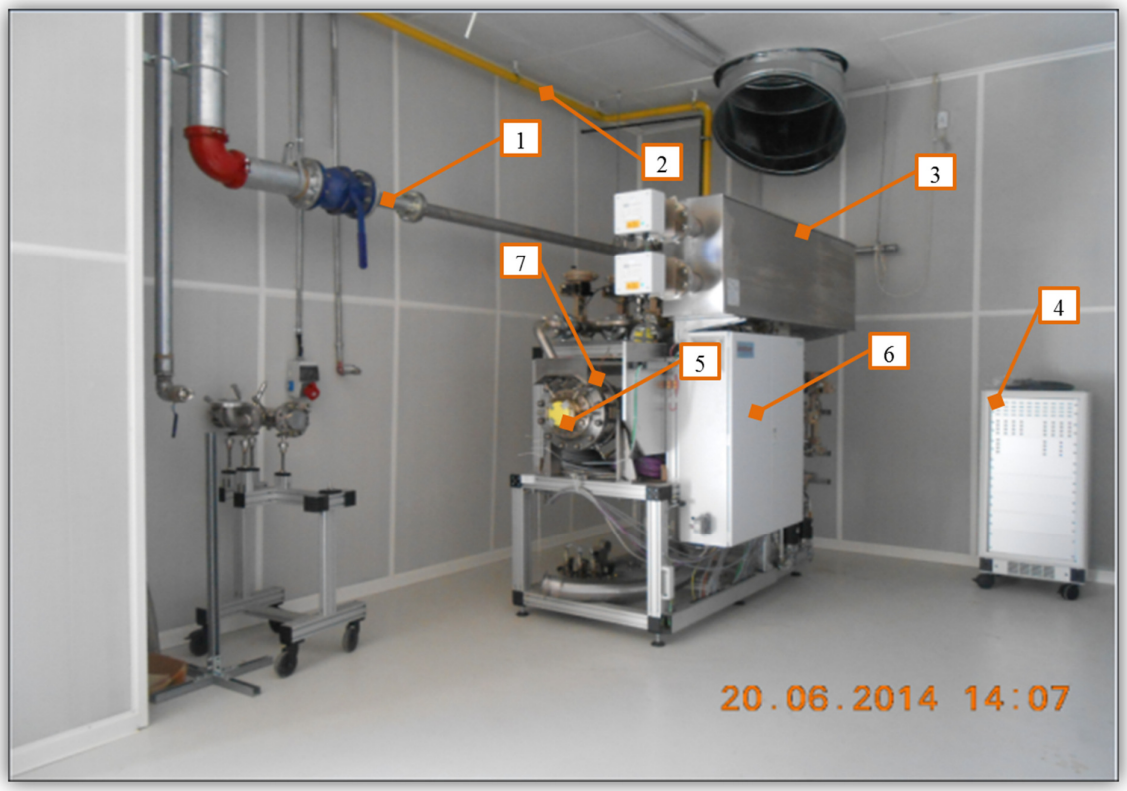

Figure 3.25. Flow Test Bench

The flow test bench consists of a natural fired burner with high flow dilution system for temperature control, dosing system for NO_x control, urea dosing system and finally the test catalyst section. The total flow and temperature in the exhaust is a function of the mass flow rate of the dilution system and the burner.

Natural gas burner is NO_x free concentration system. NO_x from engine concentrations are relatively high. There are several method to increase NO_x level for exhaust aftertreatment system SCR catalyst. The traditional method would be to inject gaseous NO_x into the exhaust from an external storage container in

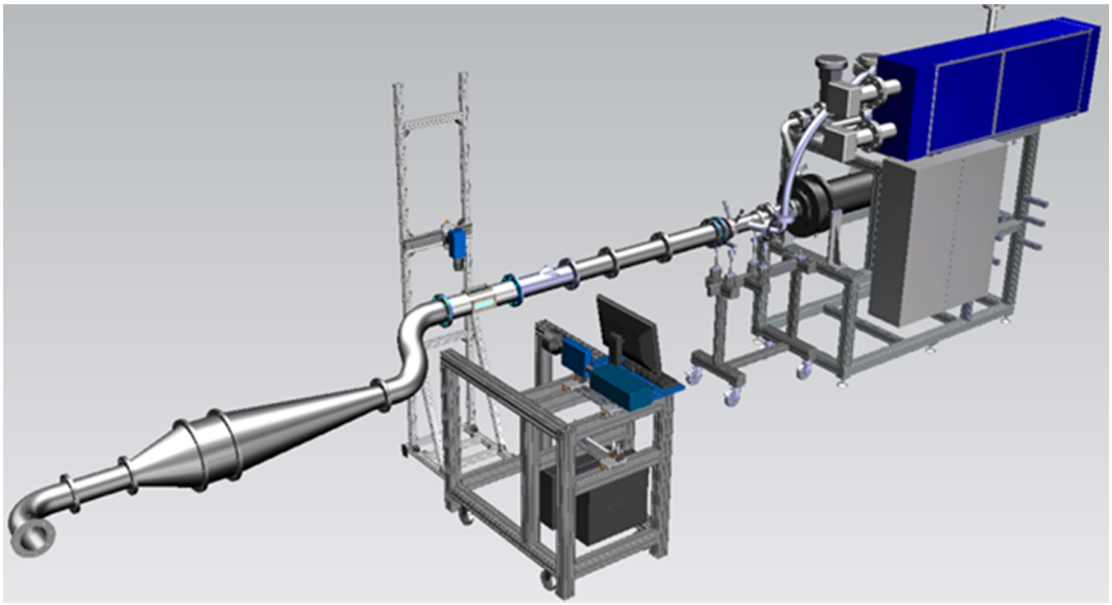

Figure **3.26**. NH_3 dosing is controlled from ECU which integrated to the burner automation system. The exhaust system of the burner was configured to heavy duty engine, a Bosch 2.2 (for injecting UWS) and a mixing tube for mixing upstream of a baseline SCR. The burner rig used a 1500 PPM range NOx sensor and controller to provide feedback for dosing control.

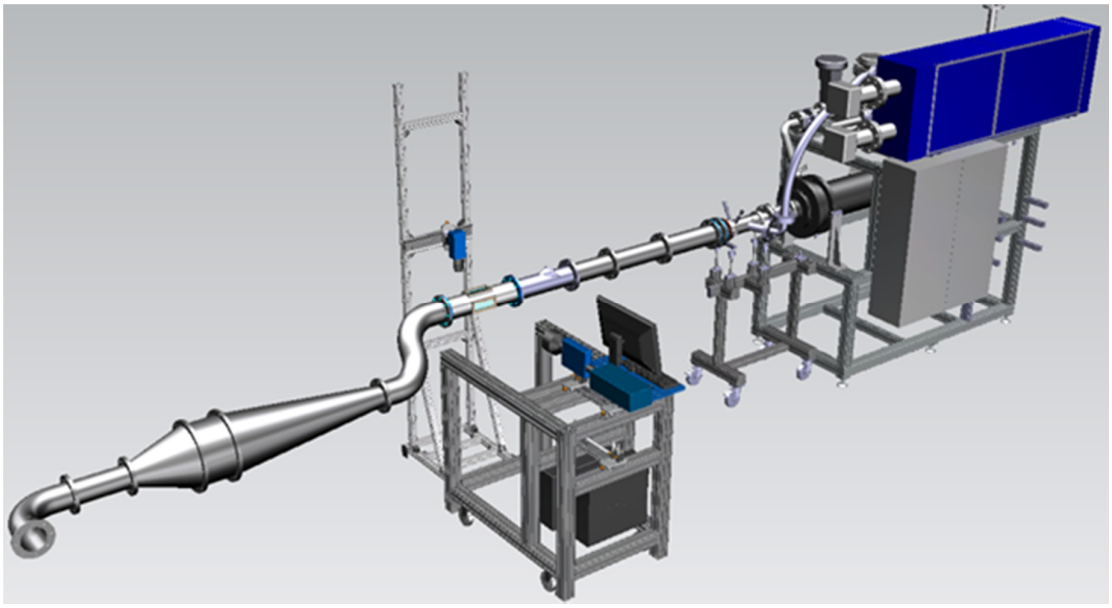

Figure 3.26. Schematic of Exhaust System Layout with Emission

The flow lab was designed to provide independent control of exhaust flow and temperature. The system control range was intended to simulate the flow and temperature from heavy-duty engine, but to also offer elevated temperatures compared to engines. Figure 3.27 shows the flow and temperature operating range of the system compared to a 12 L heavy duty engine.

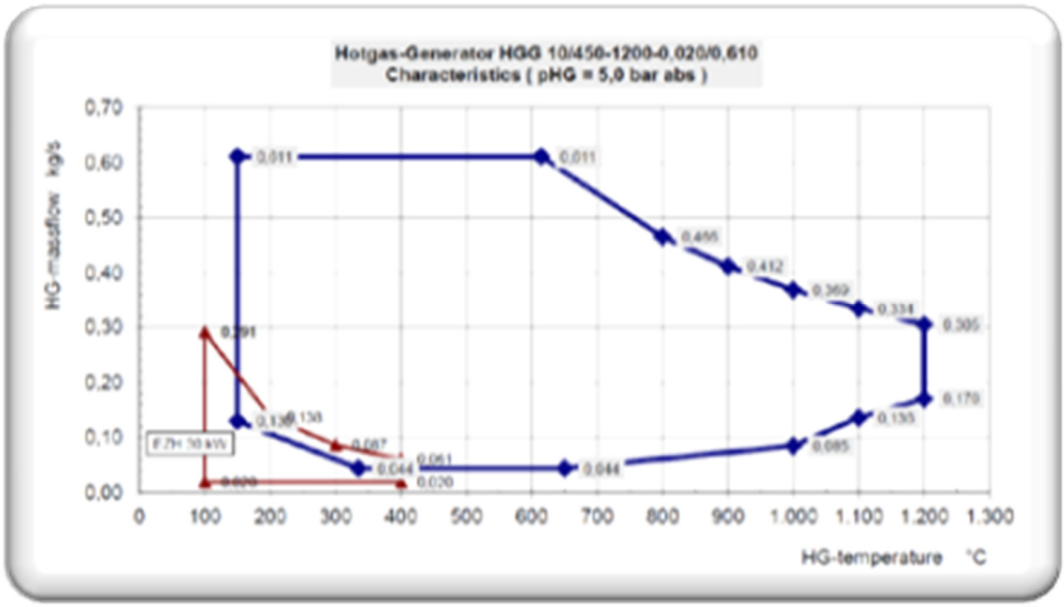

Figure 3.27. Operating condition of burner

The emissions (NO, NO2, N2O, NH3, CO and CO2) were measured at the upstream and downstream of the SCR with a FTIR analyzer. For calculation and data analysis, the raw gas NOx data (measured upstream of the SCR) and the FTIR data (measured downstream of the SCR) were used.Gas and surface temperature data were measured with K type thermocouples.

Both the flow lab and the urea injector are controlled by separate control units but they have been configured in such a way that the SCR control ECU can 'talk' to the engine ECU. This allows the exhaust temperature to be varied while maintaining the exhaust gas flow rate and urea dosing rate constant.

The test setup for examining the exhaust aftreatreatment inline system was required to peform steady emission level. WHSC cycle simulation is required to approve emission legistration. This system can be run as WHSC cycle.

3.2.3. Imaging techniques and testing methodology

In this study, UWS injection and evaporation were investigated in hot and cold air stream in transparent glass duct in flow test bench. Through different working conditions where air mass flow rate, temperature and injection rate varied, promising optical techniques were used to extracted information for velocity vector, flow streamlines through the glass window and the formation of deposit on the system was recorded when the system running on glass window.

The test section is the component where the analysis of the spray takes place. Its layout can be easily reconfigured to simulate different arrangements of the exhaust pipe. Figure 3.28 present the configuration used in the experiments was composed of an S-shaped pipe and an approximately cylindrical optically-accessible section. The urea-water injector is located upstream of the optical-accessible section and is coaxial with the air flow. Optical analysis of the urea-water spray can be performed either through PIV and shadowgraph, as detailed in the result section.

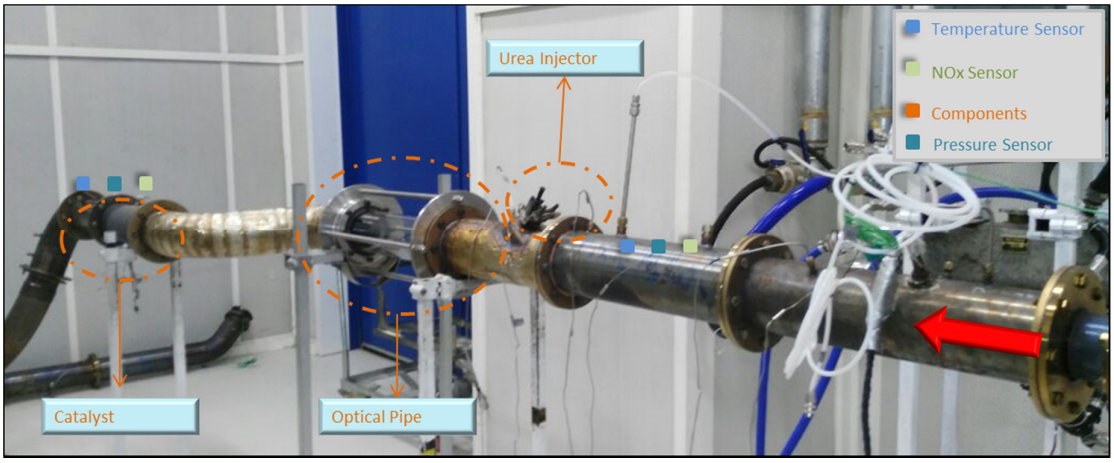

Figure 3.28. Configuration of the test section used for optical test

The optical mixer tube provided visual access to the section of glass pipe. The three flat windows of the mixer tube were made of 3 mm thick quartz glass which was installed downstream of the mixer tube before a 90° bend. This window allowed light to be introduced axially down the length of the mixer tube or for upstream images inside the mixer tube to be acquired. All joining surfaces were sealed with high temperature gaskets to prevent leakages. In this configuration, the optical mixer tube was able to safely operate at exhaust gas temperatures in excess of 500 °C. Figure 3.29 shows the 3 window optical pipe and downstream window.

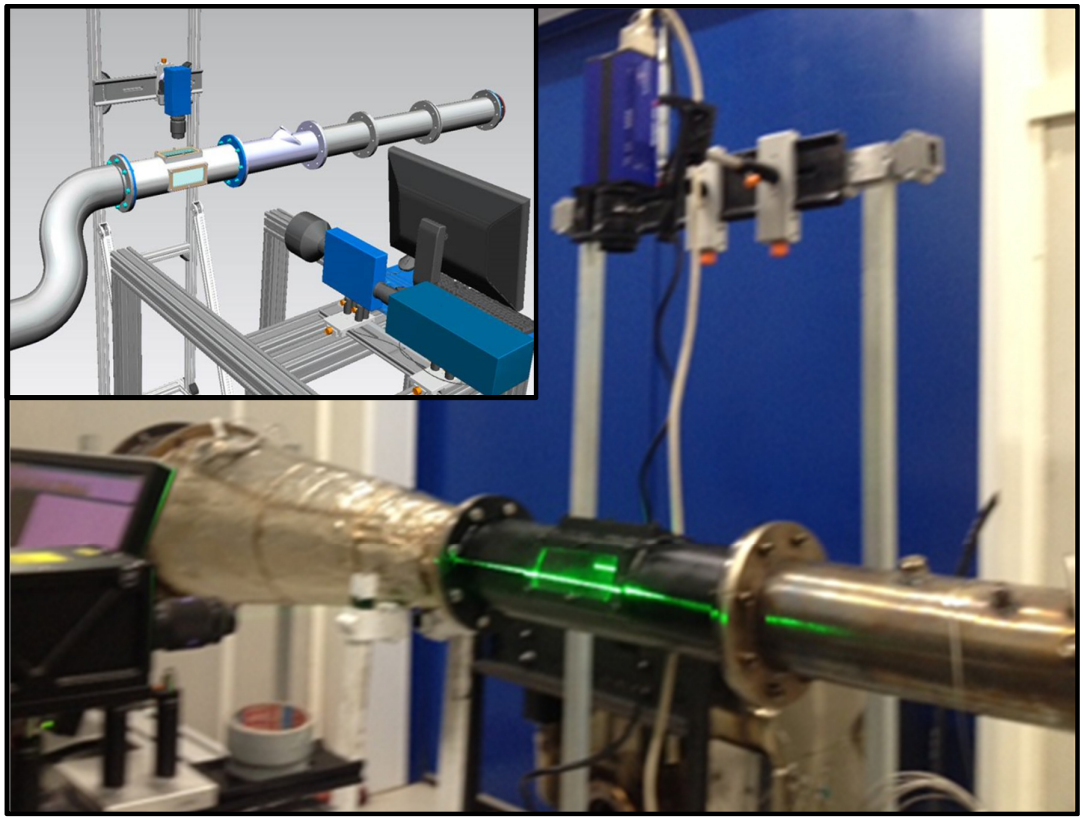

Figure 3.29. The PIV testing through 3 window pipe

3.3. Numerical Modeling of Inline Exhaust Aftertreatment System

In this chapter, urea-water-solution injection and ammonia conversion simulations are presented for inline exhaust aftertreatment system. The developed 3D numerical model accounts for all relevant physical effects. The multi modeling steps were correlated based literature data for each physics such as decomposition process. The spray and reducing agent distribution were correlated within the literature work. The influence of flow conditions, exhaust system properties and spray parameters on the film formation were be evaluated with the developed simple models.

The derived models including flow field, spray propogation and chemical reaction from validation works implemented in the Star-CCM. This complex CFD model helps to predict deposit location and deposit volume with respect to the spatial distribution of the reducing agent upstream the catalyst.

The study focuses on mixing of exhaust gas and urea spray distribution upstream of the SCR substrate and the geometry used for the simulations is therefore only downstream of the diesel particulate filter exhaust gas system. Onlt DPF are used in order to save computational time and effort to model wall filter subtrate. The flow distribution was almost uniform as %99 after the DPF due to wall filter effect. We can assume homogen flow distribution at the inlet.

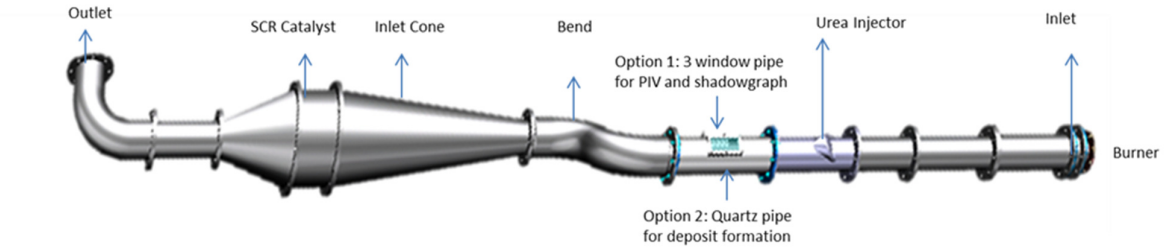

Figure 3.30. SCR Aftertreatment Inline model

The geometry of the inline exhaust aftetreatment system is displayed in Figure 3.30. The CFD model studied in this thesis consist of straight pipes, injector located pipe and mixer which is located just after the injection point. Then the quartz pipe or 3-window pipe are assemblied. The S-bend pipe and inlet cone are assemblied before the catalyst. The pipes have a circular cross section as 130 mm diameter. The mixer and s-bend are possible deposit accumulation region. The solid region of the mixer and s-bend pipe were modeled for conjugate heat transfer modeling.

The bosch injector is assemblied with three holes. All the parameters are for spray extractred from PIV results such as spray, cone angles. The initial velocity of the spray and droplet distribution are derivered also from PIV. These results are derived with spray test bench.

3.3.1. CFD model description

The mesh is created using Star-CCM with 2 million elements, including two prism layer around the mixer region to resolve the near wall conditions. The mixer wall and pipe wall are modeled as solid for conjugate heat transfer. Figure 3.30 shows the computational domain of inline exhaust aftertreatment system.

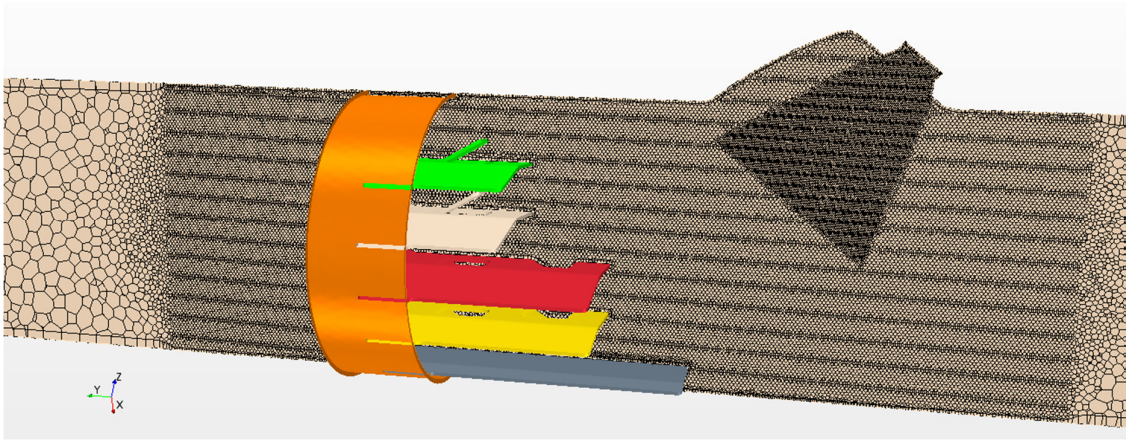

Figure 3.31. Shows the computational mesh for the mixer region

Figure 3.32 shows the computational of the full inline exhaust aftertreatment system.

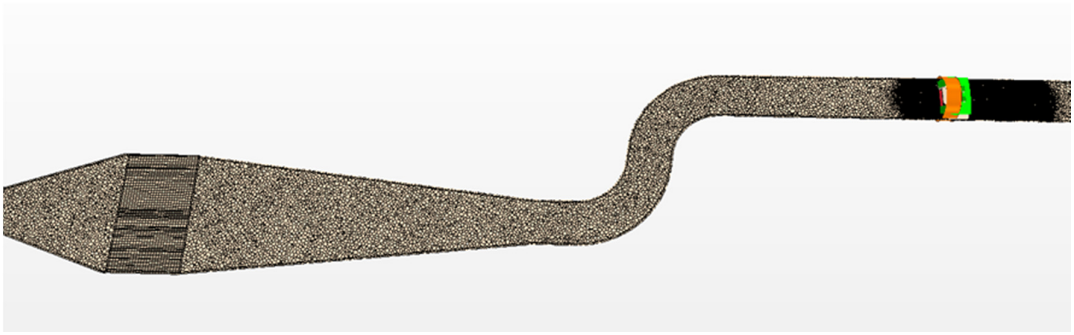

Figure 3.32. Shows the computational mesh for the whole model

Many CFD codes such as Fluent, Star-CCM and Converge were experimented for urea injection SCR cases. Fluent and Star-CCM have full capability to model SCR cases but Fluent has poor capability GT Power coupling with 3D CFD effect. Converge has

a lead technology for the spray cases as adaptive mesh technique but the deposit modeling has not developed. Star-CCM has selected for SCR cases modeling.

In **Figure 3.33** Converge spray was obtained in fron of the mixers. The spray distribution can model accurately but wall film modeling was not capable in converge.

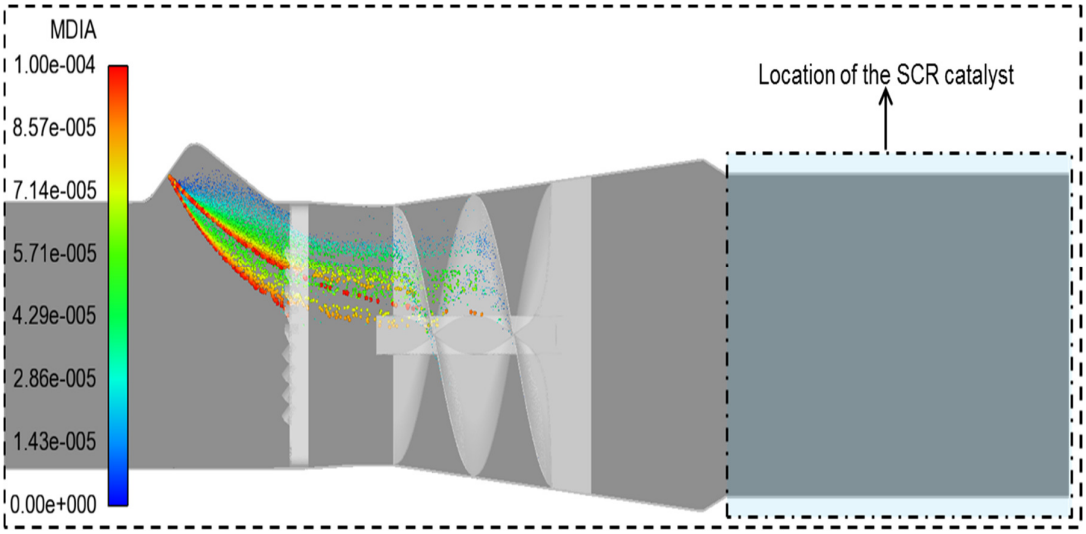

Figure 3.33. Selective Catalyst Modeling in Converge

Figure 3.34 Fluent can model spray behaviour and deposit modeling accurately. The fluent has limited capability with polyhedral mesh type. The hex mesh could not be generated easily and mesh dependency seems very high.

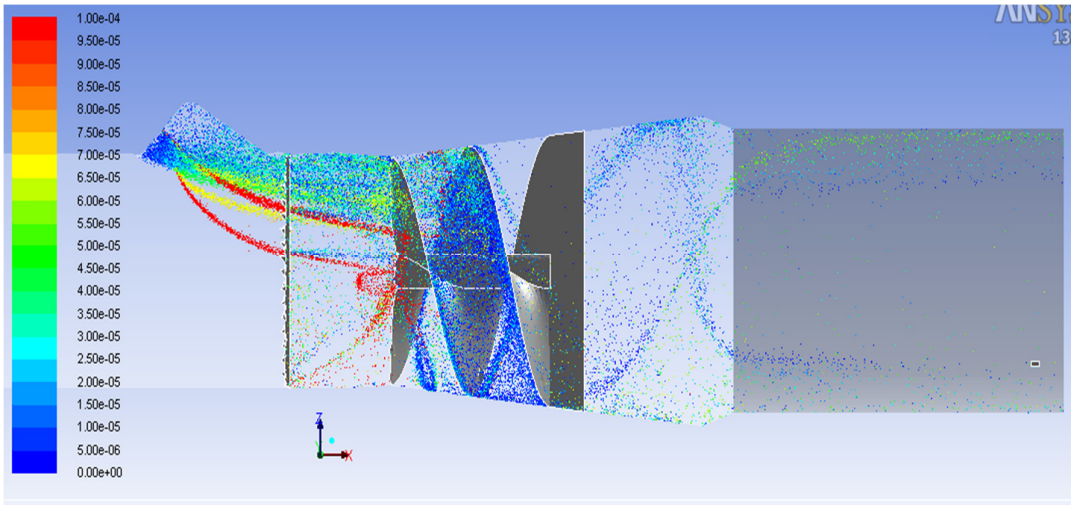

Figure 3.34. Selective Catalyst Modeling in Fluent

Star-CCM was selected after many experiment in mesh type and modeling approach investigation.

The mesh type, mesh sensitiviy and spray parcel number sensitivity works were required to accurate model for each cases.

The mesh sensitiviy work with different number and different mesh type such as tetrahedral, hexahedral and polyhedral were experimented. Hexahedral and polyhedral mesh type were less diffusivity and mesh density was optimized with polyhedral and hexahedral mesh type in Table 3.2. Hexahedral mesh type is used for catalyst region. Catalyst region is modeled with porous media. Only one direction flow is occured in porous media.

Table 3.2. Mesh type and number sensitivity

ID	Mesh Type	Outer Tube	Atomizer & Mixer		Number of Cells	Average of 29 TC
1	Tetra + Hexa	Solid	Baffle	Heat transfer	3763629	698
2	Tetra + Hexa	Solid	Baffle	Adiabatic	3463629	685
3	Tetra + Hexa	Solid	Solid	Conjugate	3763629	680
4	Poly + Hexa	Solid	Solid	Conjugate	2119982	627

5	Trimmed + Tetra	Solid	Solid	Conjugate	2359082	620
6	Experiment					630

The spray sensitiviy work was experimented to determine appropriate droplet parcel number. Less droplet parcel could not transport necessary information, high parcel numbers have time penalty and convergence issue. Different parcel number experiment work can be obtained in in Figure 3.42. 500 parcels have selected in spray simulation for each injection. The sentivity studies were experimented with many authors. [95] Spray modeling is considered two-way coupling for momentum and heat.

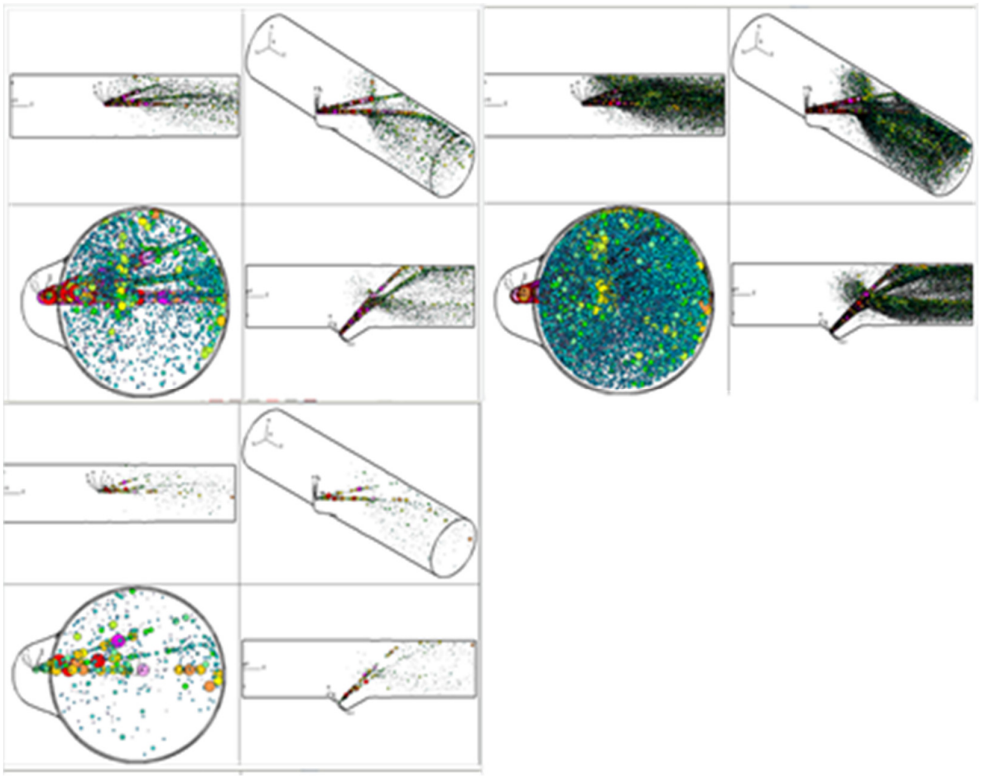

Figure 3.35. Parcel Number sensitivity testing

Catalyst are modeled as porous media in Star-CCM. The pressure drop values of the catalyst are taken from supplier and measured in inline exhaust aftertreatment system. The cofficient of the pressure drop were correlated with extracted values in flow test bench.

3.3.1.1.CFD Model Boundary Conditions

The boundary conditions are specified according the WHSC cycle point of emission registlation from Table 3.3. These 13 modes point are selected from WHSC cycle.

Table 3.3. Boundary Conditions

	Exhaust Mass Flow Rate	Temperature	NOx after DPF	Urea
	kg/h	^{0}C	ppm	mg/s
1	77	306	117	8
2	1057	320	1000	935
3	348	277	140	43
4	778	350	462	318
5	718	400	1677	1065
6	171	200	106	16
7	635	250	480	268
8	300	300	152	40
9	546	220	231	111
10	1137	330	573	576
11	482	400	941	400
12	228	250	112	22
13	83	200	126	10

A parameter studies were carried out to investigate the ammonia distribution and deposit accumulation of the system for each modes. The automatic post processing script tool is developed to generate deposit map for the work.

Star-CCM was used for CFD works. Star-CCM models the case as unsteady, turbulent, compressible flow with multi-phase reacting flow problems. Polyhedral mesh are advantages due to eliminate flow directional problem. Lagrangian modeling is used for droplet distribution. From PIV work droplet particle size are given to code with statistically. The exhaust gas is modeld in an Eulerian for chemical reactions of the

thermolysis and hydrolysis. Two-way coupling of mass, momentum and energy between liquid and gas phases are considered.

The injection frequency was givens as 1 Hz from supplier. Simulations were conducted for only 1second and the simulation run for 3 injetion for convegence.

Inlet of the inline exhaust aftertreatment systems is modeled as mass flow rate and outlet as pressure. The mass flow rate balance is monitored for convergence.

For modeling the urea spray, three hole nozzle with a spray angle of 33 degree and injection velocity of 32 m/sec is applied. The diameter distribution curve is also applied and tuned to replicate the actual spray. The droplet breakup parameters are tuned based on the PIV data specific to the injector used. The urea droplets are treated to evaporate completely as they hit the SCR inlet face. The simulation is conducted for three injection pulse and the dosing is started from the converged steady state calculation. Dosing time is calculated based on the required amount of NH3 required to convert the NOx.

Exterior walls of the solid parts are treated as fixe temperature. In addition to that, conjugate heat transfer for both the pipe wall and mixer wall is defined to include lateral heat conduction. The 2D results are monitored on the SCR inlet face to quantify the performance of the system.

The boundary conditions used for this study are shown in Figure 3.36. These values are WHSC point of the engine. These boundary conditions are required for emission prediction work.

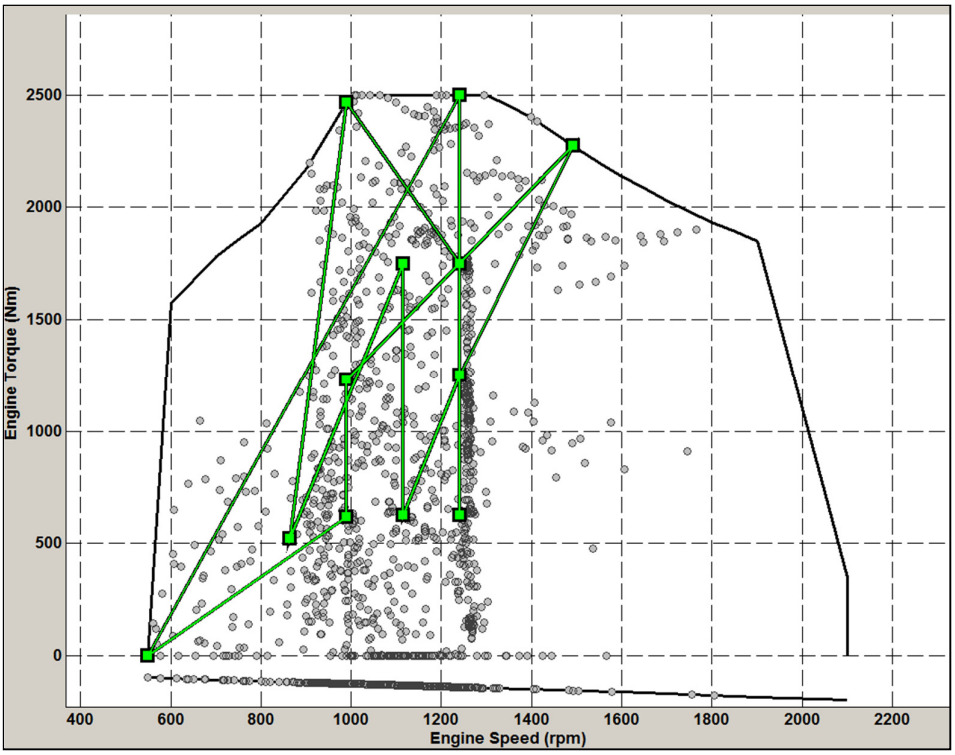

Figure 3.36. Boundary conditions of the inline exhaust aftertreatment system

3.3.2. Experimental set-up and optical diagnostics

The flow optical test bench is designed to visualize the deposit accumulation when the flow test bench provide demanded mass flow rate and temperature similar to diesel exhaust. Optical experiments such as PIV, shadowgraph can be used in flow optical test bench that are less complex than engine. For the investigation of the velocity vector, spray distribution through the window of the pipe, the variations of air mass flow rate, temperature and injection rate are considered whereas only the velocity vector downstream of the mixer and spray distribution were studied for the examination of UWS spray characterization.

The experimental setup consists of urea injector at a fixed mass flow rate, optical windows, CCM camera and laser sheet. In Figure 3.37 shows the setup of the PIV visualization. The urea injector is commercial three-hole injector. The inspected region is downstream of the injection point and mixer which causes the swirl flow structure. The distance between optical access and the injector ranges from 150 mm to 200 mm. CCM camera installed with 105 mm objective which is 90 degree of the laser sheet.

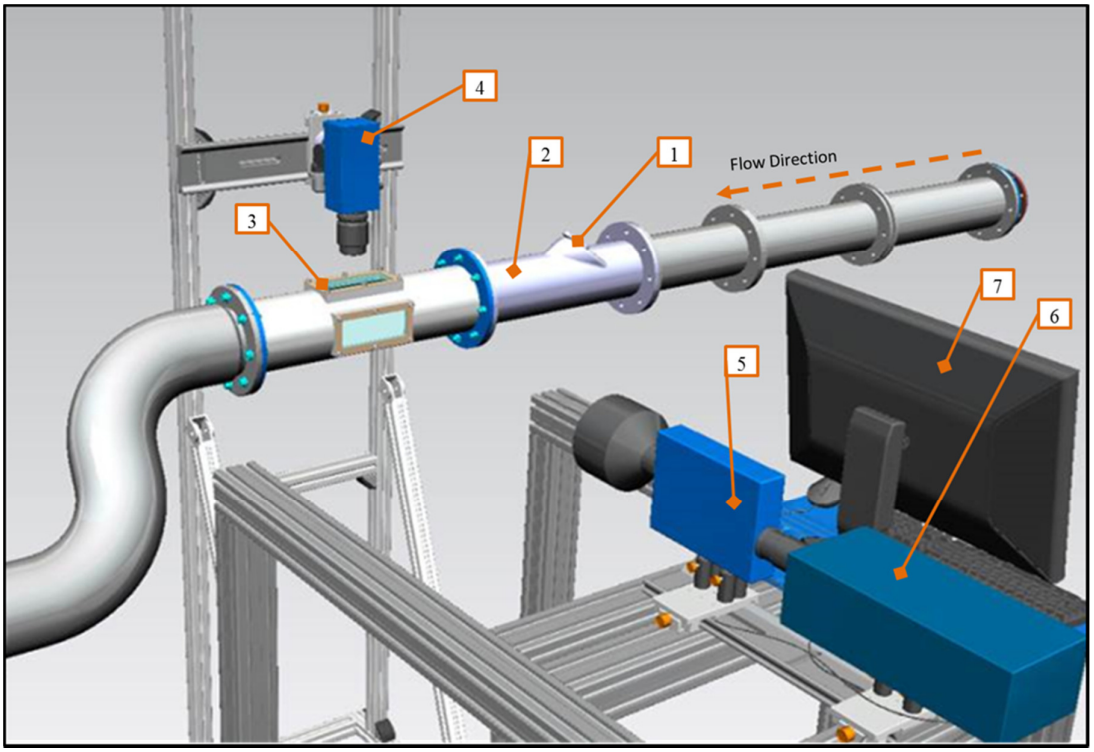

Figure 3.37. The PIV and shadowgraph setup for the optical test bench

The components of optical test bent bench is listed in Table 3.4.

Table 3.4. Components of the optical test bench

1	urea injector
2	mixer
3	optical window
4	CCD camera with 105 mm lens
5	long distance microscope
6	laser
7	computer and sencronization unit

In this cases circular part of the pipe deflects the images. The calibration plate consists of certain dimension of the dot point. The images are taken when the calibration plate inside the pipe. The distortions is corrected for calibration plate image. The same

correction values are used for velocity vector image. The distortion effect was eliminated.

UWS (32.5 wt% solution) is sprayed by urea injector inside the hot air stream. Window glass pipes are used to enable optical access. A scheme of the injection section and the optical arrangement is presented in Figure 3.38. Dashed line rectangles delineate both optical diagnostics used in the PIV visualization and shadowgraph techniques.

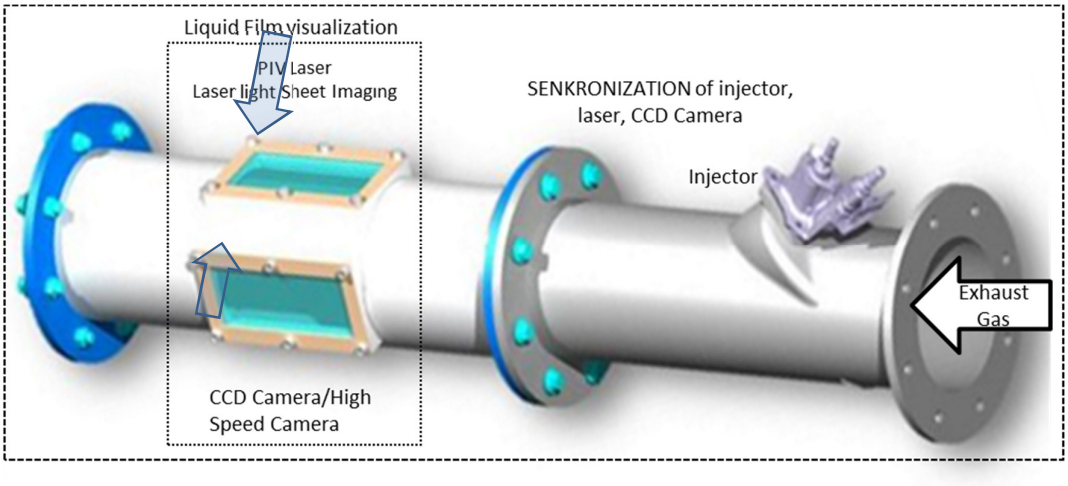

Figure 3.38. PIV measurement at the pipe window

The recirculation regions were obtained due to complex mixer structure which is located upstream of the pipe window. The highest velocity quantities are reached in the pipe center just downstream of the mixer. The mixture blades generate the vortex and recirculation that can capture with numerical and PIV measurement.

The velocity vector from PIV measurement are presented in Figure 3.39. The developed injection control system send the signals to PIV laser and CCD camera for senkronization. Many instatenious sampling data was collected and done post processing to generate velocity vector. In this figure recirculation area can be obtained at the bottom and top of the pipe window.

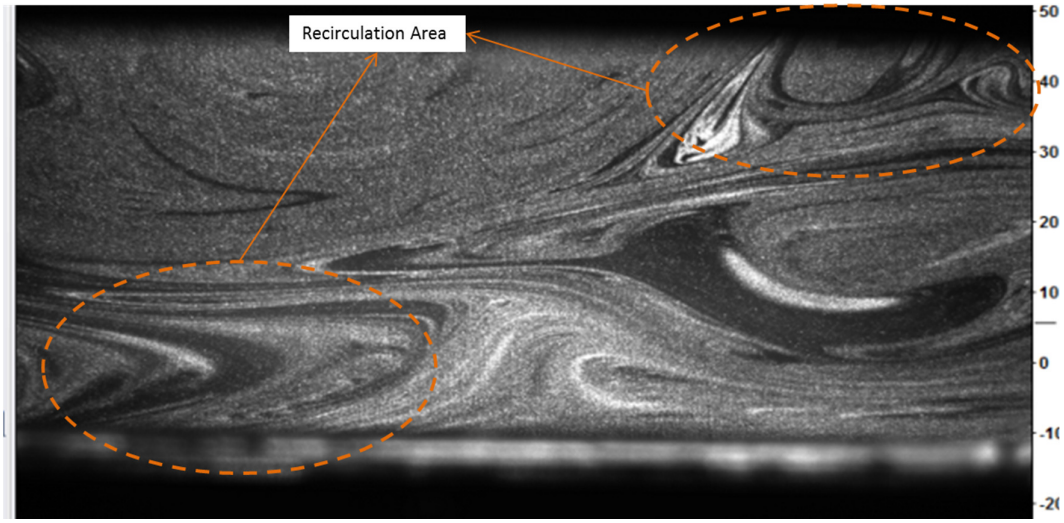

Figure 3.39. PIV measurement comparison flow field

Figure 3.40 shows the velocity vector at the pipe window. The high velocity was obtained at the center of the region. 13 m/s velocity is obtained.

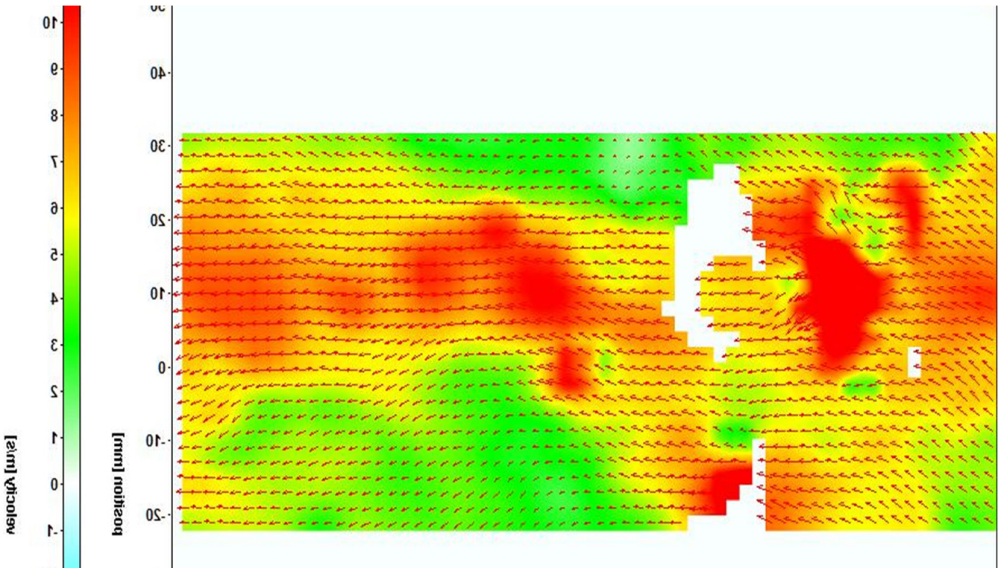

Figure 3.40. Velocity vector from PIV measurement

The velocit fields are investigated in details. The turbulence model of the RSM predict in good agreement of the flow recirculation at the upstream of the catalyst. k-e turbulence model cannot predict the swirl region upstream of the mixer in Figure 3.41.

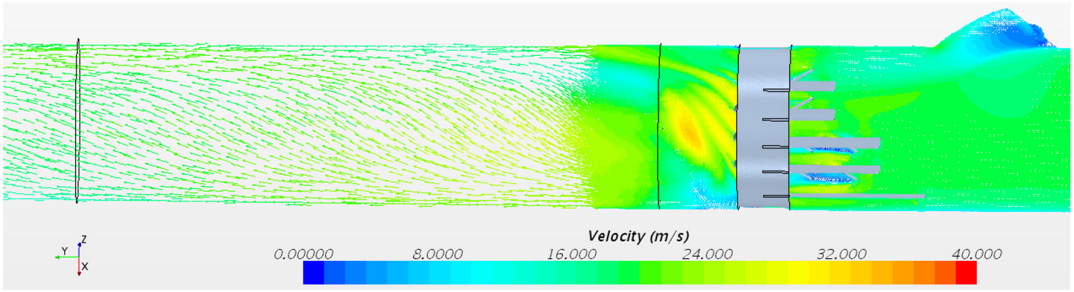

Figure 3.41. Velocity vector at the cone k-epsilon

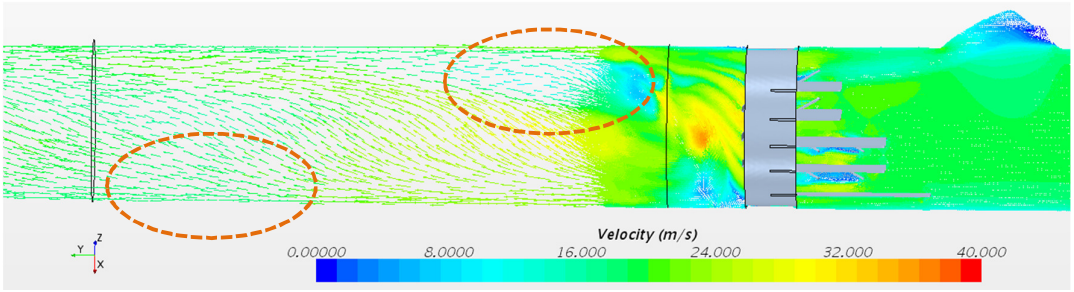

Figure 3.42. Velocity vector at the cone RMS

The velocity vector at the inlet cone was observed in Figure 3.43. Due to large diameter of the inlet cone, low velocity vector was observed. But k-e predicted swirl structure for the flow field in the upper surface of the pipe.

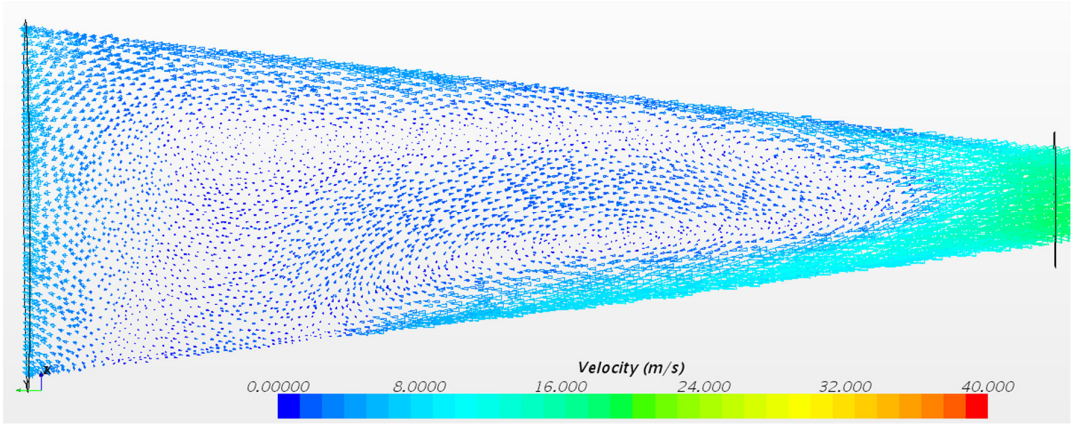

Figure 3.43. Velocity vector distribution at the cone for k-epsilon model

In Figure 3.44 the swirl flow stucture was captured in the inlet cone.

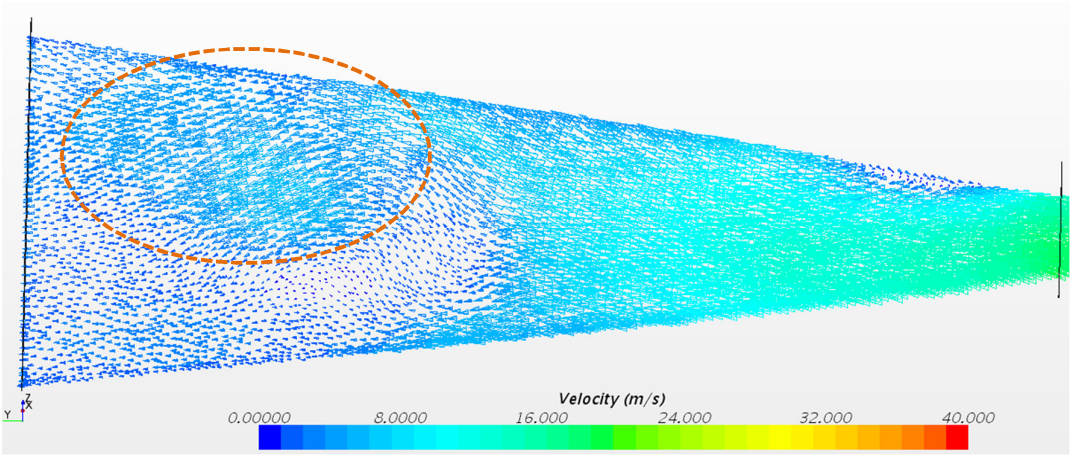

Figure 3.44. Velocity vecot distribution at the cone for RSM model

The velocity vectors of the inlet cones were observed for both turbulence models. Both turbulence models predicted swirl in inlet cone. But RSM model predict more wide swirl. This recirculation flow field of the pipes effect the SCR performance due to poor velocity distribution. It is hard to measure flow field distribution by hot-wire sensor at that region. Numerical simulation with PIV correlation and temperature distribution correlation predict all flow field characteristics.

The velocity, temperature and ammonia distributions were extracted 5 mm upstream of the catalyst.

The temperatures across the aftertreatment system and in each of the SCR bricks were measured using K-type thermocouples. As shown in Figure 2, there were 13 thermocouples in each SCR brick to measure both radial and axial temperature gradients. The SCR inlet radial temperature gradients are provided by thermocouples 1-3, located 25 mm from the inlet face of the brick.

The flow uniformity can not measured at the inlet face of the SCR. Hot wire can not installed due to package issue. Another method to measure flow uniformity upstream of the catalyst is temperature distribution method by thermocouple installation. It can give the similar distribution behaviour according the velocity distribution. 13 thermocouples are instrumented at the 10 mm, 20 mm and 45 mm downstream of the inlet face of the catalyst as seen below. These installation measure radial temperature gradients along the exhaust system.

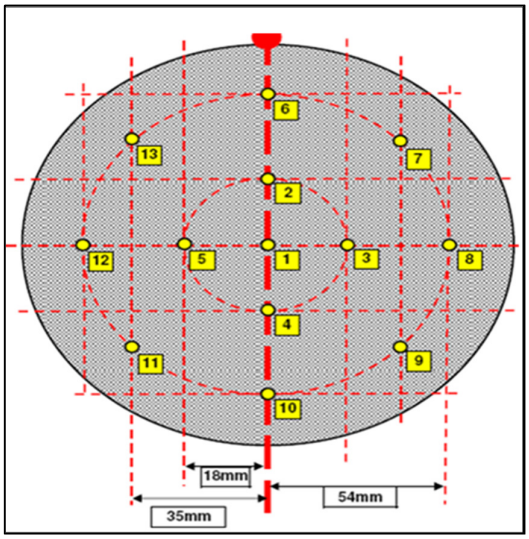

Figure 3.45. Thermocouple layout in SCR catalyst

The temperature distribution at the upstream of the catalyst are derived in Figure 3.46 The uniformity is 0.98 which shows high uniformity. It can be seen that thermocouple data is similar trend with CFD result. The temperature differences range from 40°C.

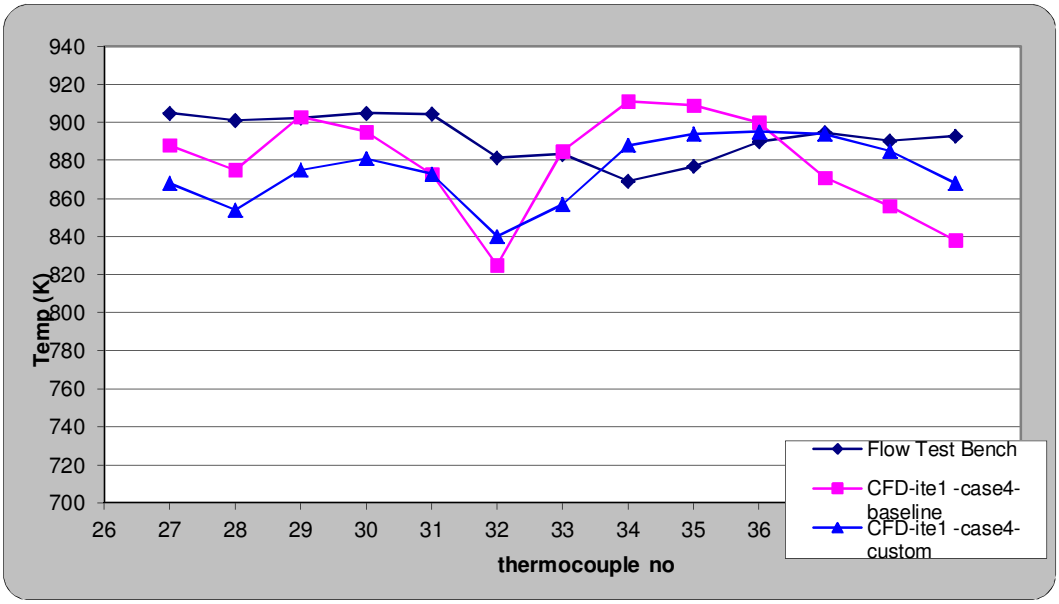

Figure 3.46. Temperature distribution correlation with flow distribution

The temperature distribution across the catalyst section are comparable with flow test bench distribution. That such validation shows us the conjugate heat transfer modelling and heat convection values are calculated in good agreement.

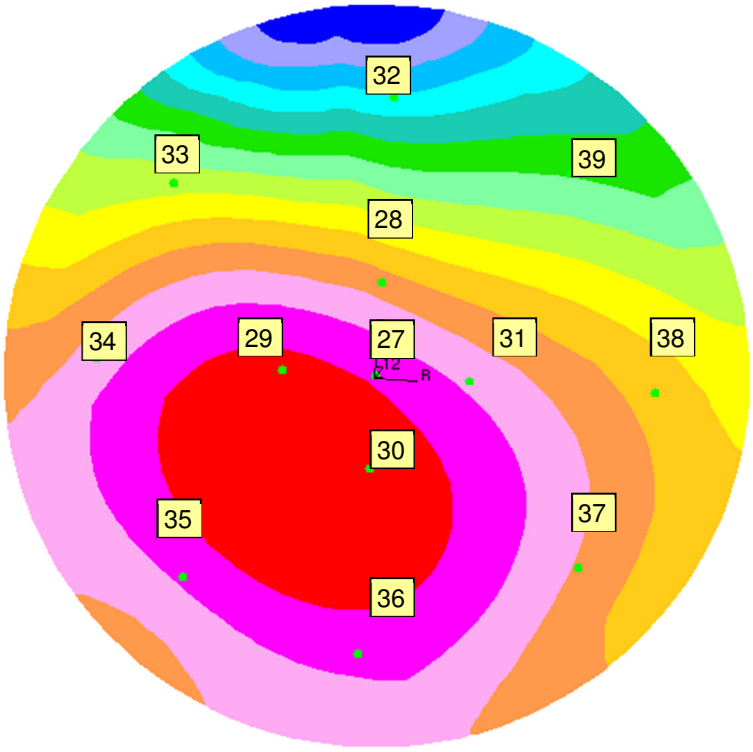

Figure 3.47. Temperature Distribution at the inlet of the SCR

3.3.3. CFD spray model setup

For this work, commercial CFD code, Star-CCM is used for the CFD simulations. In urea spray modeling, the UWS droplets are injected into the exhaust stream and the generation of NH3 and HNCO from the DeNOx evaporation is captured. The simulation approach and corresponding models activated for the spray analysis are explained in this section. The analysis is conducted in a transient run mode, where the exhaust gas phase is solved in transient approach with constant mass flow inlet condition, and spray droplets are introduced in a transient nature to simulate the flow of the injector. In this setup, the flow field from a steady state condition serves as an initial condition for the spray analysis.

Interaction of urea droplets with the exhaust gas flow is solved as a multi-phase flow,

where the droplet phase is treated as multicomponent droplets. Droplets are injected with given initial conditions, such as data from PIV experiment from previous chapter, and solved for its trajectories, momentum, mass and heat transfer. For this analysis, inbuilt modules of droplet turbulent dispersion, evaporation of urea, primary and secondary breakup and droplet wall interaction are activated. A two-way coupling approach applied to both phases; such as influence of droplets to gas phase.

Interaction of the fuel with air was modeled by using Lagrangian approach in the simulations. The entrained particle phase is modeled using the following set of ordinary differential equations for mass, momentum and energy that characterize the change in particle properties along particle trajectory as it moves through the gas continuum

3.3.4. Mathematical modeling

The most basic particle description involves only its position $r_p(t)$ and velocity $v_p(t)$. These two quantities relate through the equation of motion.

$$\frac{dr_p}{dt} = v_p - v_g \quad (3.9)$$

Individual particles are not tracked, instead a single parcel represents a set of identical particles, at some mean centroid $r_\pi(t)$. The velocity of the parcel is assumed to be the same as its constituent particles, hence its equation of motion is

$$\frac{dr_\pi}{dt} = v_p - v_g \quad (3.10)$$

In subsequent sections, a quantity which is identical for a parcel and its particles, such as velocity in the preceding paragraph, are described as a "particle" quantity and given the subscript p. The term "parcel" and the subscript π are reserved for quantities which are exclusively defined on parcels.

The equation of conservation of mass of a material particle is simply

$$\frac{dm_p}{dt} = \dot{m}_p \quad (3.11)$$

Where m_p is the mass of the particle and $\dot{m}_p$ the rate of mass transfer to the particle.

The latter is zero unless a mass transfer model is active, such as the Quasi-Steady Single-Component Droplet Evaporation model. If the Two-Way Coupling model is active, $\dot{m}_p$ is accumulated over all the parcels and applied in the continuous phase continuity equation.

The generic form of the equation of conservation of momentum for a material particle is

$$m_p \frac{dv_p}{dt} = F_s + F_b \quad (3.12)$$

Here F_s represents the forces acting on the surface of the particle, and F_b the body forces. These forces in turn are decomposed into

$$F_s = F_d + F_p + F_{vm} \quad (3.13)$$

$$F_b = F_g + F_u \quad (3.14)$$

The momentum transfer to the particle from the continuous phase is simply F_s. If the Two-Way Coupling model is active, F_s is accumulated over all the parcels and applied in the continuous phase momentum equation.

A material particle is assumed to be internally homogeneous which, from a thermal point of view, implies a low Biot number, for example, less than approximately 0.1.

The generic form of the equation of conservation of energy consistent with this assumption is

$$m_p c_p \frac{dT_p}{dt} = Q_t + Q_{rad} + Q_s \quad (3.15)$$

Here, Q_t represents the rate of convective heat transfer to the particle from the continuous phase, Q_{rad} represents the rate of radiative heat transfer.

The convective heat transfer term is formulated as

$$Q_t = fhA_s(T - T_p) \quad (3.16)$$

Where A_s is the particle surface area, and h is the heat transfer coefficient.

The heat transfer to the particle is always active in the energy equation. It can also be written

$$Q_t = \frac{f m_p c_p (T - T_p)}{\tau_T} \quad (3.17)$$

If the Two-Way Coupling model is active, Q_t is accumulated over all the parcels and applied in the continuous phase energy equation.

If the Particle Radiation model is active, heat transfer due to radiation is included in the energy equation. The radiative heat transfer, Q_{rad} , to the particle is defined as:

$$Q_{rad} = \frac{A_s}{4} Q_{a,p} (G - 4\sigma T_p^4) \quad (3.18)$$

where A_s is the particle surface area, $Q_{a,p}$ is the absorption efficiency of the particle, G is the incident radiative heat flux, and σ is the Stefan-Boltzmann constant. [94]

3.3.4.1.Droplet Breakup

The multi-component droplet evaporation model assumes droplets to be internally homogeneous, consisting of an ideal mixture of liquid components, some of which are transferred. This means that they can vaporize. There can also be inert components in both the droplet and the gas.

The rate of change of mass of each transferred component due to quasi-steady evaporation $\dot{m}_{pi}$ can be written

$$\dot{m}_{pi} = -\varepsilon_i g^* A_s \ln(1 + B) \quad (3.19)$$

in which B is the Spalding transfer number, g^* is the mass transfer conductance and ε the fractional mass transfer rate

Effectively, the transfer number represents the driving force for evaporation, which is a function of thermodynamic conditions of the liquid and vapor mixtures. On the other hand, the conductance represents geometrical and mechanical effects, such as the size and velocity of the droplet. Expressions for these quantities depend on the mode of evaporation, of which there are:

•Super-Critical is active when the droplet temperature exceeds the highest critical temperature of the transferred components, $T_p \geq \max(T_{c,i})$, The transferred components are forced to vaporize instantaneously

•Heat Transfer Limited Evaporation is active when the vapor at the droplet surface is

saturated and subcritical. The evaporation rate then depends on the balance between heat transfer from the vapor and latent heat transfer due to evaporation. The first condition for a saturated vapor is:

$$\sum_{T} X_{is} \geq 1 \quad (3.20)$$

where X_{is} is the equilibrium mole fraction of transferred component at the droplet surface. X_{is} is evaluated using Raoult's law:

$$X_{is} = \frac{p^{i}_{sat}(T_p)}{p} X_{ip} \quad (3.21)$$

in which $p^{i}_{sat}(T_p)$ is the component saturation pressure that is evaluated at the droplet surface temperature, and X_{ip} is the component mole fraction in the droplet.

The Reitz-Diwakar breakup model assumes that breakup occurs in one of two possible regimes. The droplet diameter decreases according to

$$\frac{dD_p}{dt} = \frac{D_s - D_p}{\tau_b} \quad (3.22)$$

in which D_s is the stable diameter and τ_b the breakup time-scale which depend on the active breakup regime.

The first breakup regime, bag breakup, is caused by the droplet expanding into the low-pressure wake region behind it, and eventually disintegrating when surface tension forces are overcome. It is assumed to be possible if

$$We \geq We_{crit} \quad (3.23)$$

With $We_{crit} = 12$ the default.

The second breakup regime, stripping breakup, is caused by liquid being sheared or stripped from the droplet surface. It is assumed to be possible if equation 3.21 is satisfied and additionally. [94]

$$We_{crit} > \max(2C_{s1}\,\mathrm{Re}^{0.5}, We_{crit}) \quad (3.24)$$

3.3.4.2.Bai-Gosman Wall Impingement Model

The Bai-Gosman model aims to predict the outcomes of liquid droplets impacting an impermeable boundary ("wall") or fluid film.

The Bai-Gosman model categorizes possible outcomes as being in one of six possible regimes, illustrated in the following diagram.

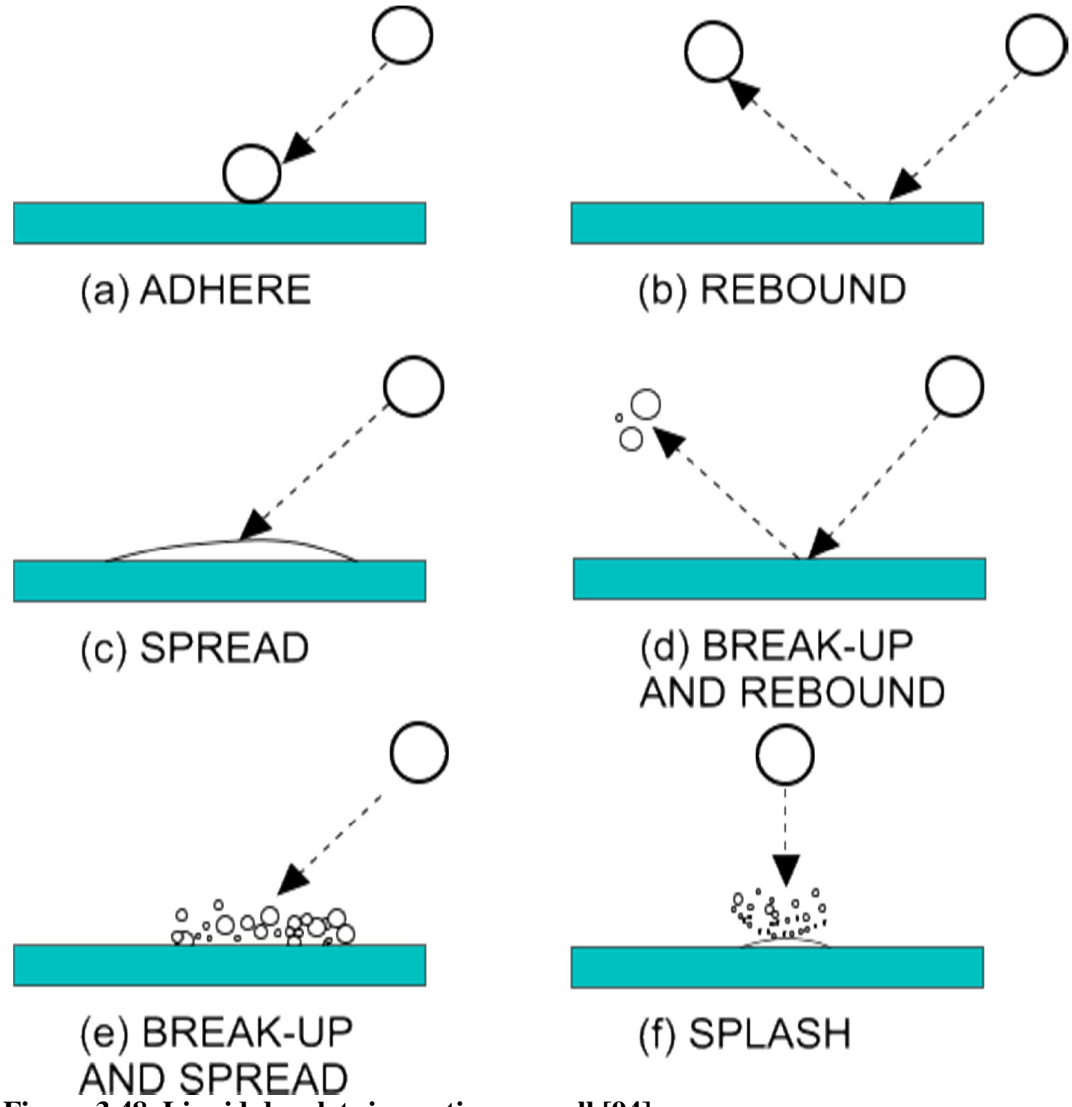

Figure 3.48. Liquid droplets impacting on wall [94]

For fluid film boundaries, momentum and kinetic energy lost by the droplets are gained by the film. The choice of regime for a given impingement event is made using four parameters:

•The incident Weber number

$$We_I = \frac{p_p v_{r,n}^2 D_p}{\sigma} \quad (3.25)$$

in which $v_{r,n} = (v_p - v_w).n_w$ is the normal component of the particle velocity relative to

the wall. n_w is the unit vector normal to the boundary.

•The Laplace number

$$La = \frac{p_p \sigma D_p}{\mu_p^2}$$

•The boundary temperature T_w (provided the Energy model is active in the physics continuum).

•The wall state; a boundary can be either wet or dry. For fluid film boundaries, this is determined by the presence or absence of a fluid film. For other boundaries, this is determined by the user-selected Wall State property. [94]

3.3.5. CFD urea-water evaporation and decomposition

Multi-component evaporation model is applied for urea-water solution. When the urea-water-solution injected hot exhaust system, the endothermic reactions are occured after injection, water evaporates into water vapor. This left urea decomposes into NH3 and HNCO though thermolysis reaction. HNCO decomoses NH3 and H2O through hydrolysis reaction. Implementation of Star-CCM is based on the two step process. The reaction rate for the is described by an Arrhenius-type equation,

$$\frac{dm_{urea}}{dt} = -\pi . A . D_d . \exp(-\frac{E_a}{RT}) \quad (3.26)$$

where A = frequency factor; Ea =activiation energy; Dd = droplet diameter; R = gas constant; T = temperature. For constants, the values are tuned in simple validation chapter such as A = 0.42 kg/ms and Ea = 6.9e3 J/mol K. [70] [66]

3.3.6. Conjugate heat transfer (CHT)

As urea-water sprays can impact upon surfaces within the exhaust system, the mixer and the SCR catalyst, CHT must be employed to account for local variations in material temperatures that impact vaporization and reactions.

The temperature response time of the fluid and solid parts have a huge difference. The flow can solve with very small time interval as 1e-4 but solid can not heat up within this time interval. This is the one of the challenge issue for conjugate heat transfer.. For the fluid side especially with spray physics can modeled only 3-4 injection due to

time penalty. The bigger time step leads the unconverge solution. The 100 times bigger time step is required for the solid to capture temperature raise effect. Thus, it is not impossible to run the numerical simulation entirely in a coupled transient solution. The trend methodology to overcome the differnce in time scales of the fluid and solid part is the fluid flow becomes frozen and solid is updated using the heat transfer coefficient (HTC) and near wall temperature. Then flow and solid are running in a coupled solution with certain time then again fluid is frozen and solid part is running. An illustration of this is given as Figure 3.49 a fluid is flowing in a cold pipe and the solid calculation allows the solid temperature to heat up the fluid flow temperature in a shorter run-time.

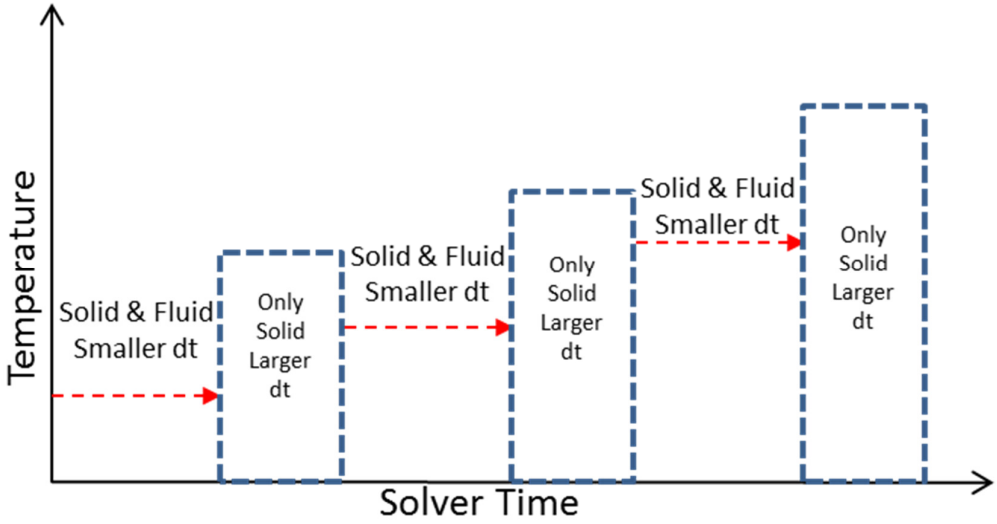

Figure 3.49. Fluid Solid Coupling Methodology

This methodology will not affect the spray, fluid film conditions when the simulation reaches a steady state.

3.3.7. Spray wall interaction

The interaction of the injected liquid spray on the impinging wall is one the major parameters in wall film formation on the walls. Based on the dimensionless wall temperature and dimensional droplet velocity, the model can predict how the spray interacts with the wall. The dimensionless wall temperature, T* and dimensionless droplet velocity, K, is defined

by, [94]

$$K = \frac{(\rho D) d^{3/4} u_d^{5/4}}{\sigma^{1/2} \mu^{1/4}} = C\alpha^{5/4} L\alpha^{3/4} \quad (3.27)$$

$$T^* = \frac{T_w}{T_{sat}} \quad (3.28)$$

The Figure 3.50 shows the different regimes in the inline exhaust aftertrreatment system.. Formation of wall film occurs by the liquid deposits, if the wall temperature, T*, is less than 1.1 and lower droplet velocity. For the higher droplet velocity, the droplets splashes into smaller droplets after impact. Some of the droplets transfer to wall film as well. If the wall temperature, T*, is greater than 1.1 and with the low droplet velocity, the droplets rebound to the gas phase. For the higher droplet velocity, droplets break into smaller one without any film on the wall. The formation of wall film in this model mainly depends on the wall temperature.

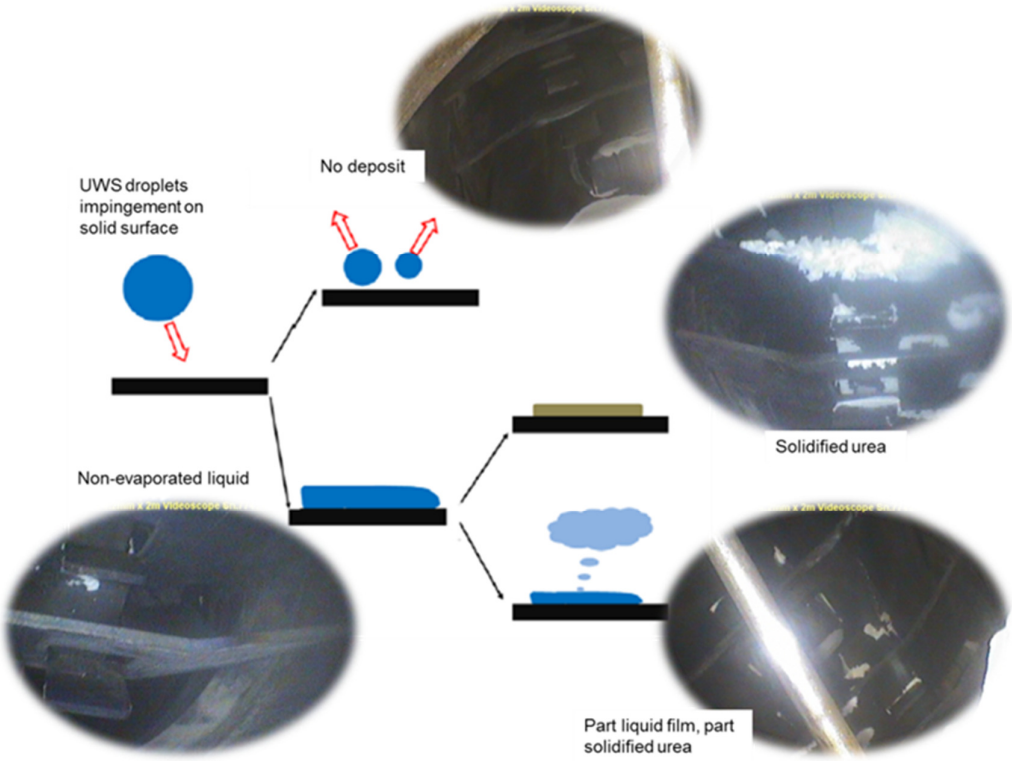

Figure 3.50. Different deposit regime in inline exhaust aftreatment

Hence the heat transfer between the impinging drop and wall temperature is quite important. This heat transfer accounts for the temperature difference, contact area, contact time and penetration coefficients of both wall and droplet properties.

3.4. CFD Deposit Prediction with test result

The endoscope with image processing software is a modular system to enable visual inspection of phenomena occurring inside of an exhaust gas aftertreatment system. The visual inspection technique is extended for thermal imaging of material surfaces such as entrance and exit faces of a catalytic converter or of any other surface.

The endoscope image with image processing code developed in matlab quantifies urea deposit formation in a SCR after-treatment system. The deposit formation can be observed directly while they are formed and recorded in pictures for further analysis.

During test, the performance parameters of the running engine, such as temperatures, pressures, emissions etc. can be recorded and synchronised with the video. The amount of solidified urea could be estimated by counting the number pixels from pictures taking over a period of time.

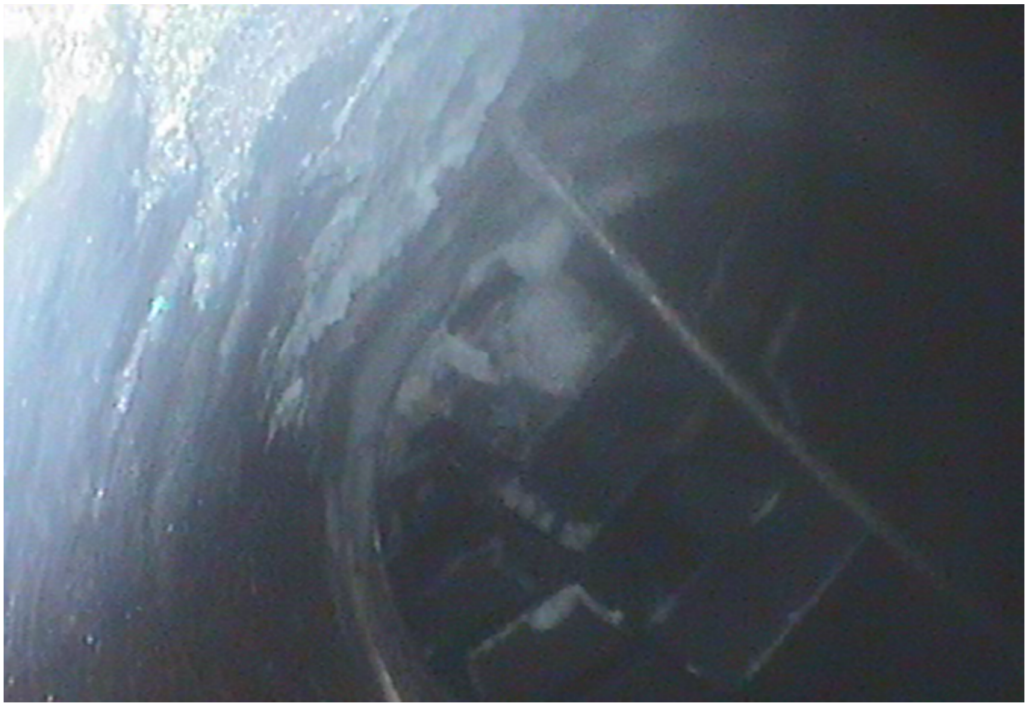

Figure 3.51. Endoscopes capture the critical region image

Two types of video cameras used for this study, namely Straight tube type which can be used for taking pictures while the flow lab is running as seen in Figure 3.52. The camera has an operational threshold limit of 250°C. Cooling air is fed into the camera

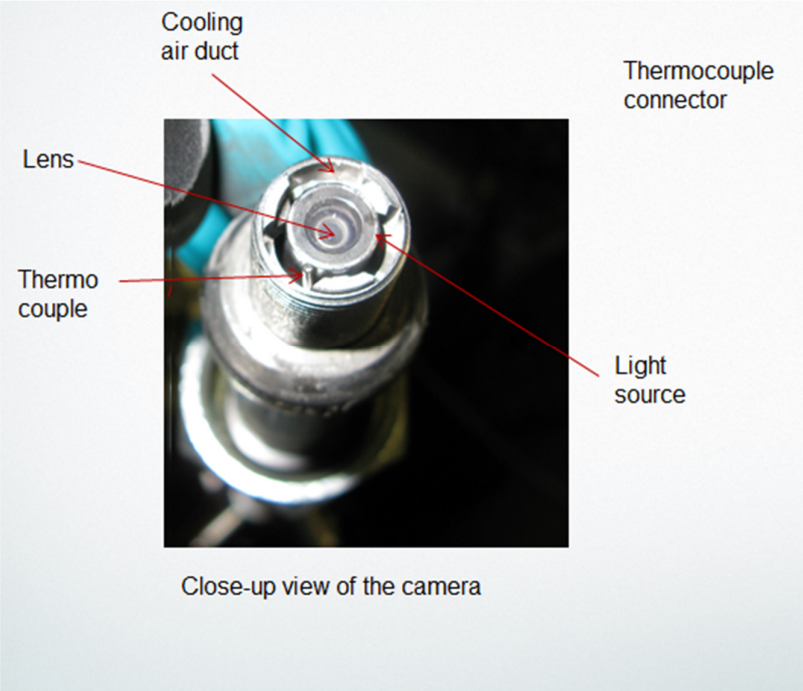

assembly to keep the lens cool by creating an 'air curtain'.

Figure 3.52. Endoscope camera

To determine the thickness and mass of the deposit image processing tool can be used. These tools make easier to identify corresponding deposit information without disassembly the exhaust system.

- All tests were started from a clean, deposit-free system.
- UWS injection was started only when steady state operating conditions were reached.
- At each specified test condition, the test will run continuously for four hours.
- Only one camera will be used for each test.
- Pictures are taken once every 13 seconds (approx.), a four hours test will produce (approx.) 1300+ pictures which will then combine together to form the

animation.

- After the test, all the excessive urea (either in liquid or in solid form) are removed by increased the engine out temperature, say 600° C.
- At such temperature, both the residual urea and accumulated soot will be removed by passive re-generation.

The purpose of the test is to generate the urea deposit map. The used image acquisition and processing software includes a calibration process which adapts certain amoun to deposit and thickness correlation using the images. The most challenging problem in processing images is to undestand deposit type as melamin, biuret. Tests basically to detect location, mass and thickness of the deposit,then compare CFD result to assign mass and thickness on the detected location.

3.5. Emission Prediction using 1D with 3D effect

3.5.1. Geometrical sector based approach

In this approach the catalyst inlet face area was divided into equal geometrical regions. The motivation for this comes from the equal region approach typically used to select sampling points for measuring spatially varying NH3 concentrations and velocities.

This approach is geometrically illustrated in Figure 3.53 using the radial and tangential regions.

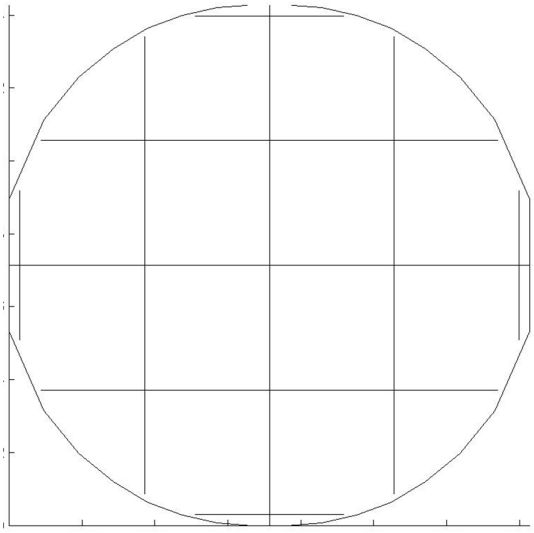

Figure 3.53. Division of substrate face into equal area geometrical sectors

3.5.2. Emission prediction model

One critical performance of aftertreatment system is back pressure as it affects engine fuel economy and combustion efficiency. In addition emission predicition is crucial requirement due to legistration. This method gives the subtrate pressure and emission prediction.

Detailed chemistry is available with Star-CCM and DARS coupling to compute NOx conversion efficiency but it requires a relatively long period of computation. The emission predicition could not acheive in 3D CFD software due to duration. The developed method is to predict emission using 1D coded but takes account 3D effect

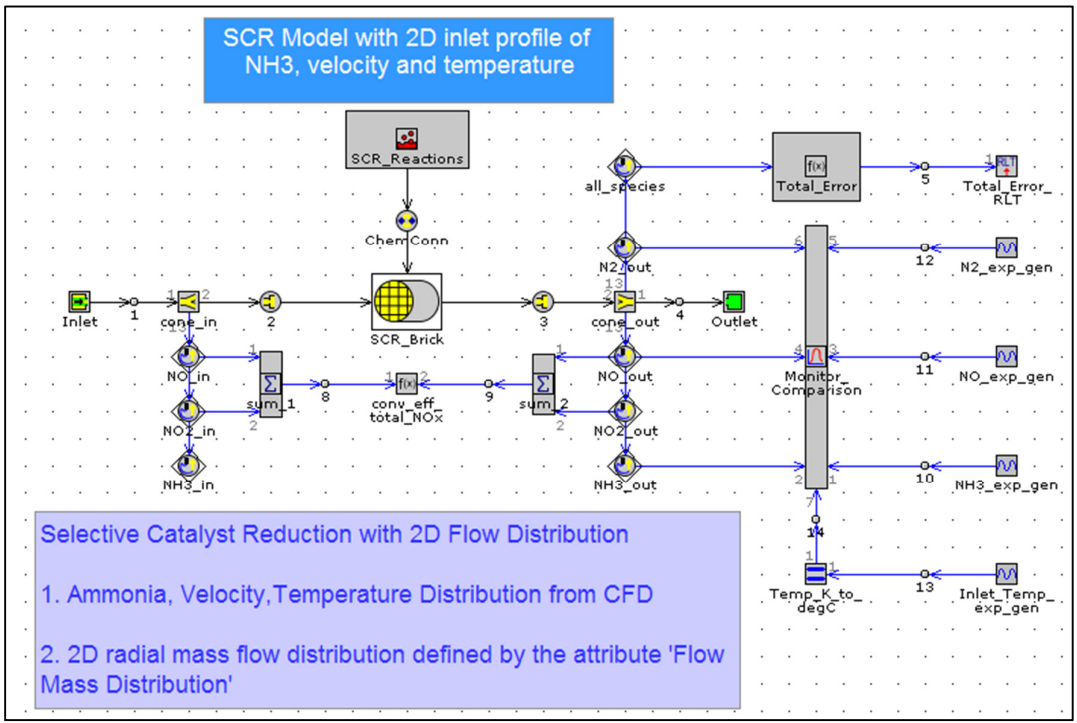

from CFD even deposit effect.

Figure 3.54. 1D modelling of the selective reduction catalyst

The 1D model is coupled with 3D CFD and developed a script for deposit mapping. 3D CFD simulation data for NOx distribution with deposit map for injection mass are used by 1D model. The 3D data that are passed to the 1D analysis include the species concentrations, temperature, pressure and velocity. Deposit map corrected the urea species and deposit that was accumulated in aftertreatment system. These values are used to solve mass conservation and surface reactions, the 1D model returns the gas concentration at the SCR exit. To improve the accuracy of the result, the SCR catalyst inlet is discretized into several geometrical sectors that are described previous chapter. These steps are described in Figure 3.55.

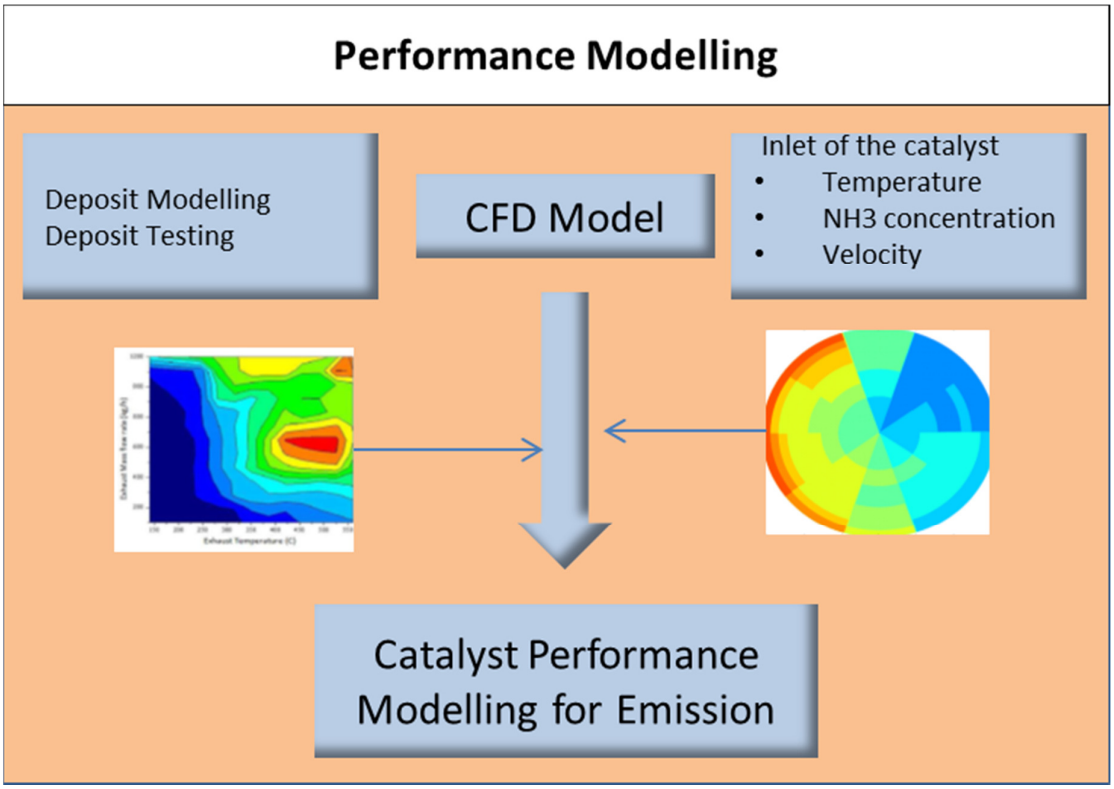

Figure 3.55. Perfomance Modelling Methodology

4. RESULTS AND DISCUSSION

In the present chapter, validated evaporation and thermal decomposition models are implemented to simulate the UWS conversion to ammonia in inline exhaust aftertreatment system. The simple cases were runs and validated againt literature result and experimental result.

The RSM (Reynolds Stress Modelling) turbulence modelling, multi-component spray approach and multi component chemistry have been developed in previous chapter and implemented in current aftertreatment system. The following simulation results are correlated with flow test bench results. The deposit results from CFD were correlated with flow lab deposit image processing results. The correlated results were passed to 1D emission modelling. 1D emission modelling are compared with engine test bench result. All the simulations were done critical emission point that can be seen in Figure 4.1.

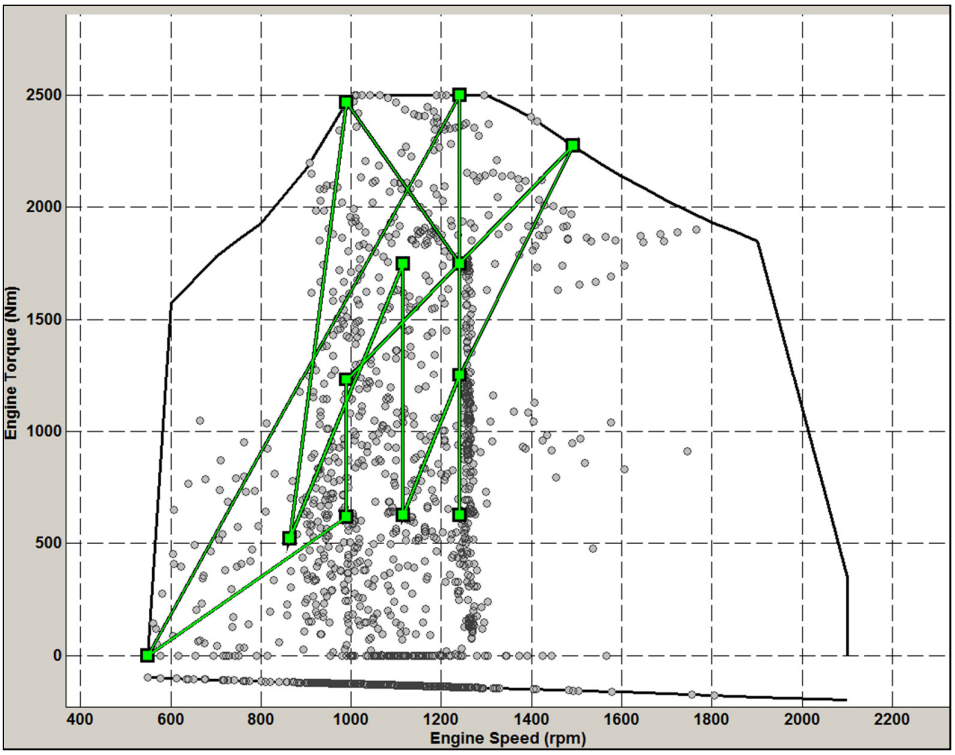

Figure 4.1. Operating conditions of deposit work

These points are World Harmonic Cycle Test point. The emission modeling ran under these conditions with combined modeling technique to asses the emission level of the system. This methodology provide the design changes on the emissions.

4.1. The Results of 3D SCR Simulation

Three dimensional (3D) simulation of inline exhaust aftreatment system with spray injection of UWS, evaporation and thermal decomposition processes have been presented results in the present chapter using Star-CCM. The deposit prediction of the CFD result were correlated with flow lab image processing. Then the deposit mass increased and ammonia mass flow rate are reduced based on the flow lab test results. The correlated values of ammonia are passes to emission prediction model.

4.1.1. The Flow field results

The acurate flow field prediction is required. Because all the modeling such as spray, deposit based on the flow field simulation. The different mesh types, number and turbulence models were experimented to get accurate solution. The comparison of

simulation and measurement for the flow field components is given in this section. The velocity in the main flow direction is shown in Figure 4.2. The simple validation cases used k-e turbulence model. LES did not used due to computational effort and cost. DES did not suitable turbulence model for in pipe application. The exhaust pipes consist of bends, mixers that built the swirl structured flow. k-e turbulence model could not predict swirl effect well. Reynolds stress turbulence models capture the swirl flow.

The flow direction is down to top. In the center of the pipe a low velocity region can be observed which is stable in the measurements down to the inlet cone of the catalyst. Due to mixer blade the vortex region can be observed.

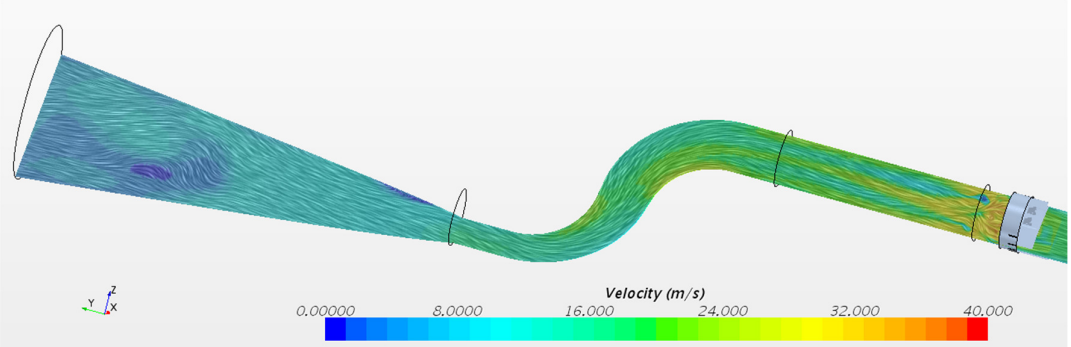

Figure 4.2. Velocity distribution for RMS model

The mixers enhance the flow distribution along the exhaust aftertreatment system. The swirl structure flow was observed after the mixer in Figure 4.2 The velocity becomes very low due to cones diameter.

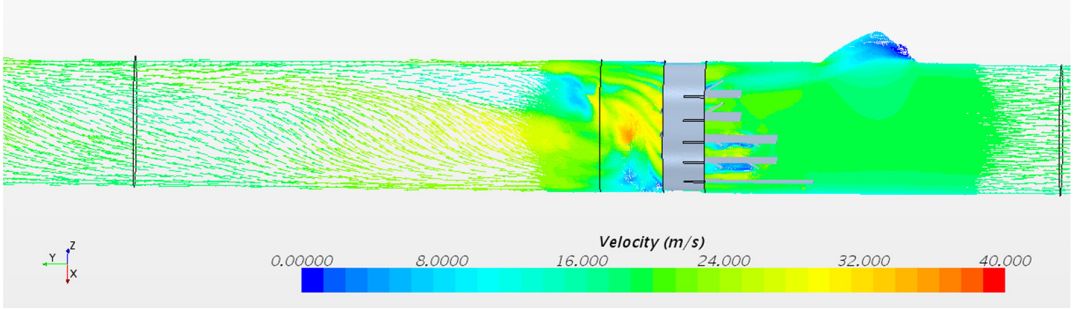

Figure 4.3. The velocity vector along the sections of the system

4.1.2. Spray particles distribution

UWS spray injection into the gas flow is shown in Figure 4.5. The individual droplet parcels follow the streamlines of the gas flow. Indeed, the gas momentum deviates the spray droplets in the flow direction towards the SCR catalyst. CFD spray models have been developed to predict the spray transport phenomena inside the exhaust pipe. Spray modeling was correlated PIV test data and literature work. This correlation was implemented to current model. Droplets are modeled as clusters of droplets which interact with exhaust gas via mass dispersion, evaporation and heat transfer. This number of clusters were worked for sensitivity on the result. The current model 80 k clusters were used.

CFD shows that at higher exhaust flow rates, the axial acceleration of the particles tends to spread the impact of the spray over a large area down the pipe, thus reducing the flux of urea onto the pipe wall per unit area. With higher exhaust mass flow rate, therefore CFD results agree with the trend of higher maximum injection rate without causing wall wetting.

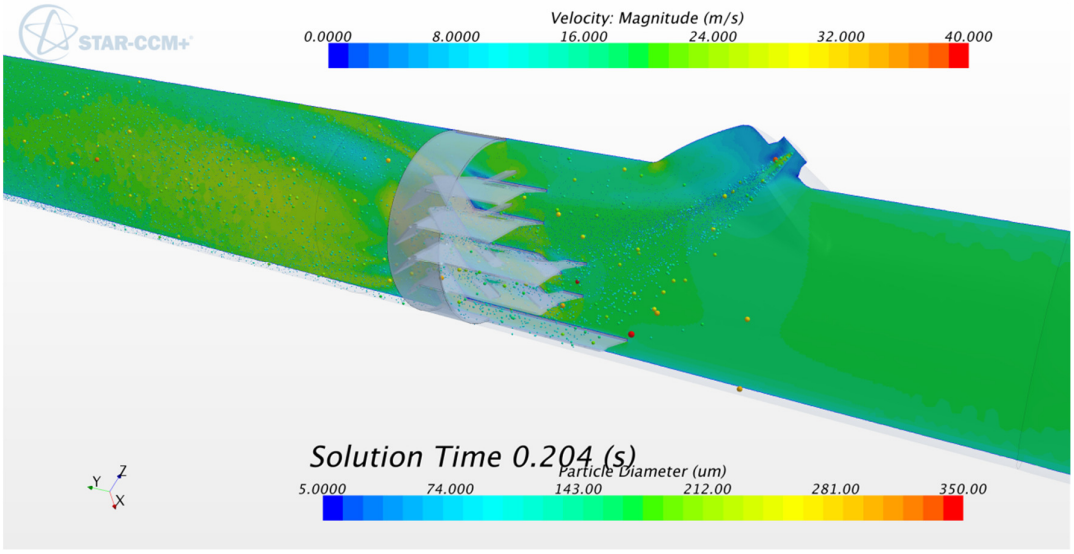

Figure 4.4. Droplet Distribution into the system

Figure 4.6, Figure 4.7 and Figure 4.8 display particle trajectories colored by diameter at different time step. The reason that downstream the exhaust line some particles still contain water may be due to the relatively low gas temperature and/or the short residence time which is related to the distance between the injector and the monolith reactor. Figure 4.11. shows the aqueous-urea diameter in droplets. According to this figure, due to the decomposition, aqueous-urea diameter decreases. However, as the decomposition is not complete, there are still a lot of droplets with high mass fraction of aqueous-urea, especially near the SCR monolith.

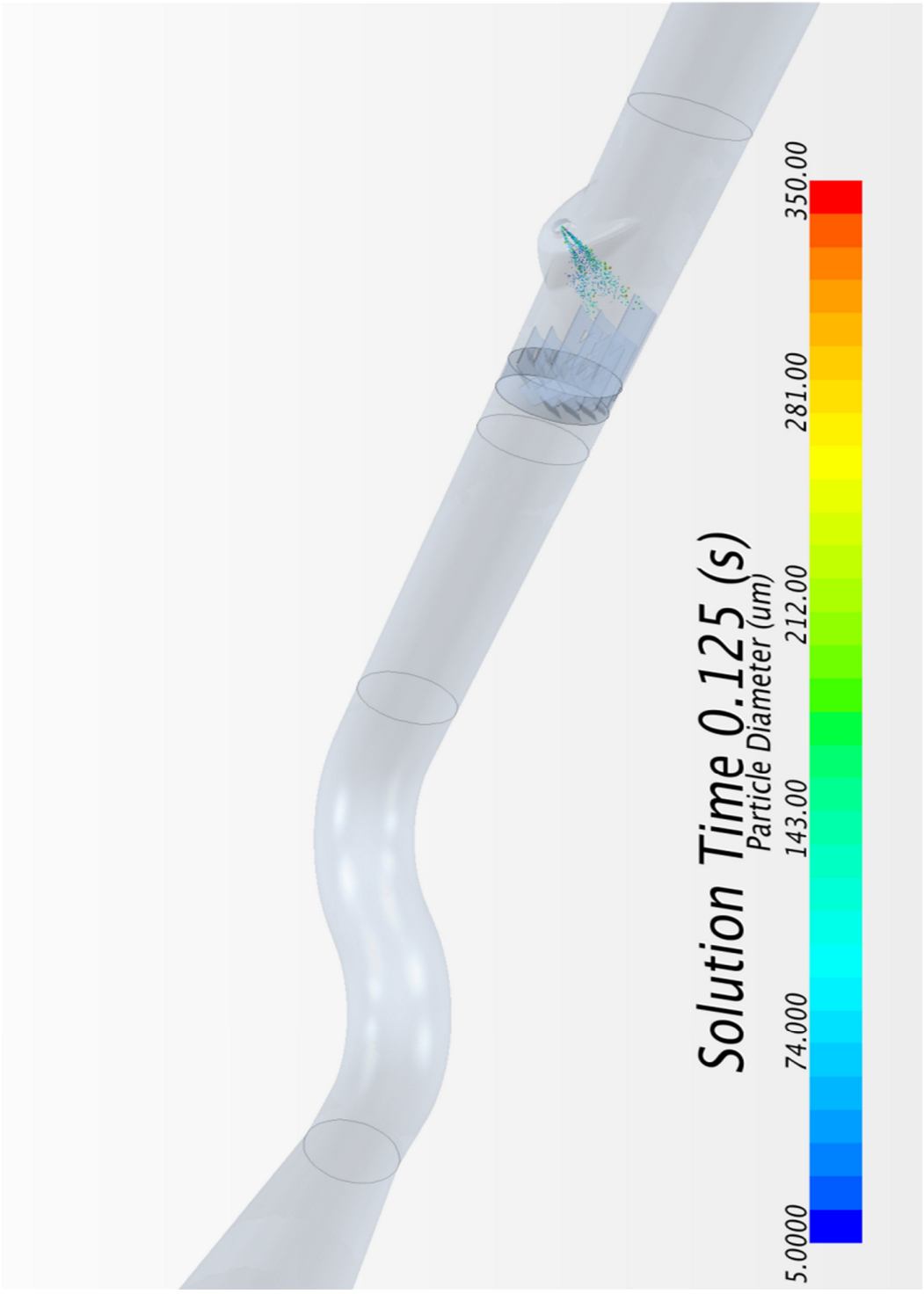

Figure 4.5. Droplet Distribution across the system at 0.125 s

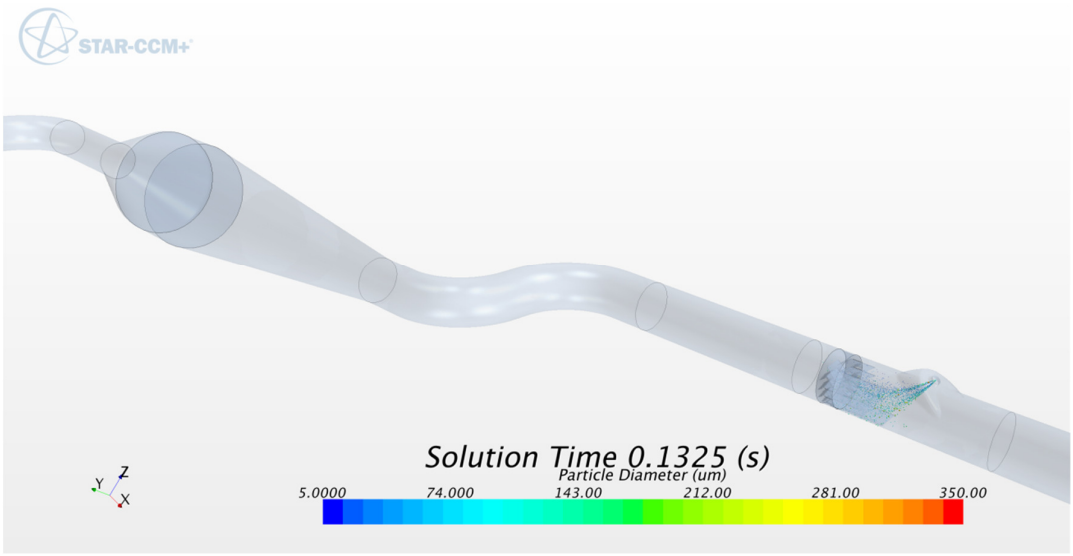

Figure 4.6. Droplet Distribution across the system at 0.1325 s

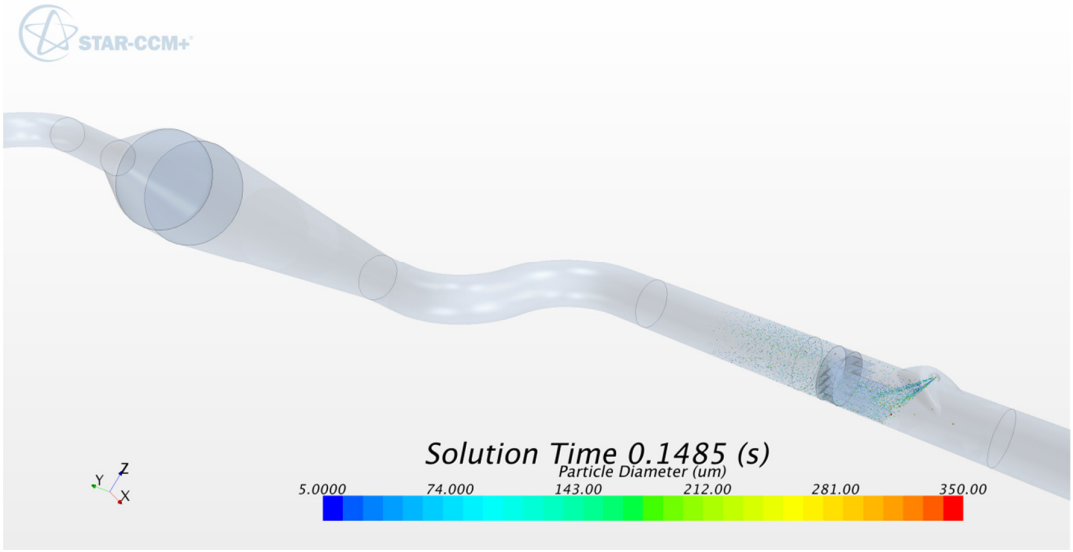

Figure 4.7. Droplet Distribution across the system at 0.1485 s

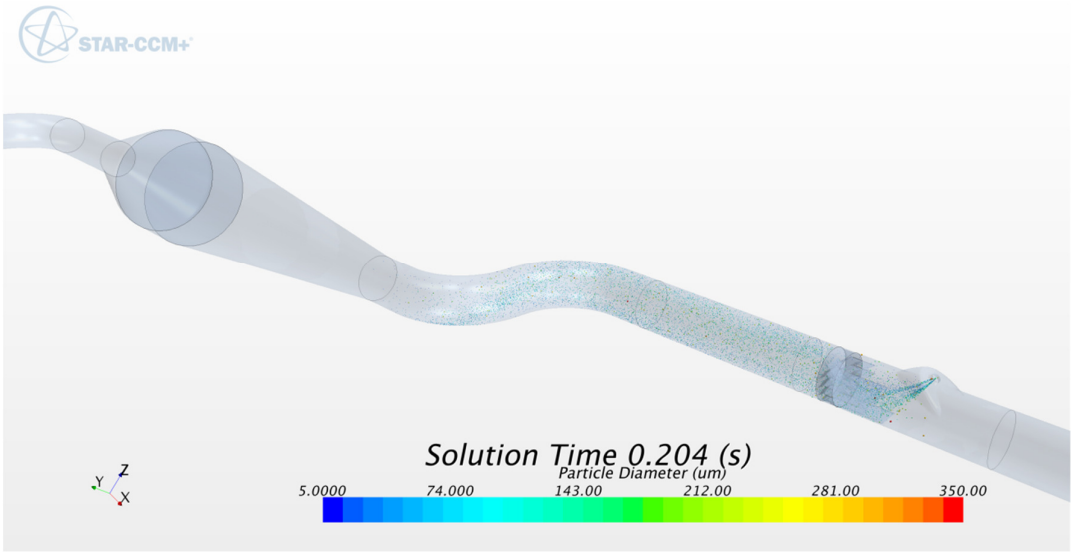

Figure 4.8. Droplet Distribution across the system at 0.204 s

The effect of in-pipe mixing devices with mixers installed in the inner pipe wall usually downstream of the injector to promote droplet evaporation, breakup and distribution of the spray. The mixer has significant effect on the break-up process. Figure 4.9 shows the application of mixer.

The following results shows the droplet distribution along the exhaust aftertreatment system for different time steps.

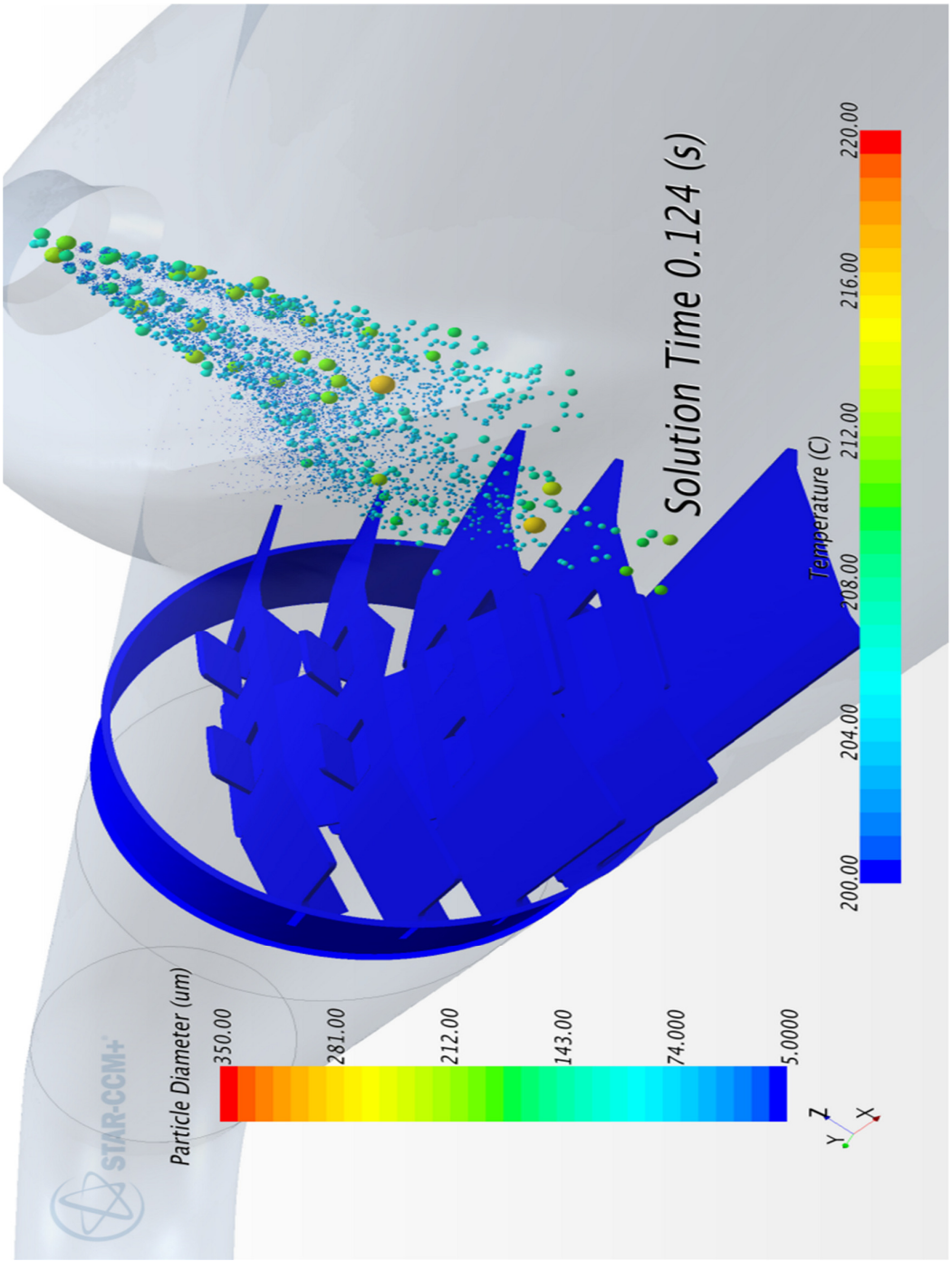

Figure 4.9. Droplet distribution through the mixer at 0.124 s

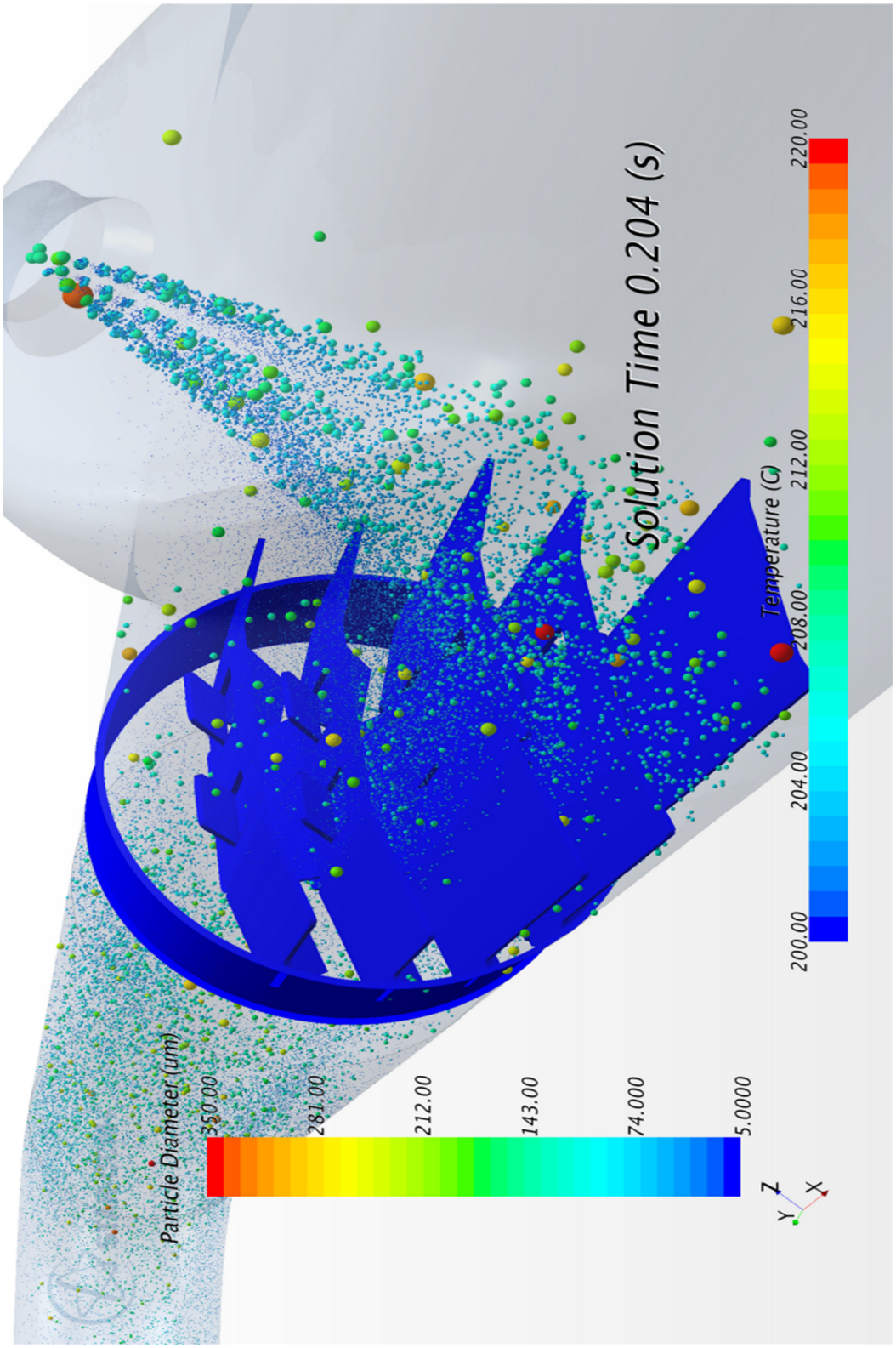

Figure 4.10. Droplet distribution through the mixer at 0.204 s

The results were plotted at the time step when the urea dosing reaches the peak value across the face selection. Figure 4.9 and Figure 4.10shows the results of the urea injection.

It is seen that particles can reach the SCR catalyst without complete decomposition. According to Figure 4.11, droplets reaching the SCR monolith contain approximately 68.8% of aqueous-urea. It means that during the passage in the exhaust line, less than 31.2 % of aqueous-urea has been decomposed. The reasons may be again the low gas temperature and/or short residence time. In practice, one way to ensure the successful evaporation and decomposition is to add a urea mixer in the exhaust line. However, at low temperature conditions, undesired deposits may form on the blades of the mixer.

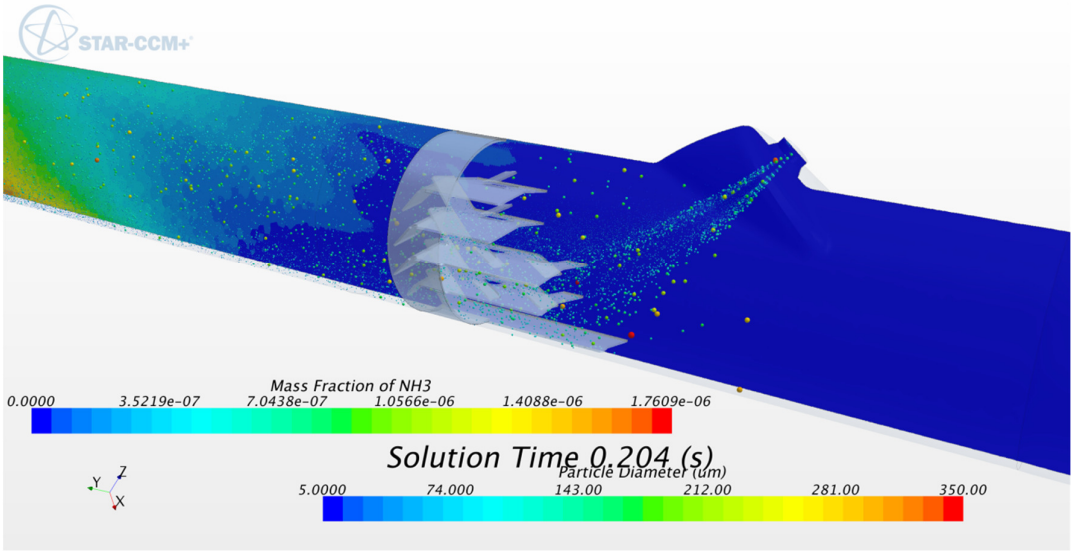

Figure 4.11. Droplet distribution along the system for time 0.01s

Figure 4.30 show droplet diameter at the upstream and downstream of the mixer. This result show us mixer's efficency in terms of the droplet breakup process. The flow cannot break up the spray particles in such reduction. This mixer reduced the droplets %50 reduction of the size.

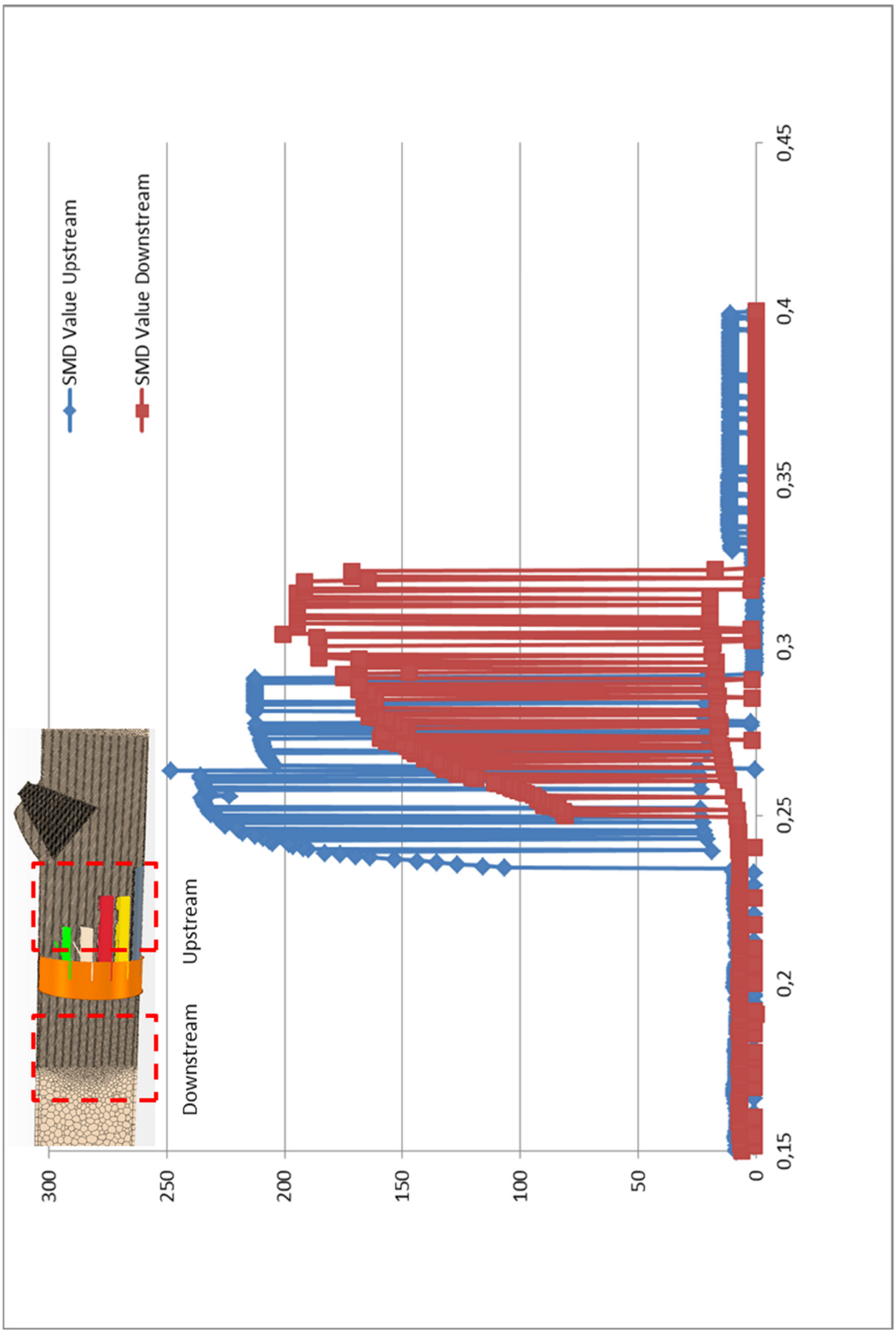

Figure 4.12. SMD Value for Upstream and Downstream of the Mixer

Hence, ammonia is produced from these droplets which are closer to the SCR monolith. Consequently, in mixer usage application more concentration of ammonia is observed near the SCR monolith. The counts of the droplet are higher

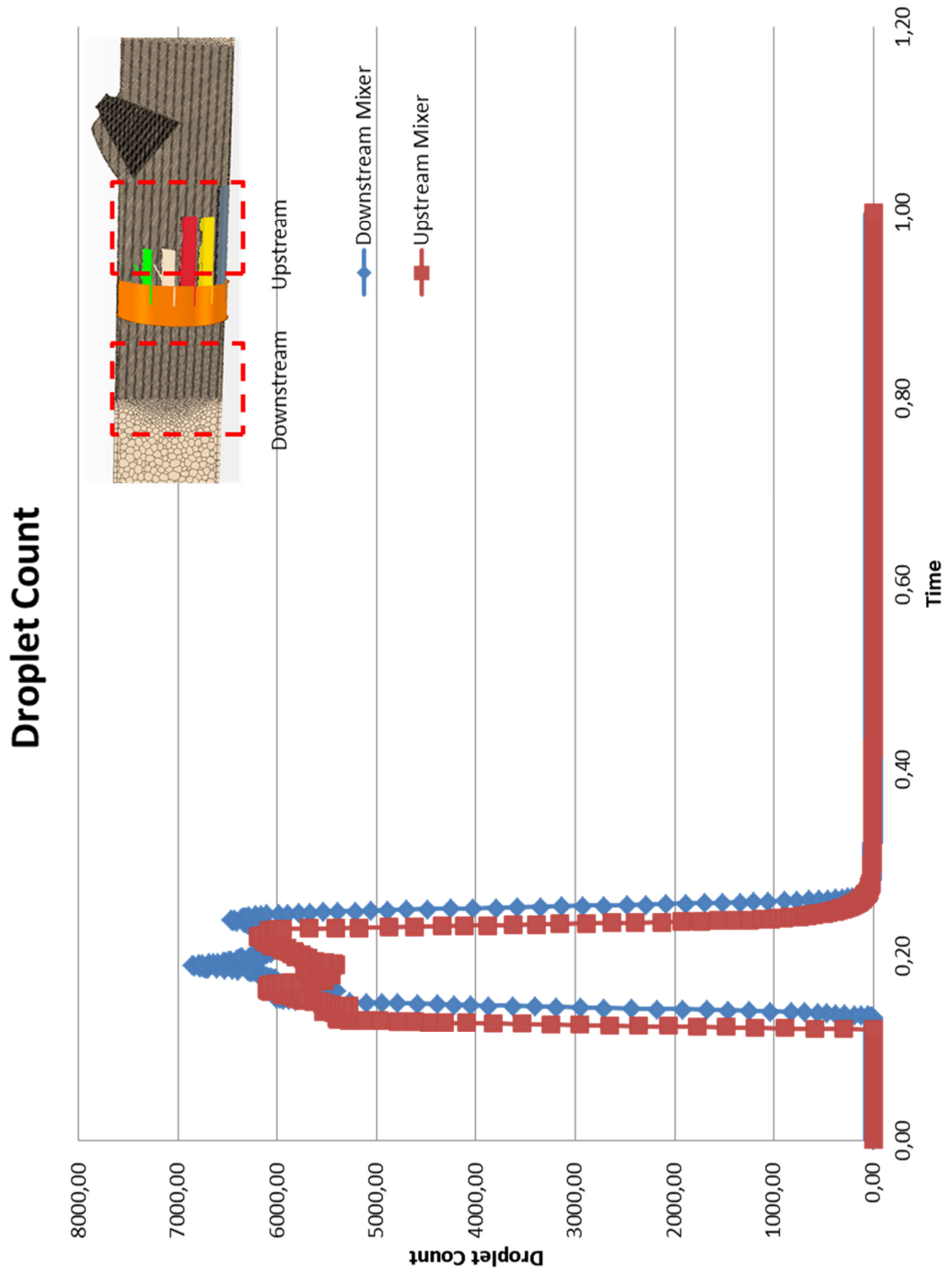

Figure 4.13. Droplet count upstream and downstream of the mixer

4.1.3. Temperature distribution

This conjugate heat transfer are modelled to account for heat transfer between liquid droplets and wall. Thus the formation of a wall film can be calculated precisely as well as the secondary breakup of droplets at the wall. Spray impingement on hot surfaces, as mixing elements or the exhaust tube walls, can lead to a better spatial distribution of the reducing agent due to thermal breakup. This also yields better conversion to ammonia, because small droplets with an enhanced heat and mass transfer are generated. Additionally heat is transferred from the hot surface to the droplets during contact and accelerates evaporation.

Pipe wall temperature and mixer temperature influence the deposit formation, was used in conjunction with spray information to predict deposits. Hence, surface thermocouples were attached to the wall to monitor the outer skin temperature and monitor surface temperature of the pipe in CFD model.

The heat transfer coefficient of the pipe wall was 10 W/m2K. Therefore, such a low resistance would result in a negligible change in temperature from the outer to the inner surface of the pipe. With radiation, the outer pipe wall is expected to cause significant radiation heat loss. But in this case insulation materials was used to reduce heat loss and retain pipe wall temperature.

It is observed that mixers not only mix urea spray effectively, also mix enthalpy effectively via enhanced convective heat transfer as a result of strong turbulence. From lab tests, it is found that in-pipe mixers are able to distribute heat from the exhaust gas to wall effectively in cross-sectional direction.

Figure 4.14 and Figure 4.15 show temperature is affected by evaporation and thermal decomposition processes. The evaporation is known to be an endothermic phenomenon. Moreover, although there are some exothermic reactions in the set of reactions mentioned in previous chapters, the overall decomposition reaction is endothermic.

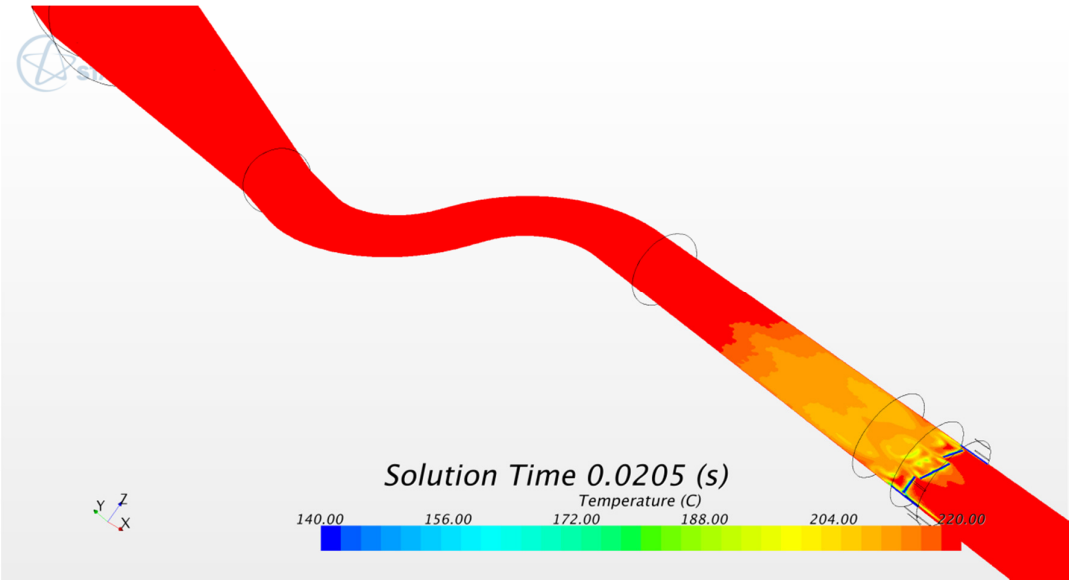

Figure 4.14. Temperature variation along the system due to process

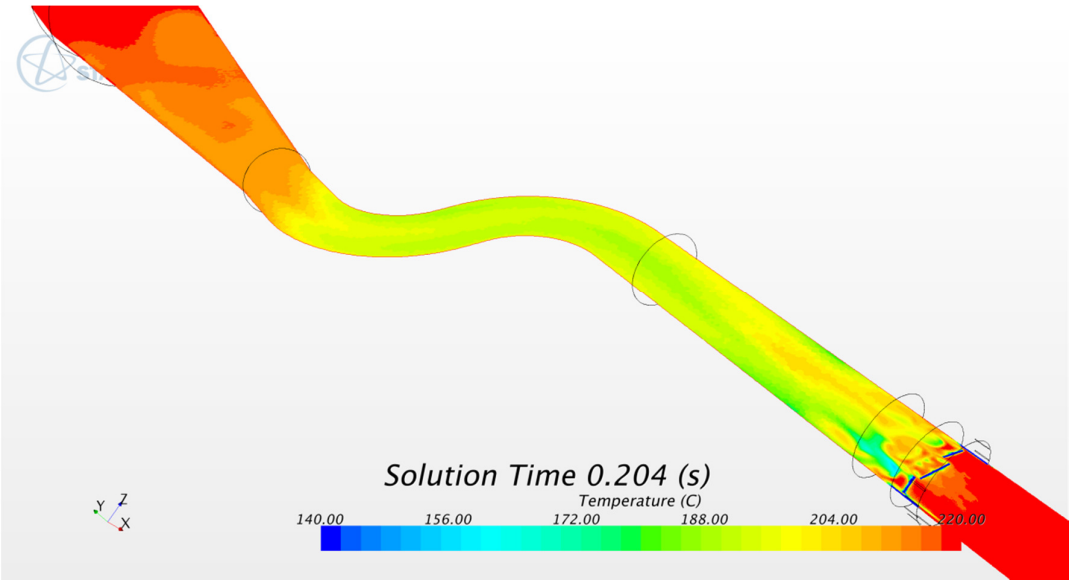

Figure 4.15. Temperature decrease due to evaporation process

Particles decrease the temperature of the gas . It is shown that the maximum decrease in gas temperature is about 60 degree C. The cooling effect due to the adblue injection induces a temperature drop. This cooling phenomenon can adversely affect the decomposition rate. The temperature decreasing region is increased in advance time due to increasing evaporation. Water vapor mass fraction and corroborates the mentioned

phenomenon: in regions with higher concentration of water vapor, lower gas temperature is obtained due to evaporation.

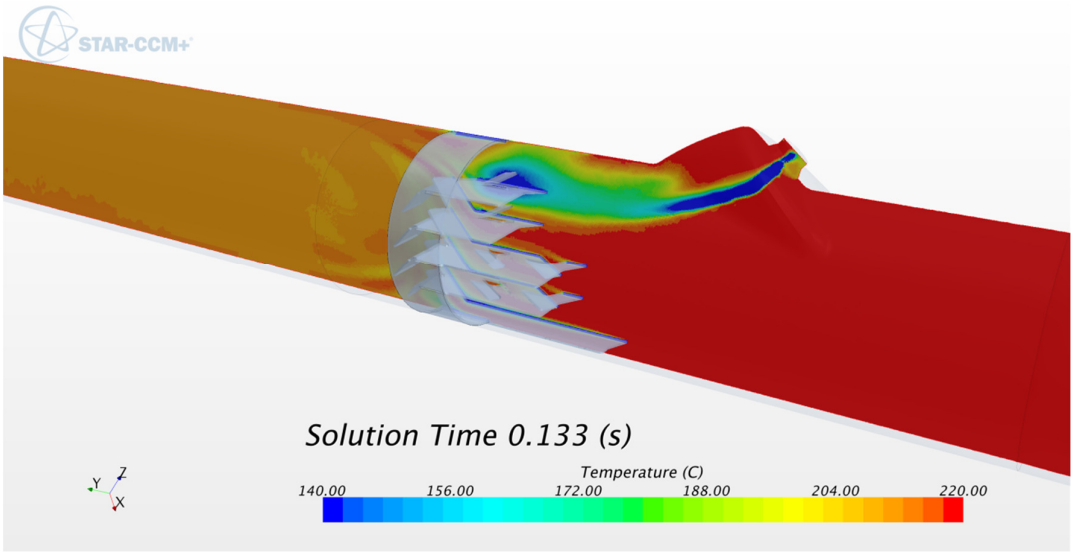

Figure 4.16. Temperature cooled down due to evaporation

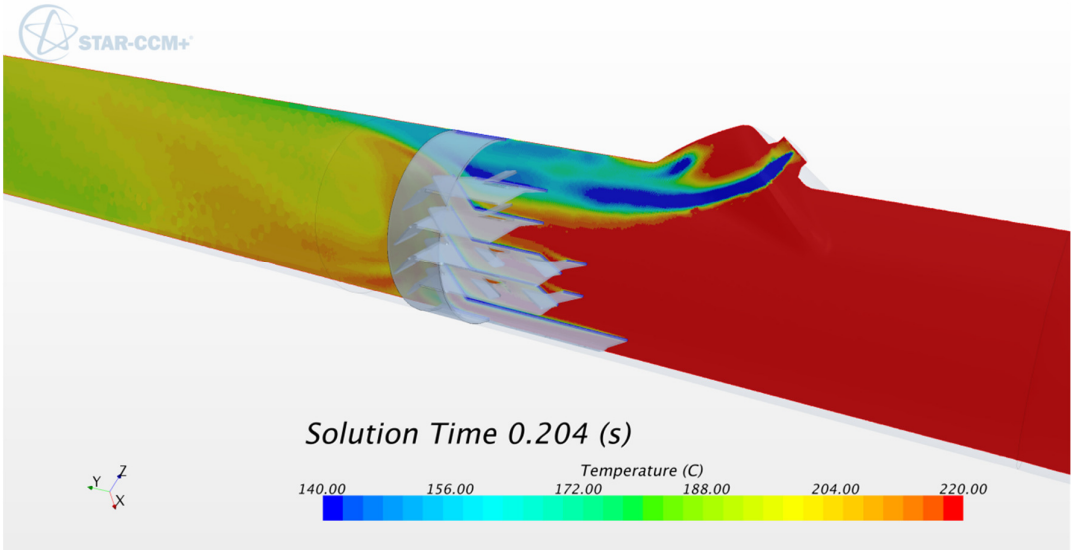

Figure 4.17. Temperature cooling down due to evaporation

Figure 4.18 shows the heat transfer rate for pipe and mixer

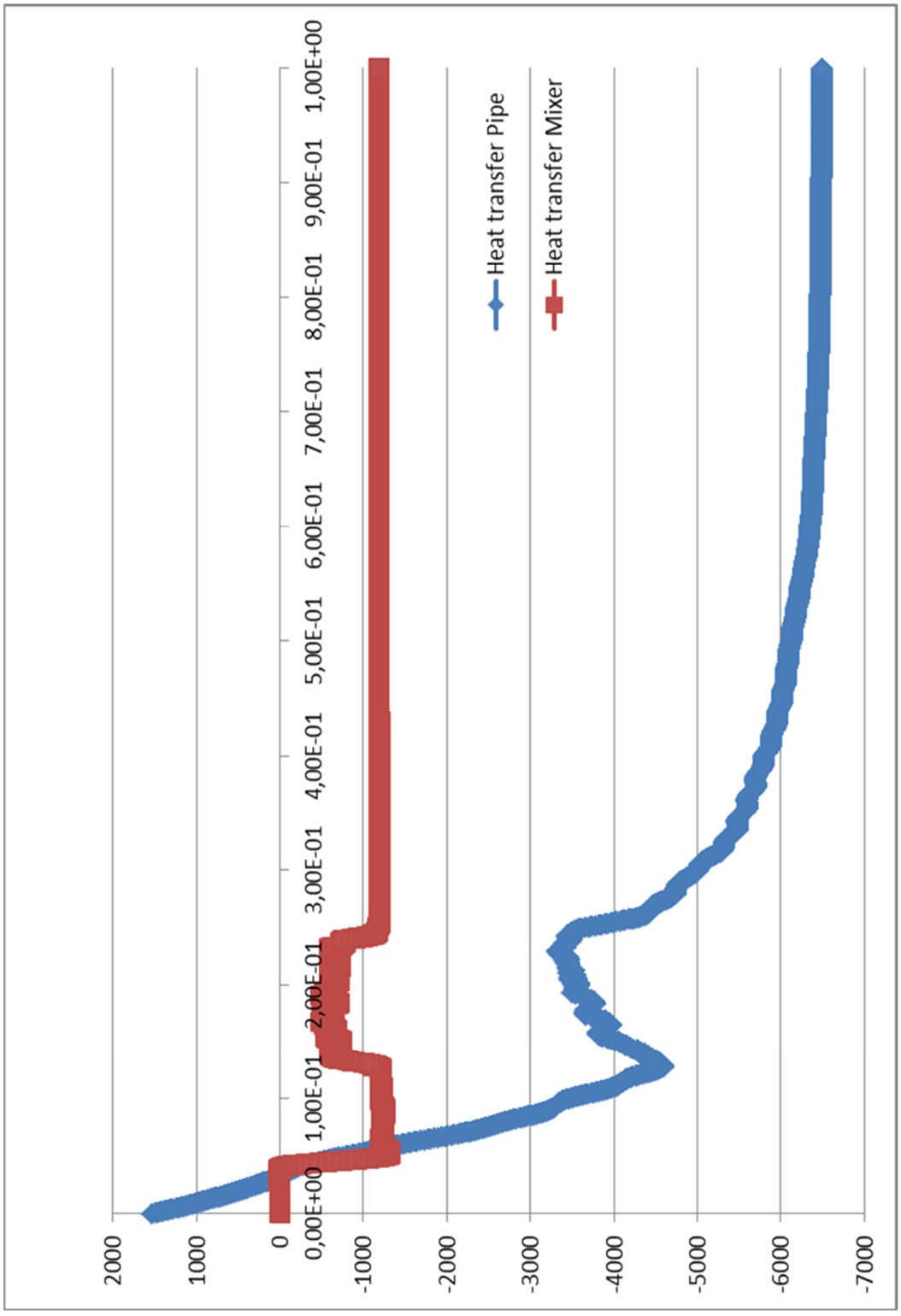

Figure 4.18. Heat Transfer on the mixer wall

4.2. Deposit Formation

Depending on different exhaust configurations, design layout and injection specifications, droplets impinging the exhaust wall may form a liquid film and/or a solid deposit.

Spray wall interaction model was developed for UWS and found out that spray impingement on hot surfaces can lead to a better spatial distribution of the reducing agent due to thermal breakup. [71] Better conversion to ammonia occurs due to the generation of small droplets with an enhanced heat and mass transfer. Additionally heat is transferred from the hot surface to the droplets during contact and accelerates evaporation. As the film is transported downstream in regions with less spray impingement, the evaporation of water from the film leads to higher urea concentrations. After evaporation of water is completed; thermolysis of urea begins in these areas. Spray impact also results in cooling of surfaces and can lead to wall film formation if the surface temperature decreases below a critical value. Deposit location is predicted with CFD calculation. The results was compared with test data. CFD is well tool predict deposit location. But CFD can predict deposit mass with lower value. In further chapter deposit mass from CFD was corrected with image processing result from endoscope.

Figure 4.19 shows the UWS spray and UWS deposited on the wall. aqueous-urea. This result shows that the deposit can form after the spray directly hit the surface. According to Figure 4.20 and Figure 4.21deposit form reduces the temperature of the mixer blades. Isocyanic acid on the mixer change the form of the deposit from melamin to ammelide.

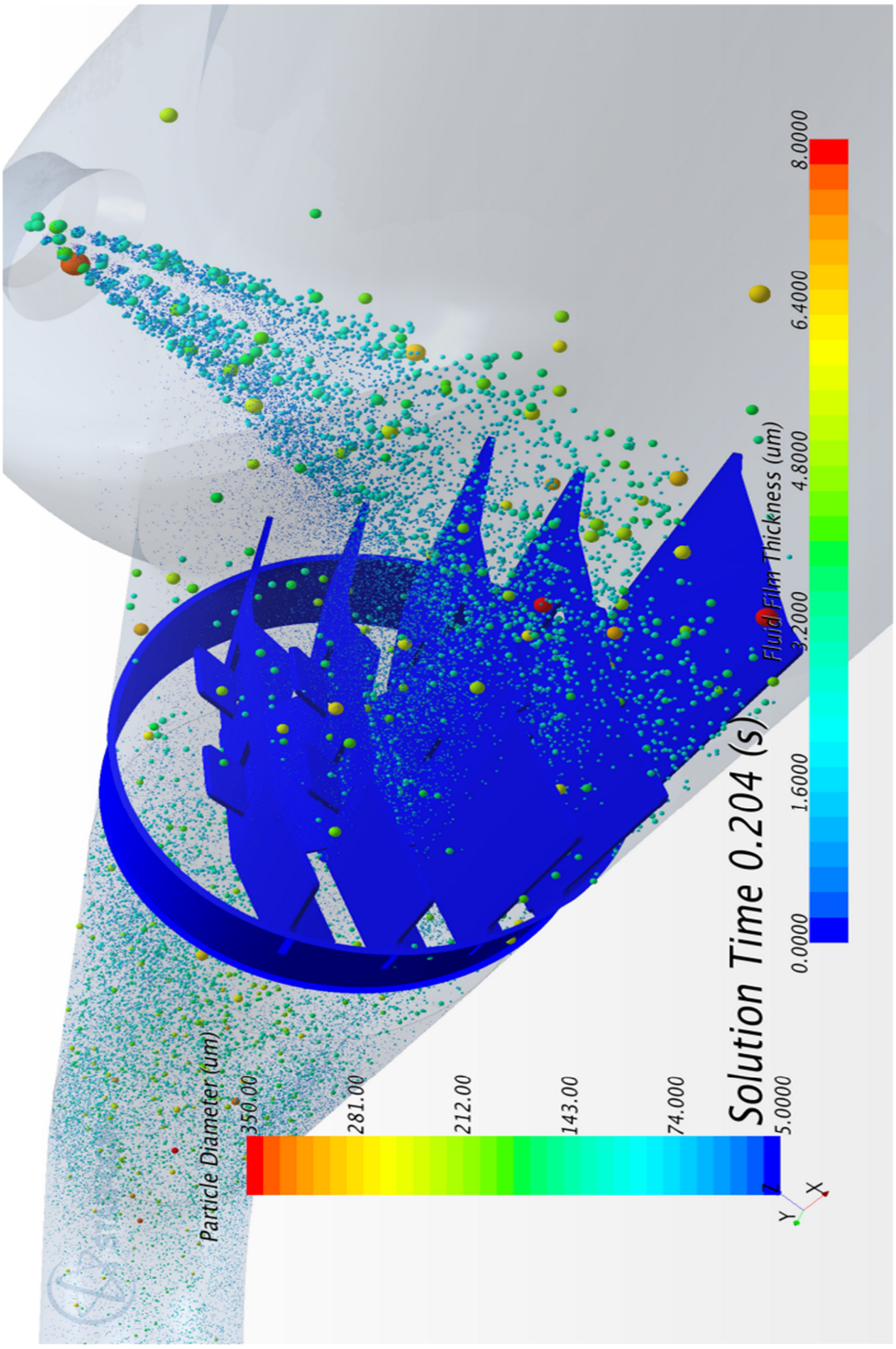

Figure 4.19. Deposit formation where the spray hits

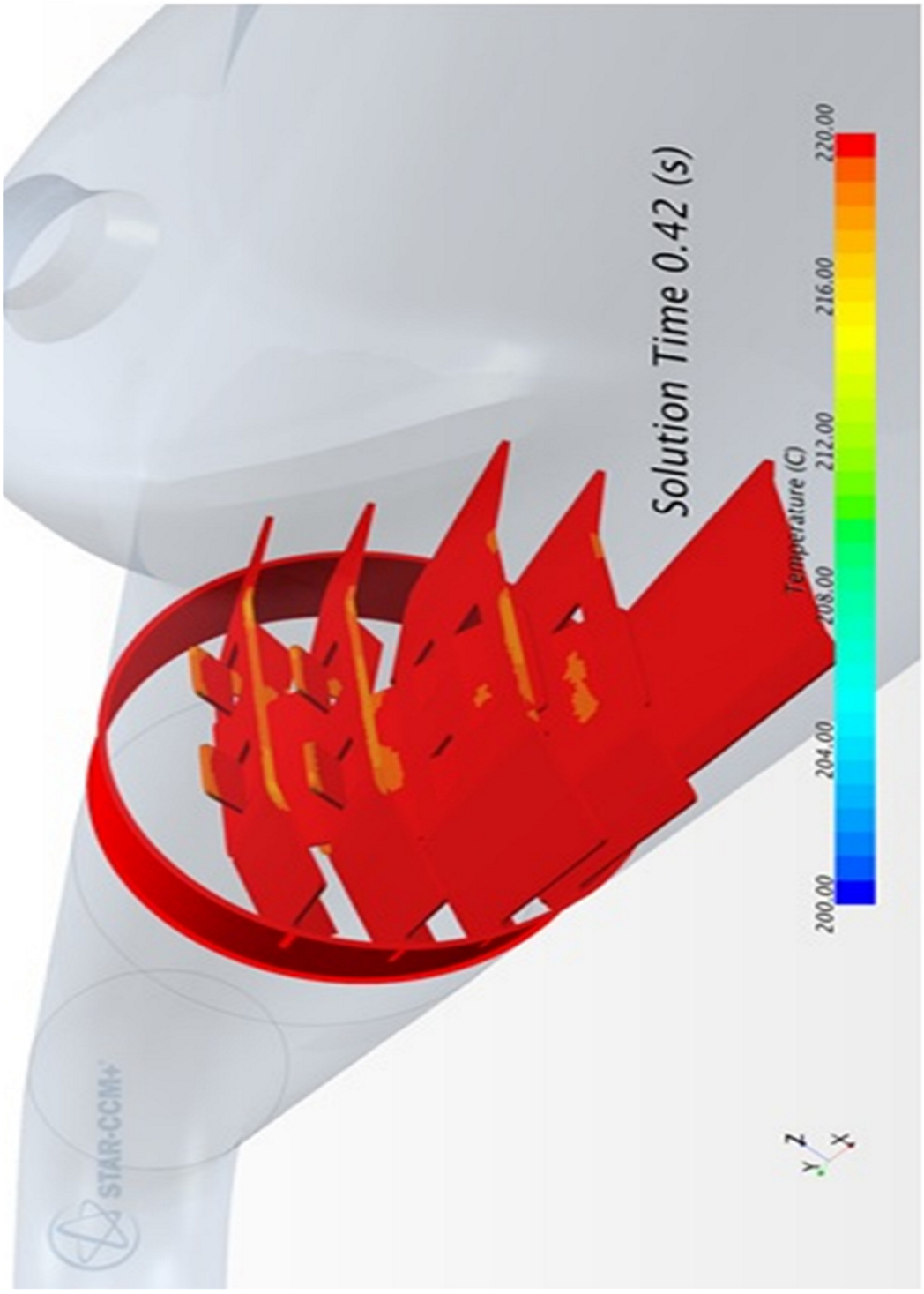

Figure 4.20. Temperature reduced on the mixer due to deposit

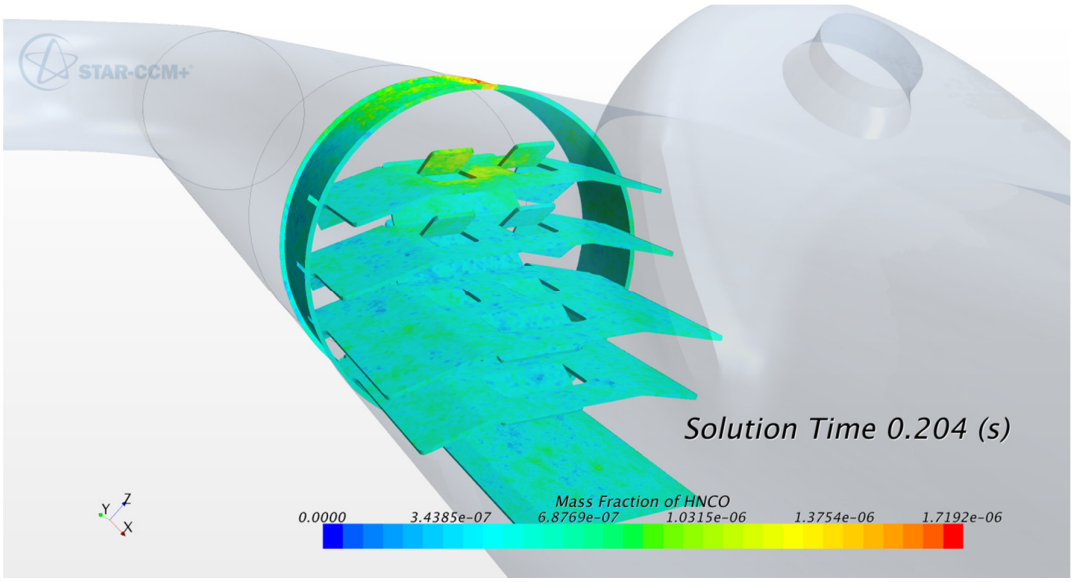

Figure 4.21. Isocyanic acid form more complex deposit

The results reveal that the particles deposited downstream of the injection contain accumulated the mixer blades. Figure 4.22. shows the deposit thickness on the mixer and Figure 4.23 shows the deposit accumulation on the system. The prediction location is well correlated with the test data but the mass is underpredicted.

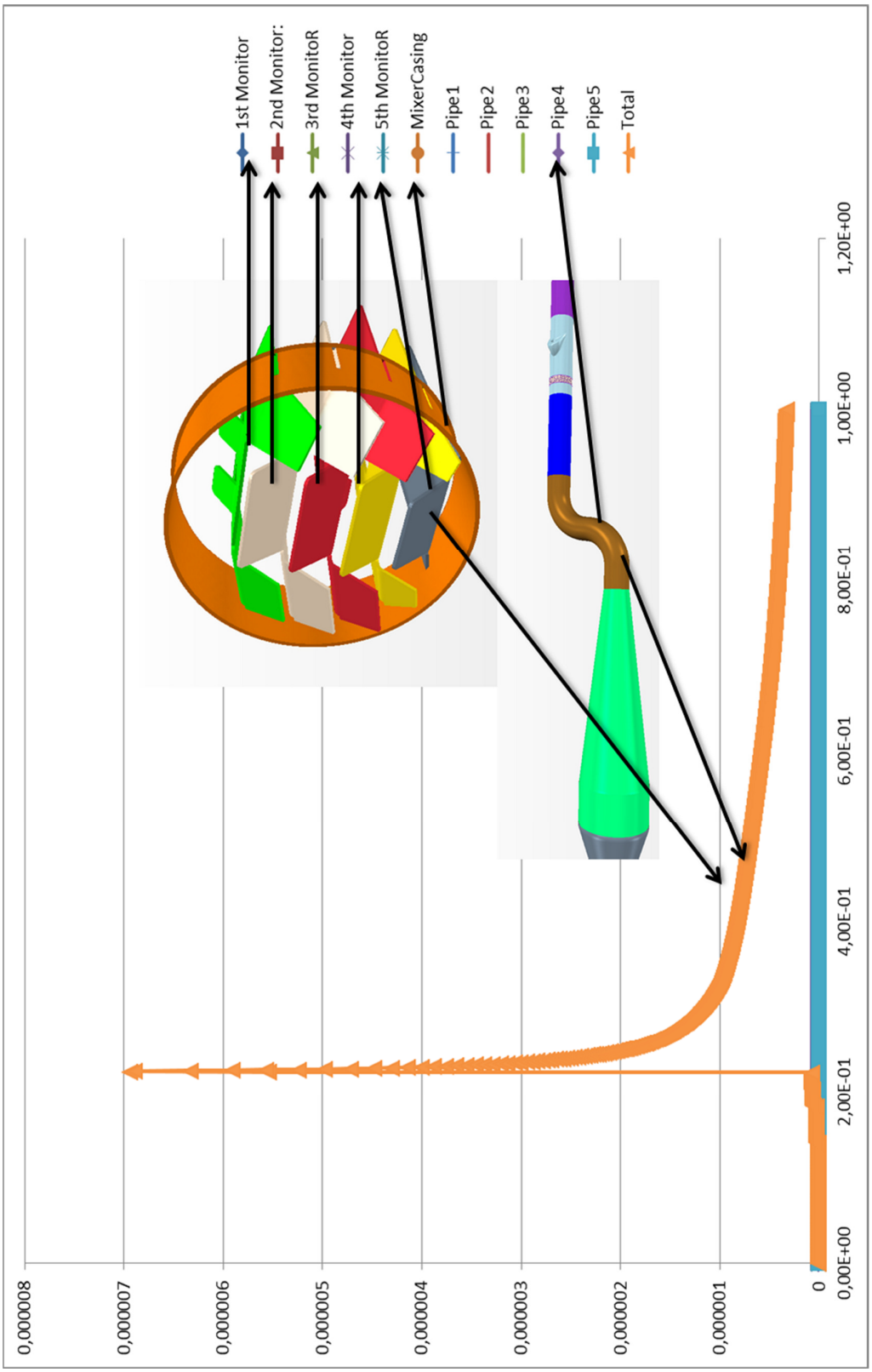

Figure 4.22. Deposit accumulation on the mixer

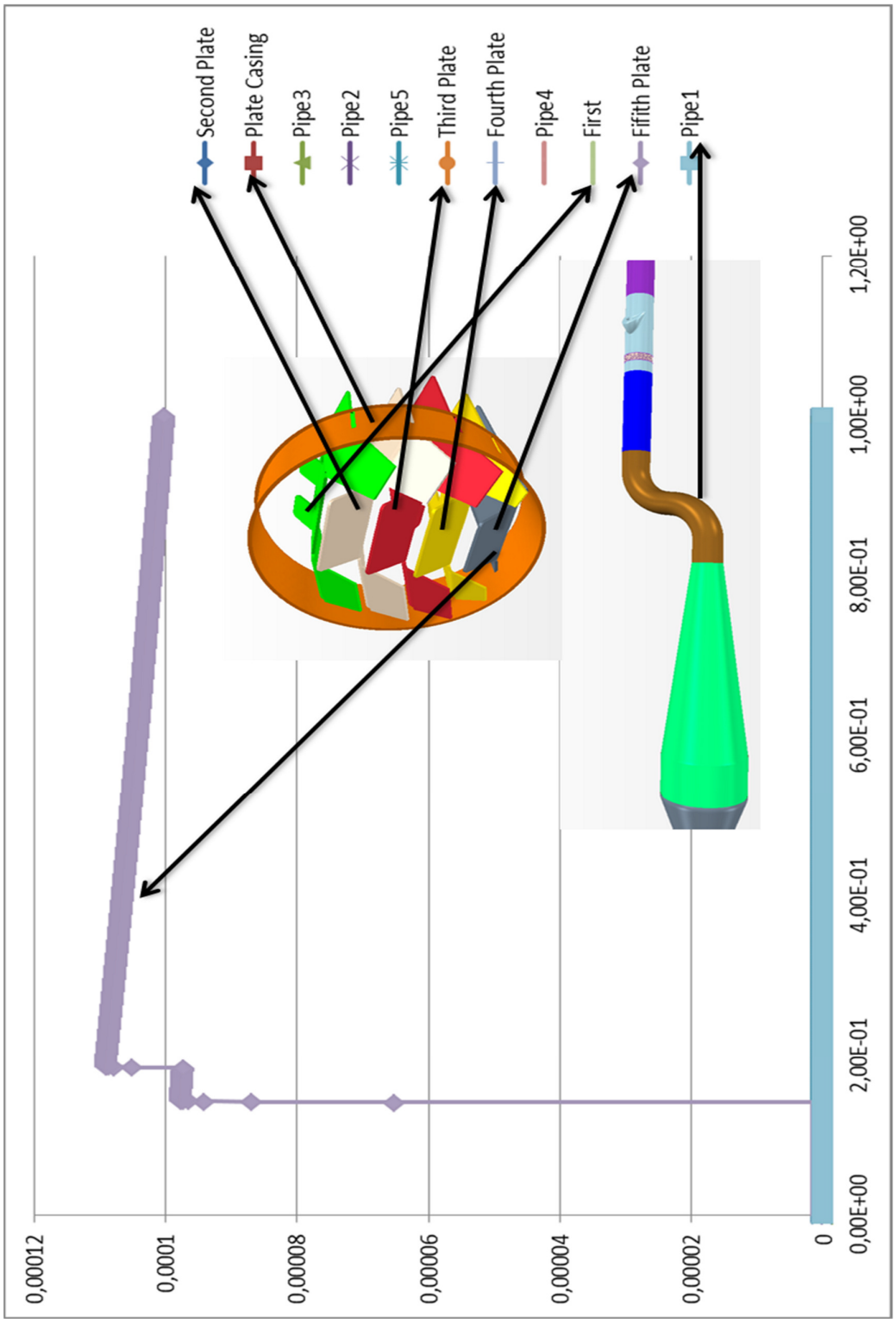

Figure 4.23. Mass Thickness on different region of the system

4.3. NH_3 distribution at the inlet of the SCR

In order to evaluate the parameters affecting ammonia production, the distributions of mean gas temperature, water vapor, ammonia and isocyanic acid are investigated in previous chapters. The contour plots are drawn at the inlet of the catalyst for different time intervals.

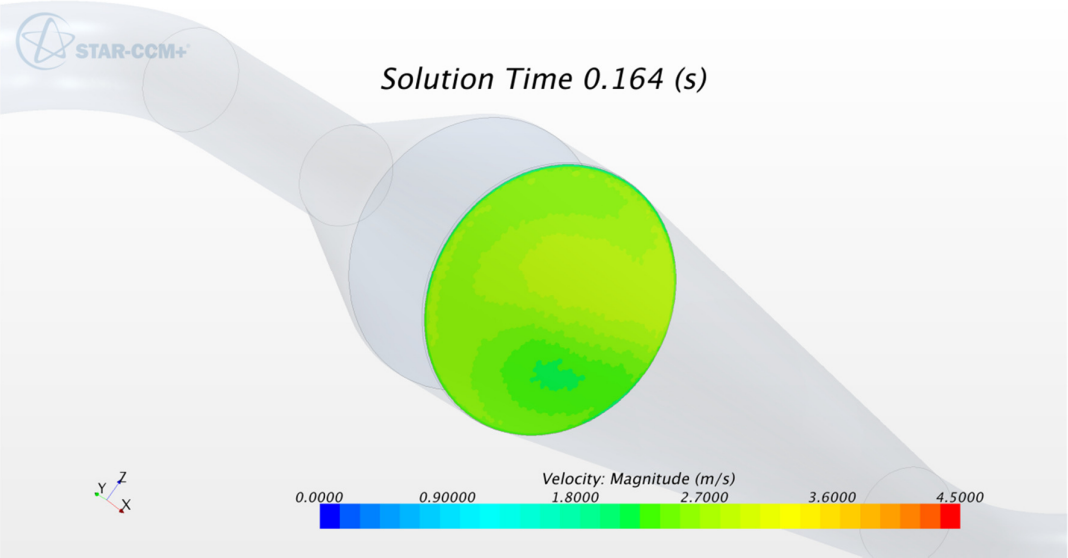

Figure 4.24. NH3 distribution at the inlet of the catalyst

The following results in

Figure 4.25, Figure 4.26 and Figure 4.27 shows the mass fraction contours of NH3 distribution on the face of 10mm inside of SCR inlet.

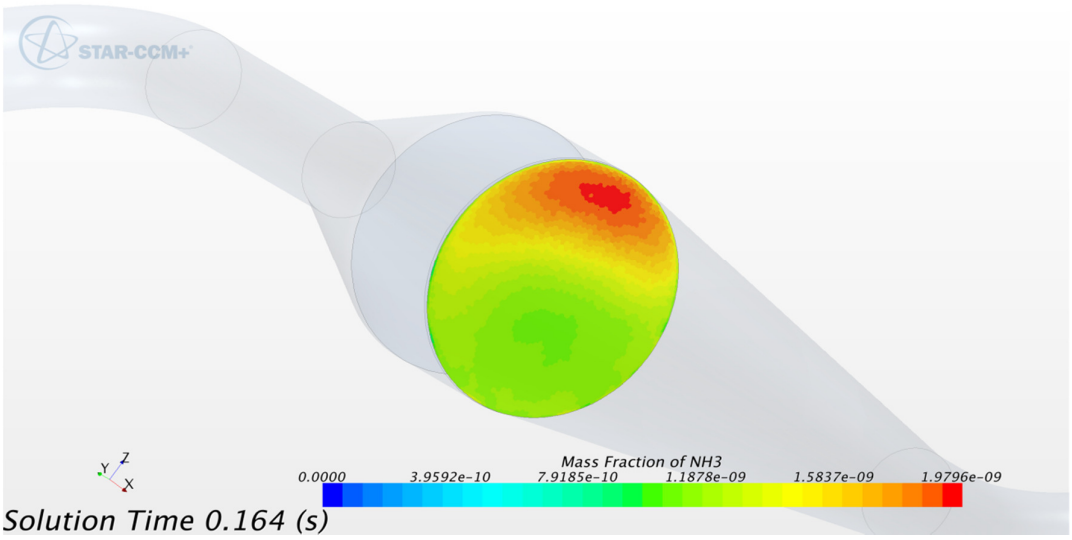

Figure 4.25. NH3 distribution at the inlet of the catalyst

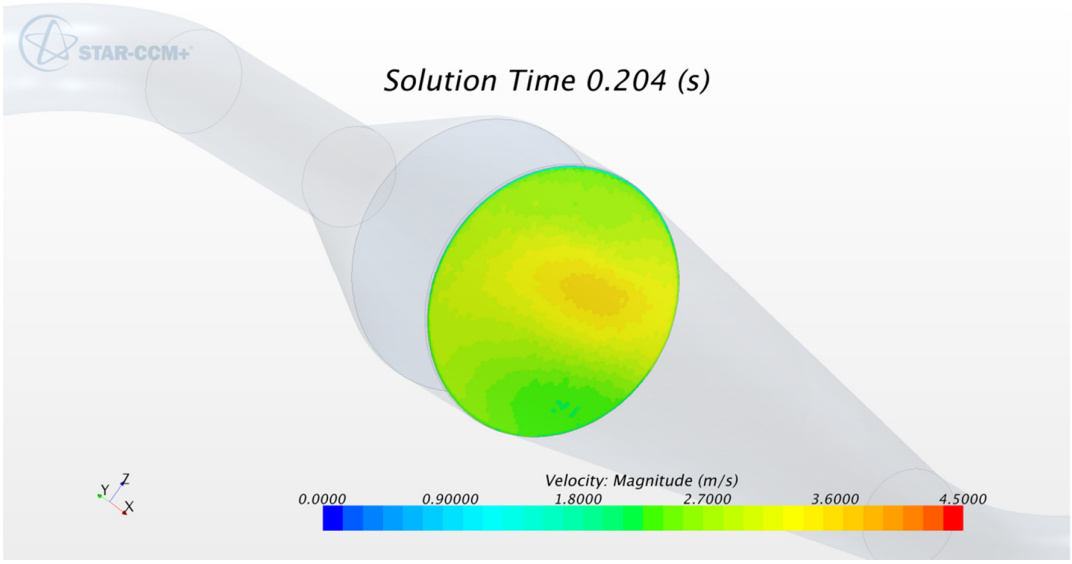

Figure 4.26. NH3 distribution at the inlet of the catalyst

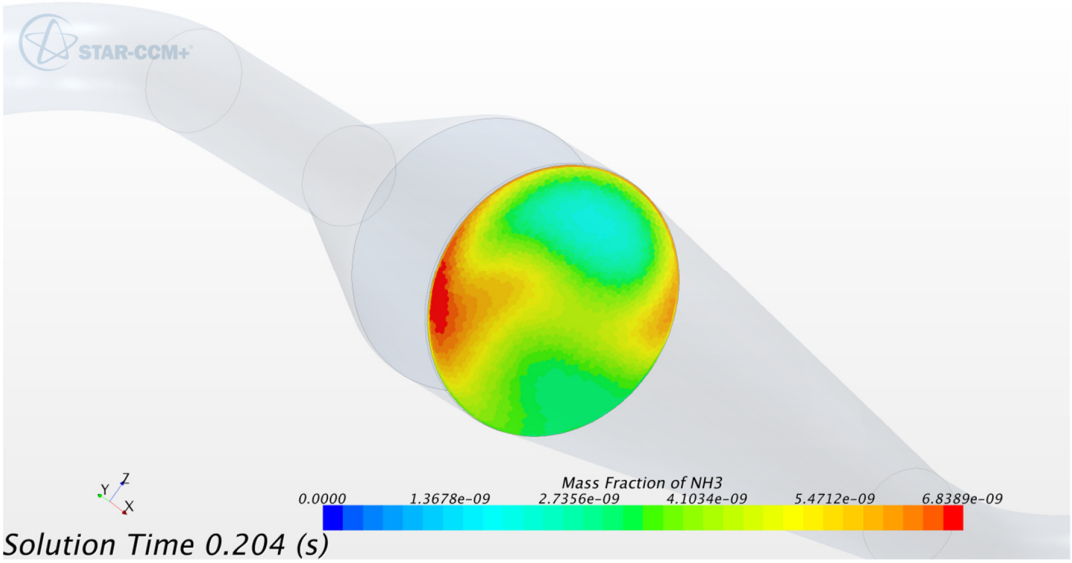

Figure 4.27. NH3 distribution at the inlet of the catalyst

The results were plotted at the time step when the urea dosing reaches the peak value across the face selection. Figure 4.28 shows the mass of the NH3 over the injection period. CFD could not predict mass deposit well. After the correlation with test result, depost mass is increased so ammonia distribution is decreased significantly. %25 mass is decreased at this operating condition. Hot operating condition with lower urea injection, deposit was not accumulated so mass of urea is not decreasing. This is the one of the worst operating condition in terms of deposit accumulation and mass of the ammonia.

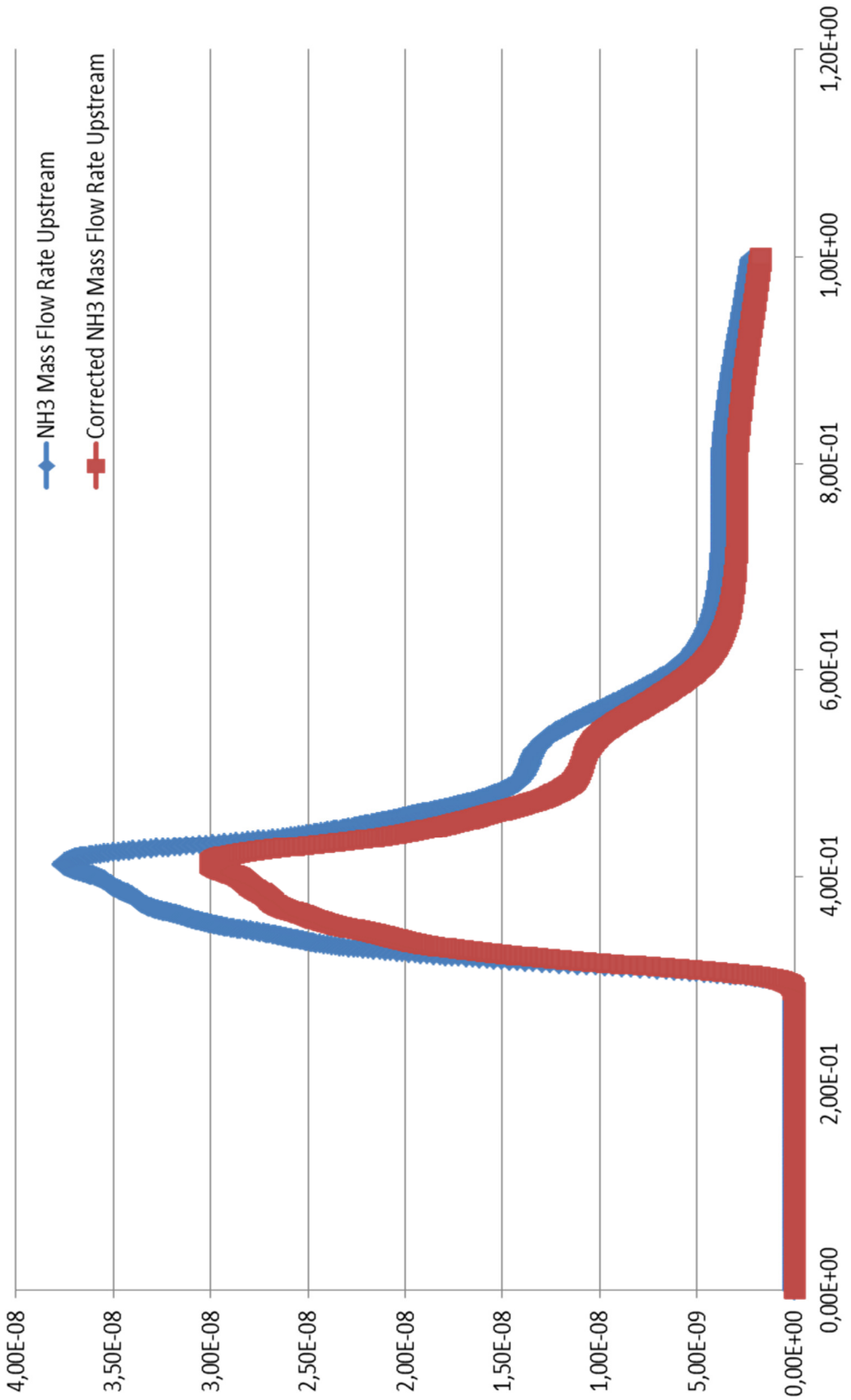

Figure 4.28. Mass of the NH3 at the inlet

Cold operating conditions with high mass of urea lead deposit accumulation into the system. CFD predicted deposit location but it cannot predict mass of deposit which influnce ammonia mass. After deposit correlation, we can obtain ammonia distribution significantly.

Beside of mass of the urea, another parameter quantify the species distribution across the SCR inlet face is uniformity index for velocity and NH3 whicj are defined below,

$$Gamma = 1 - \frac{1}{2}\sum_{i=1}^{n} \frac{[V_i - V_{mean}]}{A V_{mean}} A_i \quad (4.1)$$

where V is the average velocity, A is thethe cross section area and instead of the V the mole fraction of NH3 can be used to calculate ammonia distribution.. Time average values for the uniformity index are shown in Figure 4.29.

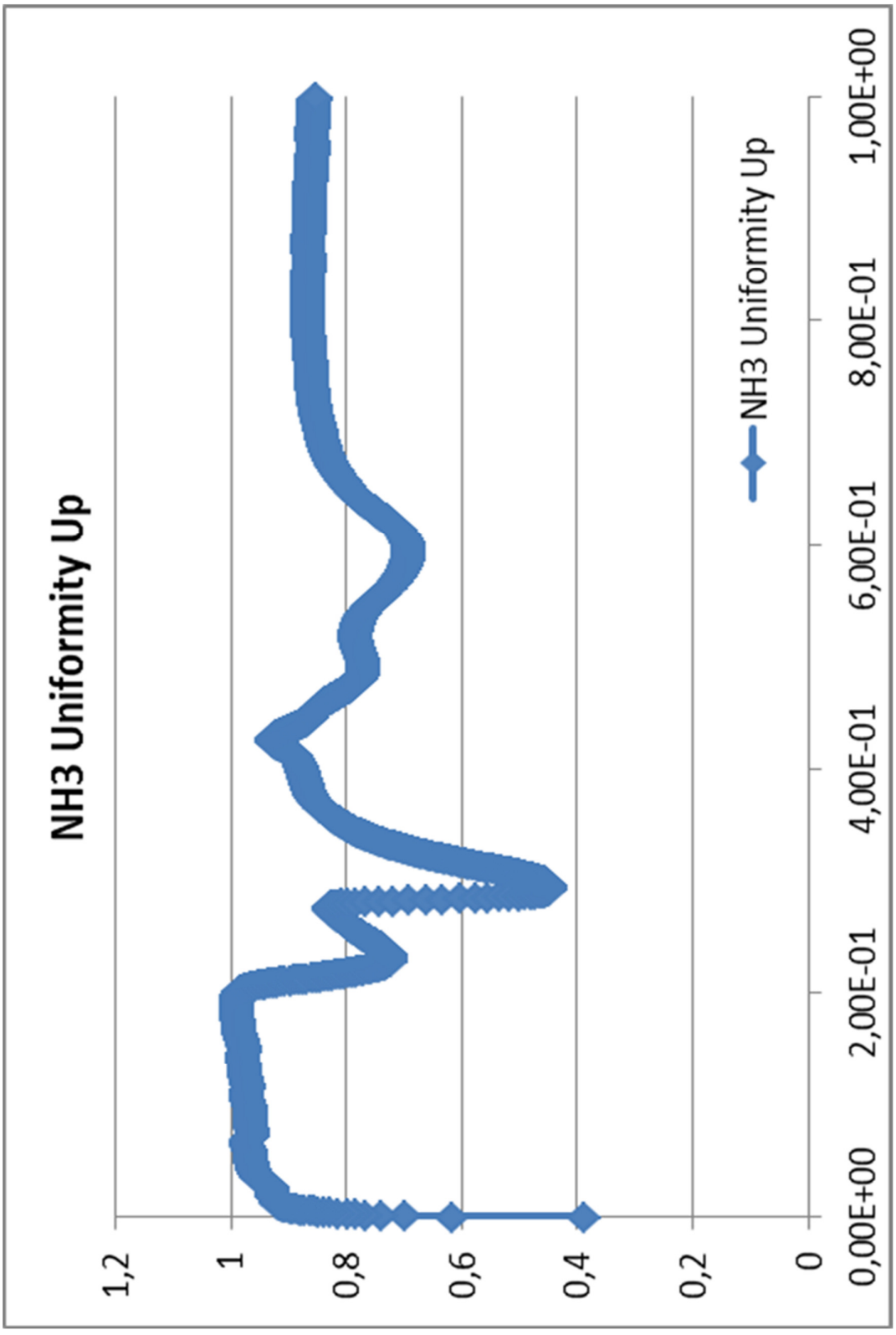

Figure 4.29. Gamma value of the NH3

Figure 4.30 show the production of urea products from urea decomposition obtained using the proposed kinetic model which validated in previous chapter. The reason is that due to the low residence time, the droplets exit the domain without complete decomposition of aqueous-urea.

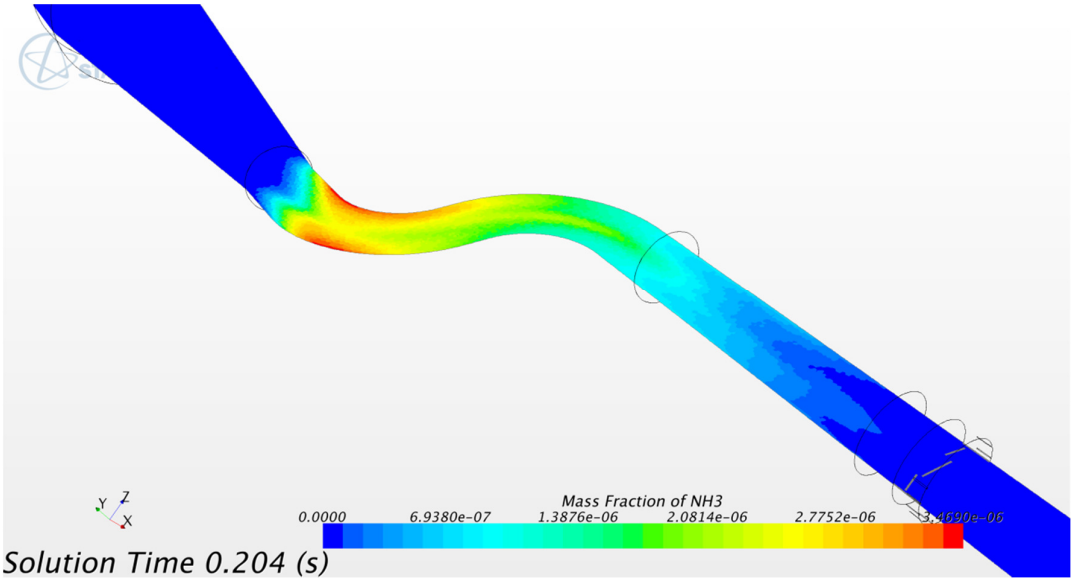

Figure 4.30. Isocyanic product can be seen along catalyst

However, since SCR systems in mobile applications operate under a range of engine speed and load conditions, such incomplete decomposition is possible in real systems in some operating conditions. In real engine operating conditions, aqueous-urea particles in spray may not completely be decomposed to by-products and gaseous species like ammonia.

4.4. Urea Deposit Mapping

The deposit test for inline exhaust aftertreatment test guide the development of test plans to evaluate the conditions of deposit formation. Deposit testing are conducted in a flow lab in Figure 4.31 that is capable of simulating flow rates, temperatures and urea injection in inline exhaust aftertreatment systems. Urea injection system is developed with ECU connection for flow lab.

It is worth mentioning that low NOx efficiency and high deposit buildup are often outcomes of poor system design. Therefore, before performing deposit mapping, it is desirable that the exhaust system has been sufficiently optimized in thermal and flow

performance, resulting in even distribution of ammonia, highest possible NOx reduction efficiency, acceptable back pressure as well as other performance measures. In general, deposit issue should not come as a result of poor system design, but rather a result of severe engine conditions such as extremely low temperature and other design constraints.

A glass window test is conducted to observe deposit formation and the critical temperature at which wall wetting occurs. For this test, wall wetting is defined as a condition where injected droplets form a liquid film. To observe the droplets, quartz window mounted below the injector where the injected droplets hit the bottom wall. Figure 4.31 shows the window test pipe and the location of the thermocouples attached to the bottom of the pipe directly below the glass window. The thermocouples are positioned across from the injector where particle impingement is most likely.

The S-bent pipe is directly assemblied to the window test pipe's flange. At each operating point, temperature and flow are held constant, while injection pulse width is gradually increased until droplet evaporation could not be sustained and wall wetting occurs. For several representative points, the urea injection rate is increased until unsustainable evaporation occurs.

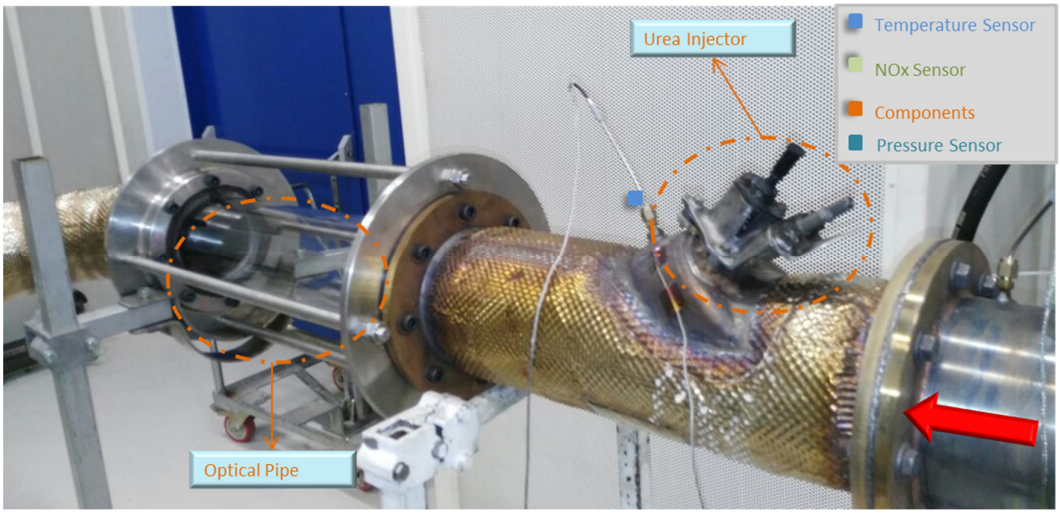

Figure 4.31. Optical window pipe

Inline exhaust aftertreatment system for deposit testing includes urea injector, quartz pipe, S bend and SCR catalyst. The quartz pipe is used for discover the root causes of deposits.In Figure 4.32. The observations in quartz pipe indicate that deposit which fails

to evaporated and start the formation due to temperature distribution extensively on the side wall of the mixer and the aerodynamic force as operating condition.

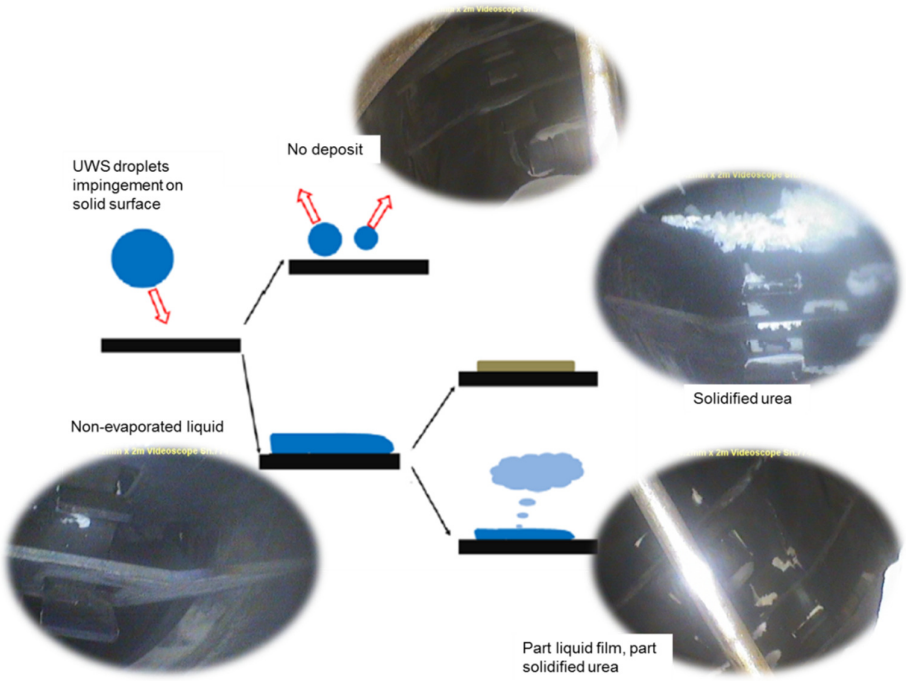

Figure 4.32. Deposit Characteristics for different impingement condition

Exhaust gas temperature and mass flow rate of exhaust system have impacts on urea deposit formation. Droplet deposition has the potential to quench temperature in local areas of the mixer, such as the blade side. The local temperature could reduced even further if evaporation took place (latent heat of evaporation). So in liquid phase form, the deposit formation seems to be dependent on the initial size of the wall film.

The blade side is the primary impingement target and wall film always accumulates at the blades. The light wash of liquid can be seen to progress and recede (tidal effect) across the field of view at some operation conditions. When this occurs, the leading edge of the wall film begin to form a crystal dam preventing further progression. Potentially, the could be the deposit nuclei to create a much bigger deposit formation. It the initial wall film size is sufficient large (say go beyond the trailing edge of the side blades), then it can broken up by the interactions with either the gas stream or fluid additions. Such interactions could cause a splatting of droplets on adjacent surface which in the conditions observed has rapidly led to crystal formation at these sites. Excessive wall film could transported off the primary injection zones into the adjacent

areas, as trailing edge of blades. However, the current study predict the liquid film location because of endoscope camera and quartz pipe. So quartz pipe can be used to detect location and correlate the CFD model but it is not sufficient to predict mass and thickness of deposit. Quartz pipe is only used to predict the deposit starting point. But it cannot give us quantified value for the deposit.

Besides of quartz pipe deposit testing, endoscope camera system with image processing tool in Matlab are developed as deposit quantify prediction work. Deposit map can be generated so it will offer insights on deposit formation across a wide range of operating conditions. Urea deposit mitigation, in turn, should fall within system level design scope along with other performance targets and constraints.

With regards to procedures of deposit mapping, typically, it is desirable to select representative engine conditions and use reliable and repeatable test procedure to quantify urea deposits. Then perform deposit tests for selected operating points with intermittent step of eliminating unnecessary test conditions. Finally, translate test findings from thermal and flow management back to those based on engine rpm and load. In many cases, the urea deposit map can often be interpreted more directly by temperature and flow conditions.

There are mainly two method to understand deposit mass and thickness. First one is measuring deposit weight for an SCR system. But it is not possible if there is compact SCR layout system. In addition if the system cools, the deposit collects moisture and amount of deposit affect significantly. This can also interpreting the severity of deposits across difference cases. Therefore, a consistent method of testing and weighing the deposits should be developed to provide reliable data interpretation and deposit evaluation. The deposit weight method is used to correlate image processing tool in many selected operating points.

The different deposit accumulated location are predicted in CFD tool in a good correlation. These images are post processed in matlab. Four critical regions are selected to measure mass and thickness of deposit. Front mixer, mixer pipe, back of the mixer and s-bend connection are deposit accumulated region. In Figure 4.33 and Figure 4.34pictures from endoscopic camera are used to generate deposit map.

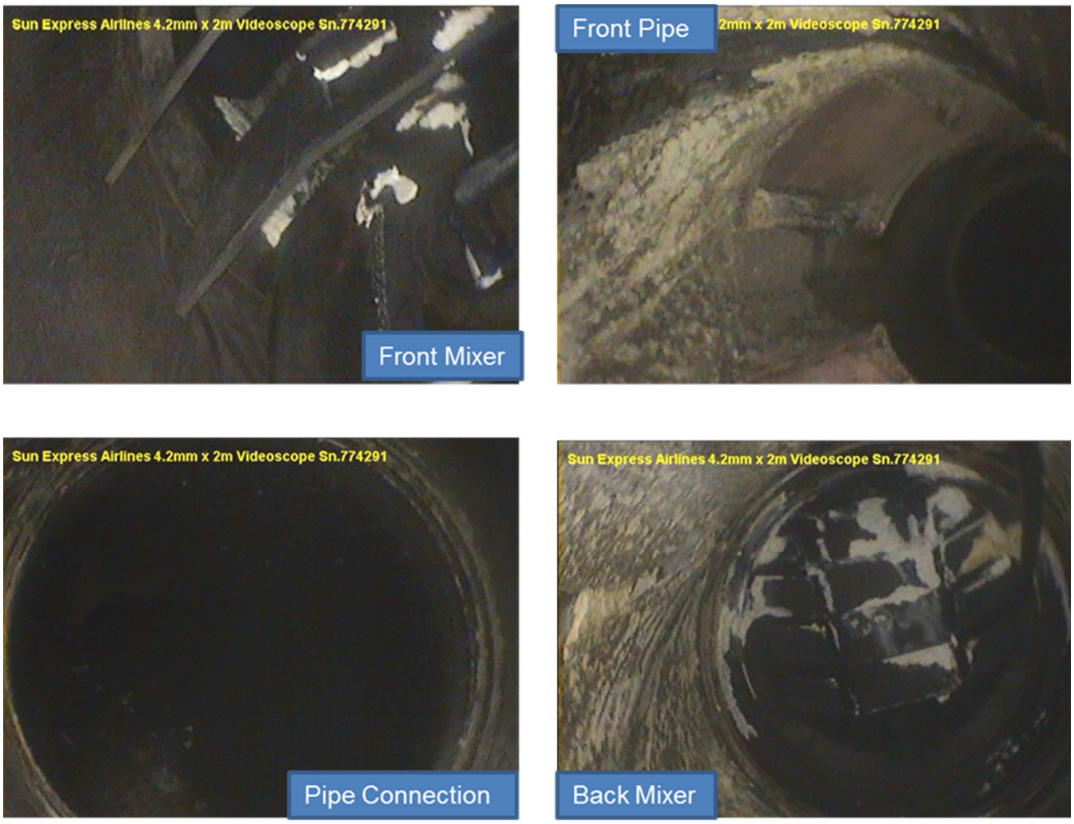

Figure 4.33. Deposit accumulation at 400 kgh/h and 200 degree C

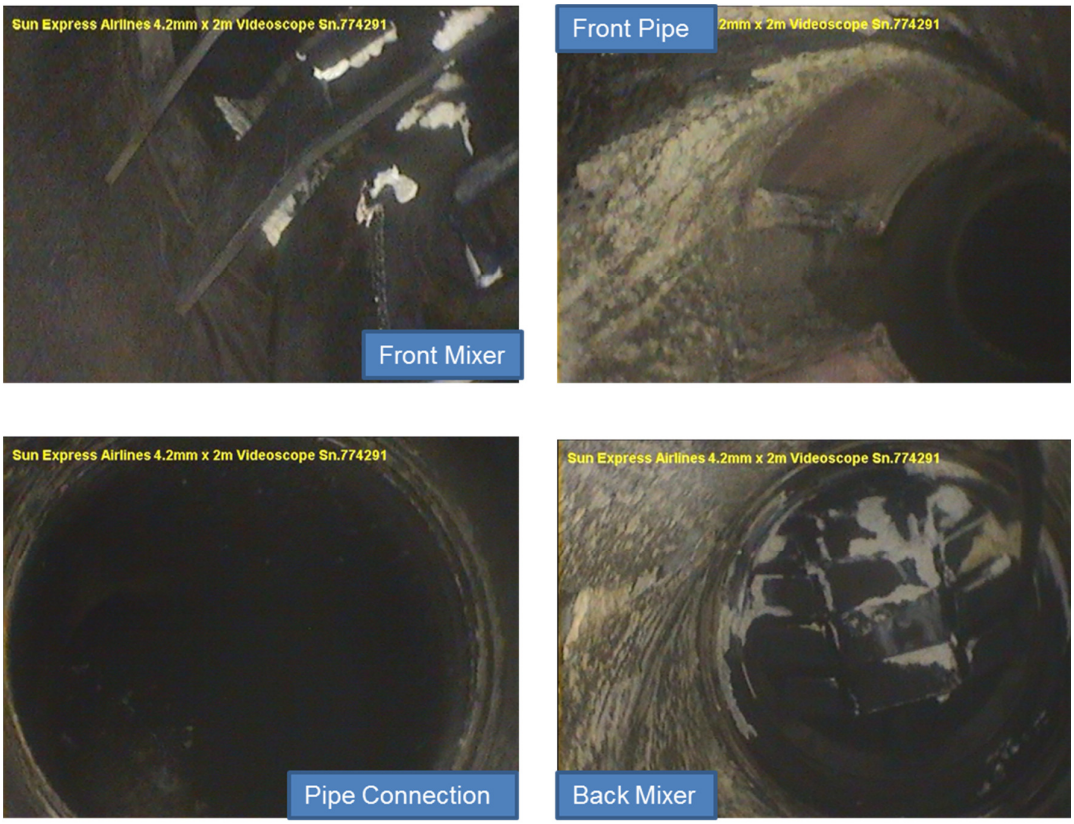

Figure 4.34. Deposit accumulation at 350 kgh/h and 300 degree C

Deposit mass are predicted by endoscope camera image processing results From

Figure 4.35. The intermediate point are generated for mapping using interpolation values in Table 4.1

Table 4.1. Predicted Deposit values for different operating conditions

Gas Temperature (C)	Exhaust Mass Flow Rates (kh/hr)					
	100	250	400	550	700	900
200	0,10	0,30	1,30	2,00	1,80	2,50
250	0,40	1,00	1,75	3,80	3,60	3,40
300	1,00	2,00	2,70	4,10	4,50	5,00
350	2,00	3,00	3,50	4,80	5,30	7,50
400	3,00	4,00	4,80	5,10	6,70	8,00

Thses map can be used as a reference surface from which multiple operating conditions for deposit tests can be selected. A set of operating conditions should be selected to adequately represent urea injection situation. Too few points would impede a full picture of the urea situation; too many points would demand too

many resources.

Intelligent screening method can be selected to determine the number of total points. For example, one approach would be to run the worst case (with the lowest temperature) conditions with the same mass flow rate, thereby possibly eliminating tests of higher temperature conditions if the worst case is free of deposit concern.

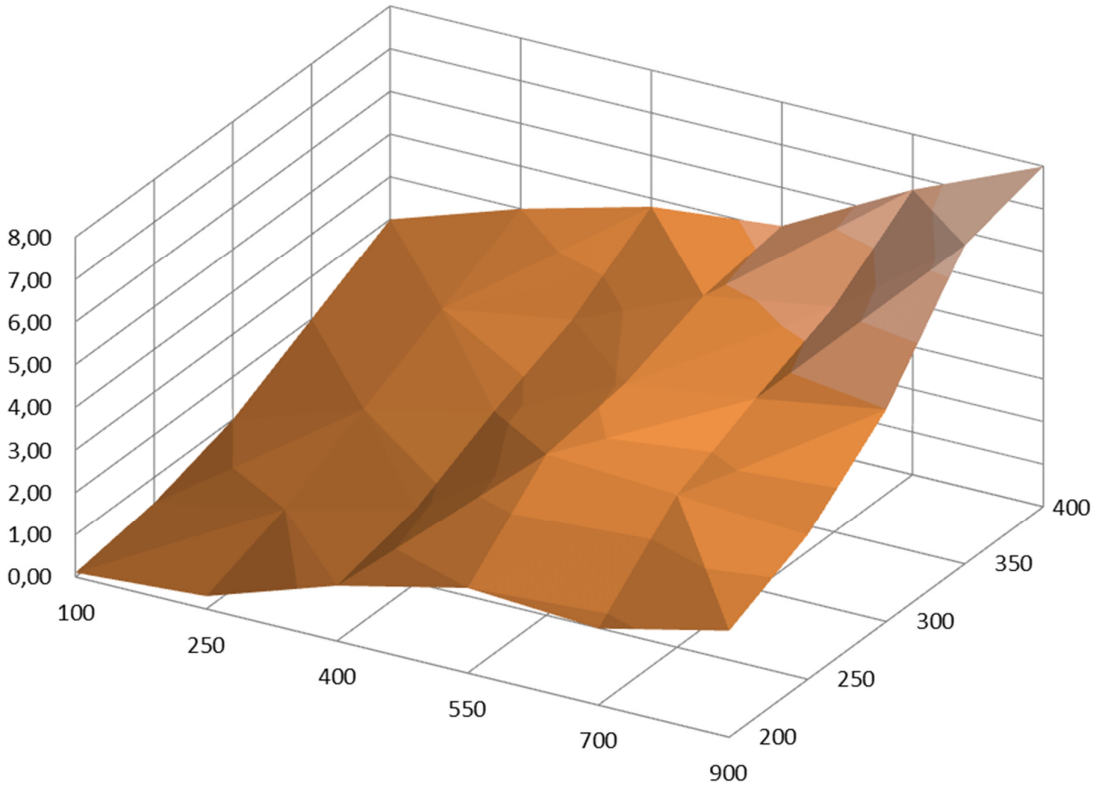

Figure 4.35. Deposit Mapping from Image Processing Tool

4.5. Emission Prediction Modelling

In order to address the 3D effects, the GTPower code has been used recently. 3D CFD flow, temperature and NH3 distribution data were used as the input file. This option will enable GT-Power to take the non-uniform flow, temperature and NH3 distribution at the entry side of the SCR into account.

For this new CAE process, radial profiles of NH3, mass flow rate of gases and temperature are extracted at the upstream of the SCR catalyst. These datas are imposed the SCR inlet at the GT-Power

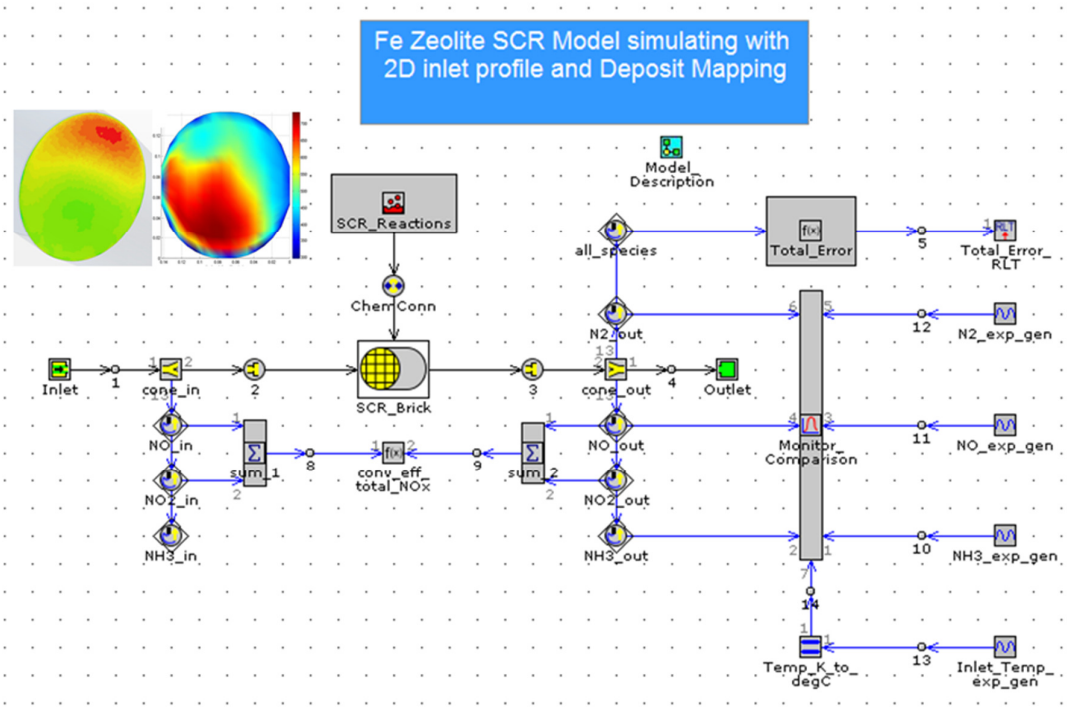

Figure 4.36. Emission Prediction Modeling with 3D CFD results

Figure 4.37 and Figure 4.38 shows corrected NH3 distribution from CFD. Ammonia distribution from CFD corrected with deposit data from image processing.

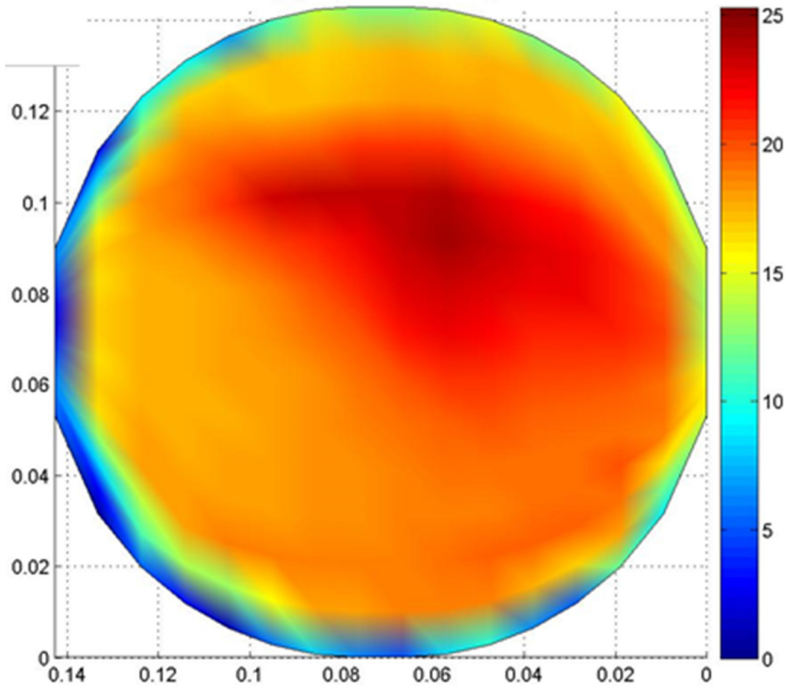

Figure 4.37. Corrected NH3 value with deposit maping result

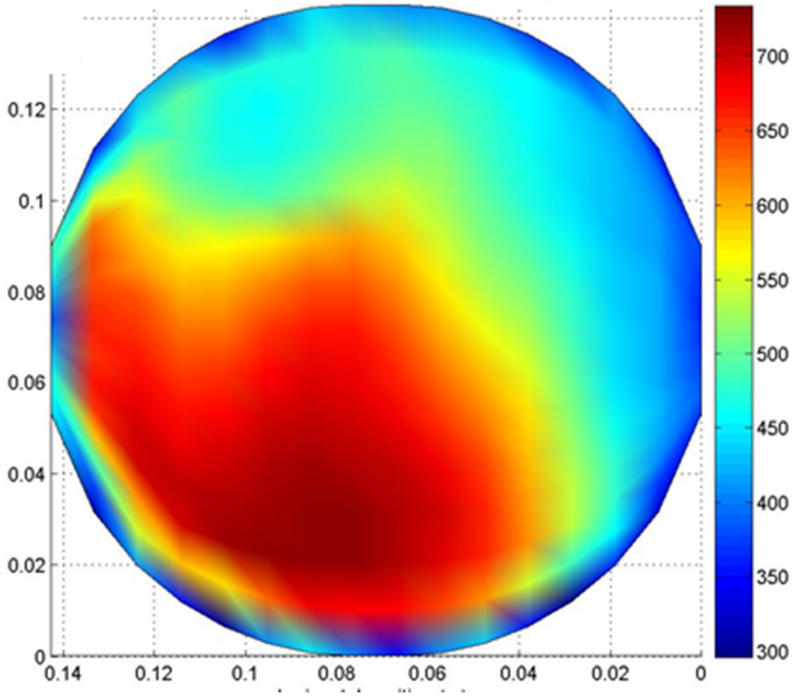

Figure 4.38. Temperature Distribution

The NH3 ammonia distibuion was corrected from deposit accumulation information. The corrected NH3 are imposed GT-Power to determine emission prediction at WHSC cycle point.

Figure 4.39 and Figure 4.40 present temperature and velocity variation across the catalyst. Figure 4.41present NOx reduction across the catalyst.

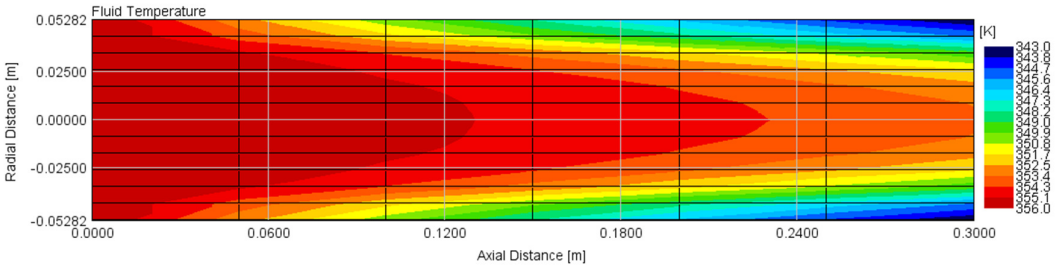

Figure 4.39. Fluid Temperature across the catalyst

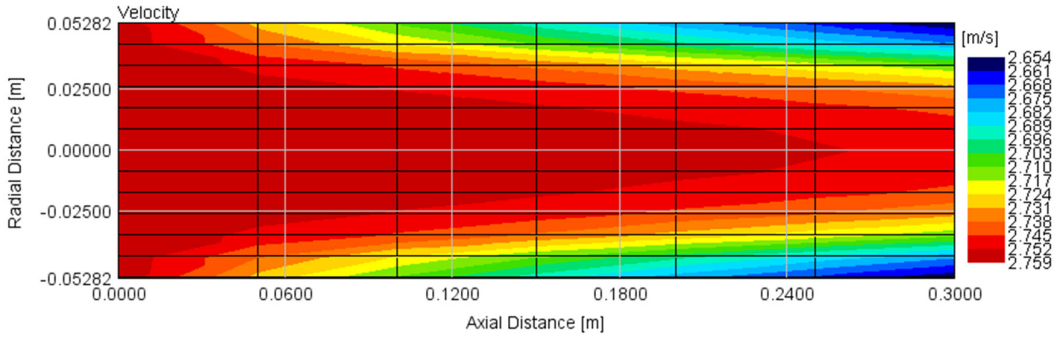

Figure 4.40. Velocity distribution across the catalyst

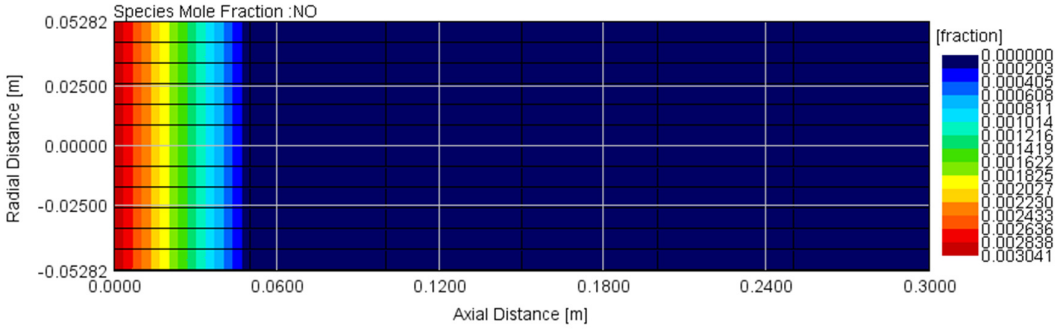

Figure 4.41. NOx reduction across the catalyst

Velocity, temperature and NH3 distribution of the inline exhaust aftertreatment system were taken from 3D CFD as the inlet boundary conditions. 1D emission prediction models were run for WHSC cycles. This comparison is reported in Table 4.2. NOx efficiency predicted using both approaches was 12% of the difference. The performance predictions using the NH3 distribution with deposit approach were slightly lower than NH3 without deposit values.

Table 4.2. NOx conversion of the NH3 distribution

	NOx Conversion	
	NH3 inlet	Corrected NH3 inlet
mode 1	82	79
mode 2	95	95
mode 3	85	80
mode 4	93	92
mode 5	85	85
mode 6	91	85
mode 7	92	86
mode 8	92	90
mode 9	83	80
mode 10	81	81
mode 11	82	82
mode 12	83	83
mode 13	85	85

The default 1D kinetic model generally over-predicted performance if the deposit is not consider. Accuracy of system out NOx emissions is improved by using CFD data corrected deposit map.

3D emission predict the local NOx conversion efficiency and give the design modification chance.

Figure 4.42 shows the average of the NH3 and NOx value for the inline exhaust aftertreatment system.

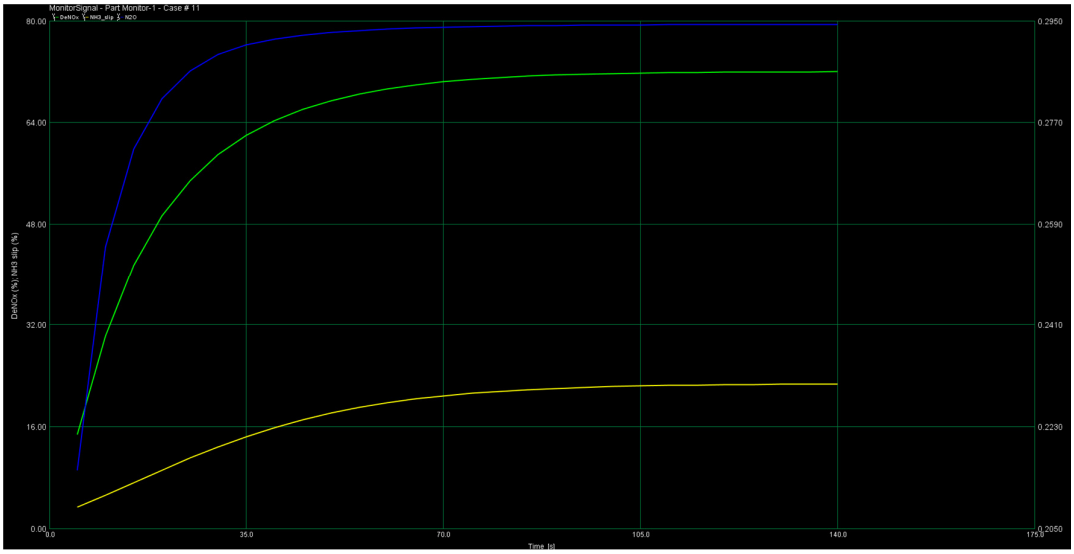

Figure 4.42 WHSC point for different NH3 distribution from CFD

Figure 4.43shows emission result of the inline exhaust aftertreatment system. For high temperature operating point NOx conversions are %98.

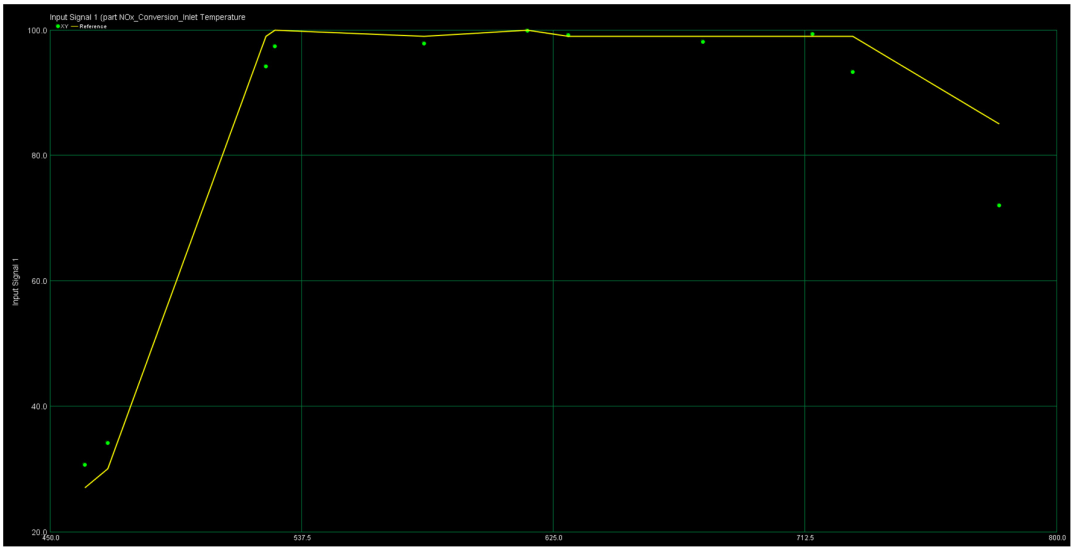

Figure 4.43. Emission Prediction on the inline exhaust aftertreatment system

5. CONCLUSIONS

The efficient design of selective catalyst reduction system is required to NOx reduction mechanism. This system design is crucial for emission legistration. In this thesis, comprehensive modeling approach has been developed to simulate active SCR system based on inline exhaust aftertreatment system from Flow Test Bench. By This method we can understand whether the desing/design changes effect on emission.

Multicomponent UWS injection modelling and muti reaction modeling as thermolysis and hydrolysis have been implemented into inline exhaust aftertreatment system and validated with literature work and flow test bench capabilities as pressure, temperature NOx and FTIR information. The PIV gives reasonable result to correlate this complex SCR system.

The developed numerical simulations for droplet and species show the dependency of the SCR system to the injection characteristics and flow field parameters. The good agreement is shown in terms of of injection and flow field between numerical model and flow test bench.

The simulation of active SCR system has been performed in spray-wall interaction framework as well. The multi component Bai impengement model has beend adopted into numerical simulation to predict deposit location but mass of deposit can not predict well. So deposit data are generated by using endoscope visualization data. The endoscope visualization data processed to generate deposit mass prediction by using image processing tool from Matlab. The deposit data are used to generate deposit map for 1D emission predictive tool.

This comprehensive 1D emission model are used to predict emission level in WHSC cycle and compared the dyno test results. These results are comparable well. Considering the results of this work, following conclusions can be drawn:

- The present work revealed that reynolds stress turbulence model is sufficient to model. PIV measurement and RSM simulations may be employed to directly validate turbulent exhaust flow field and spray simulation.
- The heat transfer correlation work of inline exhaust aftertreatment system shows conjugate heat transfer is required.

- In addition to serving their primary purpose of enhancing mixing between exhaust gas and spray, mixers are quite effective in reducing deposits. Heat transfer via spraying onto a mixer's hot surfaces results in enhanced boiling and convective heat flux. Mixers with large surface area are promising in enhancing particularly conjugate heat transfer despite the fact that mixers often reduce spray particle transport length. System design has a significiant impact on the system performance and formation of the deposit.
- The pipe surface temperature is a critical factor due to the deposits that form on the inner pipe walls of the system. Below a certain critical temperature, wall wetting and ensuing deposit formation are built.
- Modelling of deposit formation in 3D CFD is not sufficient to capture all deposit effect into the system. The developed CFD method offers a promising basic deposit prediction as deposit location for accumulation but full chemistry of deposit prediction seems very complex and ineffective for emission prediction aims.
- 1D emission prediction model has been used with WHSC cycle. These models assumed %100 water evaporation and chemical products and can not capture 2D species and velocity data at the inlet of the SCR system. This emission prediction becomes over predicted data due to very simple physics.
- 1D emission prediction models with species, velocity and temperature data from 3D CFD at the SCR inlet and deposit mapping from image processing tool shows the good validation according to engine dyno data. This predictive models can be used more complex control strategies without dyno data.

6. REFERENCES

[1] A. Winer and W. Busby, "Atmospheric transport and transformation of diesel emissions," *Diesel Exhaust: A Critical Analysis,* pp. 83-105, 1995.

[2] E. Omidvarborna , "Recent studies on soot modeling for diesel combustion," *Renewable and Sustainable Energy Reviews ,* p. Renewable and Sustainable Energy Reviews , 2015.

[3] B. Weinstock and H. Niki, "Carbon Monoxide Balance in Nature," *Science ,* p. 176, 1972.

[4] D. Fowler , "The atmospheric budget of oxidized nitrogen and its role in ozone formation and deposition," *The atmospheric budget of oxidized nitrogen and its role in ozone formation and deposition,* p. 139, 1998.

[5] "www.dieselnet.com.," 2015. [Online].

[6] R. (EC), "The European parliament and the council," 2009.

[7] R. Heck, "Catalytic Abatement of Nitrogen Oxides - Stationary Applications," pp. 519-523, 1999.

[8] T. Tarabulski and R. Krishnan , "dieselnet.com," Diesel Technical Report, January 2005. [Online]. Available: https://www.dieselnet.com/papers/0501krishnan/.

[9] P. Spurk, A. Schäfer-Sindlinger, M. Pfeifer and J. Gieshoff, "Advanced Urea SCR Catalysts for Automotive Applications," *SAE Technical Paper ,* no. 2001-01-0514, 2001.

[10] R. M. Heck and R. J. Farrauto, Catalytic Air Pollution Control, New York: John Wiley & Sons, 2002.

[11] R. Kuisell, "Butting Monoliths in Catalytic Converters," *SAE Technical Paper,* no. 96055, 1996.

[12] O. Hougen and K. Watson, "Chemical Process Principles, Part Three: Kinetics and Catalysis," *John Wiley,* p. 7th, 1959.

[13] J. Leyrer, "Advanced Studies on Diesel Aftertreatment Catalysts for Passenger

Cars," *SAE Technical Paper,* no. 960133, 1996.

[14] J. Steger, "Advances in Emission Control Technology," *Emission Control and Catalytic Combustion TOPTEC,* 1995.

[15] S. Verdier, E. Rohart, O. Larcher, V. Harle and M. Allain, "Innovative Materials for Diesel Oxidation Catalysts, with High Durability and Early Light-Off," *SAE Technical Paper,* no. 01-476, 2005.

[16] Manufacturers of Emission Controls Association, "Emission Control Technologies for Diesel-Powered Vehicles," 2007.

[17] J. Ambs and B. Ambs, "The Influence of Oxidation Catalysts on NO2 in Diesel Exhaust," *SAE Technical Paper,* no. 932494, 1993.

[18] E. Jacob, "Exhaust Gas Aftertreatment System for Euro 4 Heavy-Duty Engines," *MTZ,* no. 6/2005, 2005.

[19] P. K. Lee S., P. J. and K. B., "Characteristics of reducing NO using urea and alkaline additives, Combustion and Flame," vol. 141, 2005.

[20] D. Cobb, "Application of Selective Catalytic Reduction (SCR) Technology for NOx Reduction From Refinery Combustion Sources," *Environmental Progress,* no. 10, p. 49, 1991.

[21] K. Hirata, N. Masaki, H. Ueno and H. Akagawa, "Development of Urea-SCR System for a Heavy-Duty Commercial Vehicles," *SAE Technical Paper,* no. 2005-01-1860, 2005.

[22] Koebel and S. E. O., "Thermal and Hydrolytic Decomposition of Urea for Automotive," vol. 42, pp. 2093-2100, 2003.

[23] Y. Itaya, S. Deguchi, M. Takei, M. Yoshio, H. Matsuda and M. Hasatani, "NO reduction behavior by urea solution injection in the tubular reactor," 1997.

[24] W. Held, A. König, T. Richter and P. Pupple, "Catalytic NOx reduction in net oxidizing exhaust gas," *SAE International Paper,* p. 900496, 1990.

[25] B. R. M. A. O. M. a. I. J. Alzueta M.U., "Interactions between nitric oxide and urea under flow reactor conditions," vol. 12, pp. 1001-1007, 1998.

[26] M. Koebel, M. Elsener and M. Kleemann, "Urea-SCR: a promising technique to reduce NOx emissions from automotive diesel engines," *Catalysis Today,* pp.

335-345, 2000.

[27] J. Fisher, "Comparison of Urea-Based Ammonia to Liquid Ammonia Systems for NOx Reduction Applications," Vols. 17-20, 2002.

[28] M. Kleemann, M. Elsener and M. Koebel, "Hydrolysis of Isocyanic Acid on SCR Catalyst," *Ind. Eng. Chem. ,* p. 39, 2000.

[29] S. Sluder, J. Storey, S. Lewis and J. Lewis, "Low Temperature Urea Decomposition and SCR Performance," *SAE Technical Paper,* Vols. doi:10.4271/2005-01-1858, no. 2005-01-1858, 2005.

[30] C. Sluder, J. Storey and S. Lewis, "Low Temperature Urea Decomposition and SCR Performance," *SAE Technical Paper,* no. 2005-01-1858, 2005.

[31] J. Gieshoff, "Advanced Urea SCR Catalysts for Automotive Applications," *SAE Technical Paper,* no. 2001-01-0514, 2001.

[32] Eichelbaum, F. M.J. and C. R., "The impact of urea on the performance of metal exchanged zeolites for the selective catalytic reduction of NOx: Part I. Pyrolysis and hydrolysis of urea over zeolite catalysts," vol. 97, pp. 90-97, 2010.

[33] "http://europa.eu/legislation_summaries," Summaries of EU legislation, 2011. [Online].

[34] K. Mueller-Haas, "Emission Reduction Systems for Non-Road Applications," in *CTI Non-Road Forum*, Stuttgart, July 1-2, 2008.

[35] T. Johnson, "Diesel Emission Control in Review," *SAE Int. J. Fuels Lubr.,* pp. 68-81, 1998.

[36] H. Steven, "Development of a World-wide Harmonised Heavy-duty Engine Emissions Test Cycle," ECE-GRPE WHDC Working Group, Germany, 2001.

[37] T. Johnson, "Review of Diesel Emissions and Control," *SAE Technical Papers,* no. 2010-01-0301, 2010.

[38] G. Zhu and Q. Song, "Model-based closed-loop control of urea SCR exhaust aftertreatment system for Diesel engine," *SAE 2002 World Congress,* no. 2002-01-0287, 2002.

[39] J. Chi and F. DaCosta, "Modeling and control of a Urea-SCR aftertreatment system," *2005 SAE World Congress,* no. 2005-01-0966, 2005.

[40] C. Onder, H. Geering and C. Schar, "Control of an SCR catalyst converter system for a mobile heavy-duty application," *IEEE Transactions on Control System Technology,* vol. 14, pp. 641-652, 2006.

[41] A. Herman, W. M., D. Cabush and M. Shost, "Model based control of SCR dosing and OBD strategies with feedback from NH3 sensors," *SAE 2009 World Congress,* no. 2009-01-0911, 2009.

[42] D. Seher, M. Reichelt and S. Wickert, "Control strategy for NOx emission reduction with SCR," in *Proceedings of the International Truck & Bus Meeting & Exhibition*, 2003.

[43] P. Schaber, J. Colson, S. Higgins and D. Thielen, "Thermal decomposition (pyrolysis) of urea in an open reaction vessel," *Thermochimica Acta,* no. 2004.05.018, 2004.

[44] D. Upadhyay and M. Van Nieuwstadt, "Model Based Analysis and Control Design of a Urea-SCR DeNOx Aftertreatment System," *ASME Journal of Dynamic Systems, Measurement and Control,* p. 128, September 2006.

[45] F. Willems, R. Cloudt, E. Eijnden, M. Genderen, K. Verbeek, B. Jager and W. Boomsa, "Is Closed-Loop SCR Control Required to Meet Future Emission Targets," *SAE,* no. 2007-01-1574, 2007.

[46] M. N. J. W. M. S. T. B. T. F. G. F. G. Shost, ""Monitoring, Feedback and Control of Urea SCR Dosing Systems for NOx Reduction: Utilizing an Embedded Model and Ammonia Sensing," *SAE,* no. 2008-01-1325., 2008.

[47] M. Zöchbauer, H. Smith and T. Lauer, "Advanced SCR Flow Modeling with a Validated Large Eddy Simulation," *SAE,* no. 2015-01-1046, 2015.

[48] A. Ramadan, K. Saha and X. Li, "Modeling of the Injection and Decomposition Processes of Urea-Water-Solution Spray in Automotive SCR Systems," *SAE Technical Paper,* no. 2011-01-1317, 2011.

[49] G. Zheng, F. Wang, S. Zhang and F. Zhang, "Development of Compact SCR Systems with Closely Coupled Injector Configurations," *SAE Technical Paper,* no. 2014-01-1546, 2014.

[50] S. B. R. L. T. K. C. Fischer, "Impact of the Turbulence Model and Numerical

Approach on the Prediction of the Ammonia Homogenization in an Automotive SCR System," *SAE Int. J. Engines,* no. 1443-1458, 2012.

[51] S. El-Tahry, "A Comparison of Three Turbulence Models in Engine-Like Geometries," *In International Symposium on Diagnostics and Modelling of Combustion in Reciprocating Engines,,* no. 203-213, 1985.

[52] S. El-Tahry, "Application of a Reynolds Stress Model to Engine-Like Flow Calculations," *J. Fluids Eng ,* no. 3242508, pp. 444-450, 1985.

[53] S. Fischer, Simulation of the UWS Preparation and ammonia-homogenization with a validated CFD model for the optimization of automotive SCR system, Wien, 2012.

[54] F. Birkhold, U. Meingast and P. Wassermann, "Analysis of the Injection of Urea-water-solution for automotive SCR DeNOx-Systems: Modeling of Two-phase Flow and Spray/Wall-Interaction," *SAE,* 2006-01-0643.

[55] A. D. Z. E. M. M. Rota R., "Experimental and modeling analysis of the NOxOUT process," *Chem.Engr.Sci,* pp. 27-38, 2002.

[56] A. A. Mckinely T.L., "Urea Decomposition Modeling Framework for SCR," *SAE Int.J.Fuels Lubr,* pp. 612-626, 2009.

[57] A. Munnannur and Z. Liu, "Development and Validation of a Predictive Model for DEF Injection and Urea Decomposition in Mobile SCR DeNOx Systems," *SAE International,* no. 2010-01-0889, 2010.

[58] H. Ström, A. Lundström and B. Andersson, "Choice of urea-spray models in CFD simulations of urea-SCR systems," *Chemical Engineering Journal,* no. 150, 2009.

[59] P. P. S. G. K. A. Zheng G., "Mixer Development for Urea SCR application," *SAE,* no. 01-2879, 2009.

[60] L. S. K. W. L. C. Jeong S., "Simulation on the optimum shape and location of urea injector for urea SCR system of HDDE to prevent NH3 slip," *SAE,* no. 01-3886, 2005.

[61] Y. Y., "Development of a 3D Numerical Model for Predicting Spray, Urea Decomposition and Mixing in SCR," *SAE,* no. 01-3985, 2007.

[62] R. S., "Improved NOx reduction using wiremesh thermolysis mixer in urea SCR

system," *SAE,* no. 01-2636, 2008.

[63] V. Ebrahimian and C. Habchi, "Towards a predictive evaporation model for multicomponent hydrocarbon droplets at all pressure conditions," *Int.J.Heat Mass Trans,* no. 2011.03.031, 2011.

[64] L. T. Perman E.P., "Vapour Pressure and heat dilution of aqueous solutions," *Trans. Farad. Soc.,* p. 22, 1926.

[65] B. G. D. G. P. V. Ferro D., "Vapor Pressure and sublimation enthalpies of urea and some its derivates," *J. Chem. Thermodynamics,* pp. 915-923, 1987.

[66] J. Kim, R. Ryu and J. Ha, "Numerical prediction on the characteristics of spray-induced mixing and thermal decomposition of urea solution in SCR system," *2004 Fall Technical Conference of the ASME Internal Combustion Engine Division,* 2004.

[67] J. Grünwald, "Verbesserung der Reduktionsmitteldispersion und verdunstung in SCRAbgasanlagen," 2007.

[68] R. Van Helden, R. Venbeek and F. Willems, "Optimization of Urea Scr Denox Systems for HD Diesel Engines," *SAE,* no. 2004, 2004-01-0154.

[69] E. Aburamadan, K. Saha and X. Li, "Modeling the Depleting Mechanism of Urea-Water-Solution Droplet for Automotive Selective Catalytic Reduction Systems," *AIChE J.,* no. DOI 10.1002/aic.12523, 2011.

[70] F. Birkhold, Selektive katalytische Reduktion von Stickoxiden in Kraftfahrzeugen, Stutgart: PhD Thesis, 2007.

[71] F. Birkhold, U. Meingast, P. Wasserman and O. Deutschmann, "Analysis of the Injection of Urea-Water-Solution for Automotive SCR DeNOx-Systems: Modeling of Two-Phase Flow and Spray/Wall-Interaction," *SAE Paper,* no. 2006-01-0643, 2006.

[72] A. Herr , Thermische Zersetzung von Festharnstoff für mobile SCR Katalysatoranwendungen, Technischen Universität Kaiserslautern, 2004.

[73] G. Faeth, "Evaporation and combustion of sprays," *Progress in Energy and Combustion Science,* pp. 1-76, 1983.

[74] W. Sirignano, "Fuel droplet vaporization and spray combustion theory," *Progress*

in Energy and Combustion Science, no. 9, pp. 291-322, 1983.

[75] C. Bai and A. Gosman, Development of Methodology for Spray Impingement Simulation, 1995, p. doi:10.4271/950283.

[76] D. Kuhnke, Spray/wall- interaction modelling by dimensionless data analysis, Technische Universitat Darmstadt, 2004.

[77] H. L. Fang and H. DaCosta, "Urea thermolysis and NOx reduction with and without SCR catalysts," *Applied Catalysis B: Environmental,* no. 46:17–34, 2003.

[78] H. Dong, S. Shuai and J. Wang, "Effect of Urea Thermal Decomposition on Diesel NOx-SCR Aftertreatment Systems," *SAE Technical Paper,* no. 2008-01-1544, 2008,.

[79] G. Zheng, A. Kotrba, M. Golin and T. Gardner, "Overview of Large Diesel Engine Aftertreatment System Development," *SAE Technical Paper ,* no. doi:10.4271/2012-01-1960, 2012.

[80] T. Johannessen, "3rd Generation SCR System Using Solid Ammonia Storage and Direct Gas Dosing - Expanding the SCR window for RDE," in *2012 DEER conference*, Amminex., 2012.

[81] L. Xu, W. Watkins, R. Snow and G. Graham, "Laboratory and Engine Study of Urea-Related Deposits in Diesel Urea-SCR After-Treatment Systems," *SAE Technical Paper,* no. 2007-01-1582, pp. doi:10.4271/2007-01-1582, 2007.

[82] G. Zheng, A. Fila, A. Kotrba and R. Floyd, "Investigation of Urea Deposits in Urea SCR Systems for Medium and Heavy Duty Trucks," *SAE Technical Paper,* no. 2010-01-1941, 2010.

[83] T. Wang, S. Beak and S. Lee, "Experimental Investigation on Evaporation UWS Droplet for SCR Applications," *AIChE Journal,* no. 12:3267-3276, 2009.

[84] S. Musa, M. Saito and M. Arai, "Evaporation Characteristics of a Single Aqeuous Urea Solution Droplet," *ICLASS,* no. ICLASS06-195, 2006.

[85] D. Yim, S. Kim, J. Baik, I. Nam and Y. Mok, "Decomposition of Urea into NH3 for the SCR Process," *Ind.Eng.-Chem.Res,* vol. 43, no. 4856–4863, 2004.

[86] F. Fischer, R. Bitto, T. Lauer and C. Krenn, "Validation of Turbulence Models for an Automotive SCR System with Laser Doppler Anemometry Measurements,"

SAE, no. 2013-01-1579, 2013.

[87] A. Lundstorm, B. Andersson and L. Olsson, "Urea thermolysis studied under flow reactor conditions using DSC and FITIR," *Chemical Engineering Journal,* no. 150:544-550, 2009.

[88] A. Nishioka, Y. Sukegawa, K. Katogi, H. Mamada, T. Kowatari and T. Mukai , "A study of a New Aftertreatment(2):Control of Urea Solution Spray for Urea-SCR," *SAE,* no. 01-0644, 2006.

[89] J. Seo, "Aftertreatment Package Design for SCR Performance Optimization," *SAE,* no. 01-1135, 2011.

[90] M. Argentero and L. Stradella, "A study of the thermal decomposition of urea, of related compounds and thiourea using DSC and TG-EGA," *Dipartimento di Chimica inorganica,* no. 1016/0040-6031(93)80508-8 , 1993.

[91] J. Chen and K. Isa, "Thermal Decomposition of urea and urea derivatives by simultaneous," *J. Mass Spectrom,* vol. 46, p. 4, 1998.

[92] S. W. Prakash S., "Liquid Fuel droplet heating with Internal Circulation," *International Journal of Heat and Mass Transfer,* pp. 885-889, 1978.

[93] R. Reid, J. Prausnitz and B. Poling, The properties of gases and liquids, New York: McGraw-Hill, 1987.

[94] C. adapco, "Star-CCM User Guide," CD adapco, London, 2014.

[95] M. Koebel, M. Elsener and T. Marti, "NOx-reduction in diesel exhaust gas with urea and Selective Catalitic Reduction," *Comb. Sci. and Techn,* pp. 85-102, 1996.

[96] D. Kuhnke, "Spray/Wall-Interaction Modelling by Dimensionless Data Analysis.," *PhD thesis,* vol. Universitat Darmstadt, 2004.

[97] S. Bhattacharjee and C. Haworth, "CFD Modeling of Process Upstream of the Catalyst for Urea SCR Reduction System in HDD," *SAE,* no. 01-1322, 2011.

[98] S. Schmieg and J. Lee, "Evaluation of Supplier Catalyst Formulations for the Selective Catalytic Reduction of NOx with Ammonia," *SAE,* no. 2005-01-3881, 2005.

[99] L. Xu, R. McCabe and R. Hammerle, "NOx Self-Inhibition in Selective Catalytic Reduction with Urea over a Cu-Zeolite Catalyst in Diesel Exhaust," *Applied,* no.

39:51–63, 2002..

[100] O. Krocher, M. Devadas, M. Elsener, A. Wokaun, N. Soger, M. Pfeifer, Y. Demel and L. Mussmann, "Investigation of the Selective Catalytic Reduction of NO by NH3 on Fe-ZSM5 Monolith Catalysts," *Applied Catalysis B : Environmental,* no. 66:208–216, 2006.

[101] G. Piazzesi, M. Devadas, O. Krocher, M. Elsener and A. Wokaun, "Isocyanic Acid Hydrolysis over FeZSM5 in Urea-SCR," *Catalyst Communications,* no. 7:600–603, 2006.

[102] M. Devadas, O. Krocher and A. Wokaun, "Catalytic Investigation of FeZSM5 in the Selective Catalytic Reduction of NOx with NH3," *Reaction Kinetics and Catalysis Letters,* no. 86(2):347–354, 2005.

[103] H. Steven, "Development of a Worldwide Harmonised Heavy-duty Engine Emissions Test Cycle," UN, 2001.

ÖZGEÇMİŞ

Adı Soyadı **:** İsmail Hakki SAVCI

Doğum Yeri ve Tarihi **:** Erzurum, 02.01.1984

Yabancı Dili **:**İngilizce, Almanca

E-Posta **:**i_hsavci@yahoo.com

Öğrenim Durumu

Derece	**Bölüm/Program**	**Üniversite/Lise**	**Mezuniyet Yılı**
Üniversite	**Makina**	**İstanbul Teknik Üniversitesi**	**2007**
Y. Lisans	**Makina**	**Marmara Üniversitesi**	**2010**

İş Deneyimi

Yıl	**Firma/Kurum**	**Görevi**
2014-	**Ford Otosan**	**Ekip Lideri**
2012-2014	**Ford Otosan**	**Teknik Uzman**

Bilimsel Eserler:

1. Leong A., Savci, İ.H., Hatton A., Scott J. "On Using a CFD Based Global Kinetic Reaction Model to Simulate Catalyst Exotherm with Exhaust Fuel Dosing Device (Fuel Vaporizer)", SAE,2012-01-1290,2014
2. Savci, İ.H., Leong A., Hatton A., Scott J. "Using 3D CFD to model exhaust dosing device (fuel vaporizer) and oxidation of hydrocarbon",I.Mech Conference,2014

Patentler:

1. Savci I..H.; Sarioglu K.; Kandemir N. "A COOLING DEVICE" EP2035763 (A1);2009-03-18
2. Savci I.H, Alkan H. "A MIXER PIPE", WO2015084281, 2015-06-11

3. Savci I.H, Akgul E. “A MIXER”, WO2015076765 (A1), 2015-05-28
4. Savci I.H, “AN EXHAUST GAS REDUCER”, WO2015026305 (A2), 2015-02-26
5. Savci I.H, Kaya Y. “STATIC MIXER” CN103899389 (A), 2014-07-02,
6. Savci, I.H. “ EXHAUST SYSTEM” CN103867270 (A) 2014-06-18
7. Savci, I.H. “MIXER SYSTEM” CN103867265 (A)” 2014-06-18

8 patents are in investigation.

Projelerde Yaptığı Görevler:

1. Yerli Üre Enjeksiyon Sistemi Geliştirilmesi Ve Motor Testleri, Dr Özgür Ertunç, İsmail Hakki SAVCI, Tahsin Hacıbekir, Ardep Proje
2. Ecotorq Exhaust Afterteatment Project
3. Heavy Duty R&D Lab

Bilimsel Kuruluşlara Üyelikler:

1. ASME

Ödüller:

1. Heavy Duty R&D Lab